Chem Soc Rev

REVIEW ARTICLE

View Article Online
View Journal | View Issue

Cite this: *Chem. Soc. Rev.*, 2023, **52**, 1024

Noncancerous disease-targeting AIEgens

Yanhong Duo, †*[ab] Guanghong Luo, †*[abg] Wentao Zhang,†[f] Renzhi Wang,[g] Gary Guishan Xiao,[c] Zihuang Li,[a] Xianming Li,[a] Meili Chen,[a] Juyoung Yoon *[d] and Ben Zhong Tang *[e]

Noncancerous diseases include a wide plethora of medical conditions beyond cancer and are a major cause of mortality around the world. Despite progresses in clinical research, many puzzles about these diseases remain unanswered, and new therapies are continuously being sought. The evolution of bio-nanomedicine has enabled huge advancements in biosensing, diagnosis, bioimaging, and therapeutics. The recent development of aggregation-induced emission luminogens (AIEgens) has provided an impetus to the field of molecular bionanomaterials. Following aggregation, AIEgens show strong emission, overcoming the problems associated with the aggregation-caused quenching (ACQ) effect. They also have other unique properties, including low background interferences, high signal-to-noise ratios, photostability, and excellent biocompatibility, along with activatable aggregation-enhanced theranostic effects, which help them achieve excellent therapeutic effects as an one-for-all multimodal theranostic platform. This review provides a comprehensive overview of the overall progresses in AIEgen-based nanoplatforms for the detection, diagnosis, bioimaging, and bioimaging-guided treatment of noncancerous diseases. In addition, it details future perspectives and the potential clinical applications of these AIEgens in noncancerous diseases are also proposed. This review hopes to motivate further interest in this topic and promote ideation for the further exploration of more advanced AIEgens in a broad range of biomedical and clinical applications in patients with noncancerous diseases.

Received 21st October 2022

DOI: 10.1039/d2cs00610c

rsc.li/chem-soc-rev

[a] *Department of Radiation Oncology, Shenzhen People's Hospital (The Second Clinical Medical College, Jinan University, The First Affiliated Hospital, Southern University of Science and Technology), Shenzhen, 518020, Guangdong, China. E-mail: lgh0506@126.com*

[b] *Department of Microbiology, Tumor and Cell Biology (MTC), Karolinska Institutet, Stockholm, Sweden. E-mail: yanhong.duo@ki.se*

[c] *State Key Laboratory of Fine Chemicals, Department of Pharmacology, School of Chemical Engineering, Dalian University of Technology, Dalian, China*

[d] *Department of Chemistry and Nanoscience, Ewha Womans University, 52 Ewhayeodae-gil, Seodaemun-gu, Seoul, 03760, Korea. E-mail: jyoon@ewha.ac.kr*

[e] *Shenzhen Institute of Aggregate Science and Technology, School of Science and Engineering, The Chinese University of Hong Kong, Shenzhen, Shenzhen, 518172, Guangdong, China. E-mail: tangbenz@cuhk.edu.cn*

[f] *Department of Orthopedics, The Eighth Affiliated Hospital, Sun Yat-Sen University, Shenzhen, 518033, Guangdong, China*

[g] *School of Medicine, Life and Health Sciences, The Chinese University of Hong Kong, Shenzhen, Shenzhen, 518172, Guangdong, China*

† These authors contributed equally to this work.

Yanhong Duo

Yanhong Duo received her PhD degree from Tsinghua University and Lanzhou University (joint training), and she did her postdoctoral study at Karolinska Institutet. She is currently a distinguished professor in Research Institute of Tsinghua University in Shenzhen, and a guest professor in Shenzhen People's Hospital and The Eighth Affiliated Hospital, Sun Yat-Sen University, Major project partner of Peking University Shenzhen Hospital. Her research focuses on the design of AIEgens for biological applications.

Guanghong Luo

Guanghong Luo received his PhD degree from Shanghai University in 2018. Later, he conducted his postdoctoral work at Jinan University in collaboration with Prof. Xianming Li and Zhenyou Jiang. He is currently an assistant researcher in Shenzhen People's Hospital (The Second Clinical Medical College, Jinan University, The First Affiliated Hospital, Southern University of Science and Technology). His research focuses on the designation and biological applications of AIEgens.

1. Introduction

Noncancerous diseases encompass a long list of diseases beyond and unrelated to cancer,[1] such as neurodegenerative diseases,[2] metabolic diseases,[3] autoimmune diseases,[4] cardiovascular diseases (CVDs),[5] orthopedic diseases,[6] infectious diseases,[7] inflammatory diseases,[8] mental disorders,[9] and various kinds of rare diseases. In addition to cancer, accidents and natural disasters, these diseases are responsible for the majority of death around the world.[10] Thus, they pose a heavy burden and serve as a serious threat to the public health, quality of life, and also social development.[1] Throughout the history of medicine, researchers and clinicians have made significant efforts in order to exploit effective strategies and treat various diseases. The goal has been to use advancements in diagnosis and imaging technologies, drugs, to therapeutic biomedical devices in order to improve treatment outcomes and give patients a better, healthier life. Although great progresses has been achieved, the therapeutic outcomes are still far below expectations in most cases. Moreover, for some diseases, little progress has been made and the research is in its infancy. Therefore, there is still an extremely urgent need for additional efforts geared toward the development of more effective strategies for the treatment of human diseases.

Pathological processes are usually characterized by an abnormal amplification of specific DNA copies, expression and modification of specific proteins, secretion of cytokines, and the resultant cascades that reformed the physiological environment.[11,12] Strategies for the detection, diagnosis, bioimaging and treatment of diseases are based on these known aberrations in cellular components and structures. At present, surgery and chemotherapy focused on a specific target remain the primary methods for the treatment of noncancerous diseases. In chemotherapy, clinical drugs used for disease treatment are usually small molecule drugs, which shows a lot of shortcomings, including their poor targeting capability, very short retention time at the site of disease, rapid clearance rates, and systemic side effects, among others. Thus, novel drugs that provide better

Wentao Zhang

Wentao Zhang received his PhD degree from Chinese PLA General Hospital, Chinese PLA Medical School. He is currently a distinguished professor in The Eighth Affiliated Hospital, Sun Yat-Sen University. His research focuses on the fields of sports medicine and rehabilitation.

Renzhi Wang

Renzhi Wang received his PhD degree from PhD in Neurosurgery, Kitasato University Hospital, Japan, and he joined Peking Union Medical College Hospital, Peking Union Medical College and Chinese Academy of Medical Sciences in 1989. He is currently a distinguished professor and chief physician in The Chinese University of Hong Kong, Shenzhen. His research focuses on the fields of treatment of head and neck diseases.

Gary Guishan Xiao

Gary Guishan Xiao received his PhD degree from the Institute of Biophysics, the Chinese Academy of Sciences in 1995. He conducted his postdoctoral research at the UT MED CTR in 1995–1998. He Joined Dalian University of Technology in 2014, where he is currently a professor in the State Key Laboratory of Fine Chemicals, Department of Pharmacology, School of Chemical Engineering. His research focuses on the cancer metabolism and precision medicine, tumor molecular diagnosis and small molecule drug therapy, and the malignant tumor pathogenesis and drug resistance mechanism.

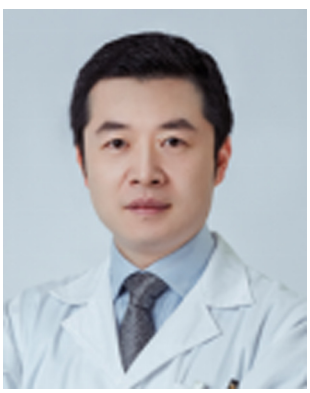

Zihuang Li

Zihuang Li received his PhD degree from Southern Medical University. He is currently a distinguished professor and senior doctor in Shenzhen People's Hospital (The Second Clinical Medical College, Jinan University, The First Affiliated Hospital, Southern University of Science and Technology). His research focuses on the fields of radiosensitization strategies based on AIEgens.

therapeutic outcomes are a key pursuit in clinical practices. Fortunately, with the development of multiple disciplines, including biology, medicine, chemistry, and physics, bio-nanomedicines that have many advantages over small molecule drugs have been developed and also innovated the ways of drug delivery. For example, Doxil received the approval from the US Food and Drug Administration (FDA) for the treatment of advanced ovarian cancer, multiple myeloma, and HIV-associated Kaposi's sarcoma. Since then, bio-nanomedicine has received much attention from the research community, and hundreds of nanomedicines are being explored in clinical trials while some have already been approved. In the past few decades, developments in multidisciplinary science have enabled the design and fabrication of many novel nanomaterials, which have been rapidly developed and applied to create therapeutic modalities in a range of diseases, these nanomaterials include colloidal gold, liposomes, graphene, two-dimensional nanomaterials, perovskites, hydrogels and so on. At the same time, owing to the evolution of clinical practices, the focus has shifted to more precise clinical management, including the detection, diagnosis, bioimaging, and bioimaging-guided therapeutics. This branch of precise treatment is called theranostics.

So far, the most popular agents for disease detection and imaging have been traditional fluorescent dyes or probes, these probes allow the real-time monitoring of biological processes in a non-invasive manner, and the colour and intensity of fluorescence provide the information of physiological alterations under pathological conditions. However, these aberrant biological molecules often in aggregated state, leading to aggregation-caused quenching (ACQ) of traditional fluorescent dyes or probes. As a result, they can only be used up to a certain range of concentrations, resulting in a reduction in their broader applications for disease detection and treatment. Moreover, these fluorescent dyes and probes cannot serve as effective therapeutic agents, in another word, the less totipotency of these detection and imaging fluorescent agents required more complicated and rational designs for the as-expected outcomes in the treatment of noncancerous diseases.

However, given the current scenario, nanomaterials with multifold potential in detection, diagnosis, bioimaging and bioimaging-guided therapeutics appear to be necessary tools in bio-nanomedicine and warrant further clinical exploration. In 2001, Prof. Ben Zhong Tang discovered the aggregation-induced emission (AIE) effect that was opposed to the ACQ

Xianming Li

Xianming Li received his PhD degree from Soochow University. He is currently a distinguished professor and senior doctor in Shenzhen People's Hospital (The Second Clinical Medical College, Jinan University, The First Affiliated Hospital, Southern University of Science and Technology). His research focuses on the fields of radiosensitization strategies based on AIEgens.

Meili Chen

Meili Chen received her MD degree from Yichun University in 2012. At present, she is currently an associate chief physician in Shenzhen People's Hospital. Her research focuses on the intelligent designation and biological applications of chemotherapy in head and neck diseases.

Juyoung Yoon

Juyoung Yoon received his BS degree from Seoul National University in Korea (1987) and his PhD from The Ohio State University. Then, he joined the faculty at Silla University in 1998. In 2002, he moved to Ewha Womans University, where he is currently a professor in the Department of Chemistry and Nano Science. He is a Fellow of the Korean Academy of Science and Technology, a Fellow of the Royal Society of Chemistry and a Distinguished Professor of Ewha Womans University. His research interests include the development of fluorescent probes, activatable photosensitizers, and new organic functional materials.

Ben Zhong Tang

Ben Zhong Tang received his PhD degree from Kyoto University in 1988. He conducted his postdoctoral research at the University of Toronto in 1989?1994. He joined HKUST in 1994 and was promoted to Chair Professor in 2008 and Stephen K. C. Cheong Professor of Science in 2013. He was elected to the Chinese Academy of Sciences in 2009. In 2021, he joined the Chinese University of Hong Kong, Shenzhen. In 2001, he coined the concept of aggregation-induced emission (AIE). His research interests include the exploration of new advanced materials, new luminescence processes and new polymerization reactions.

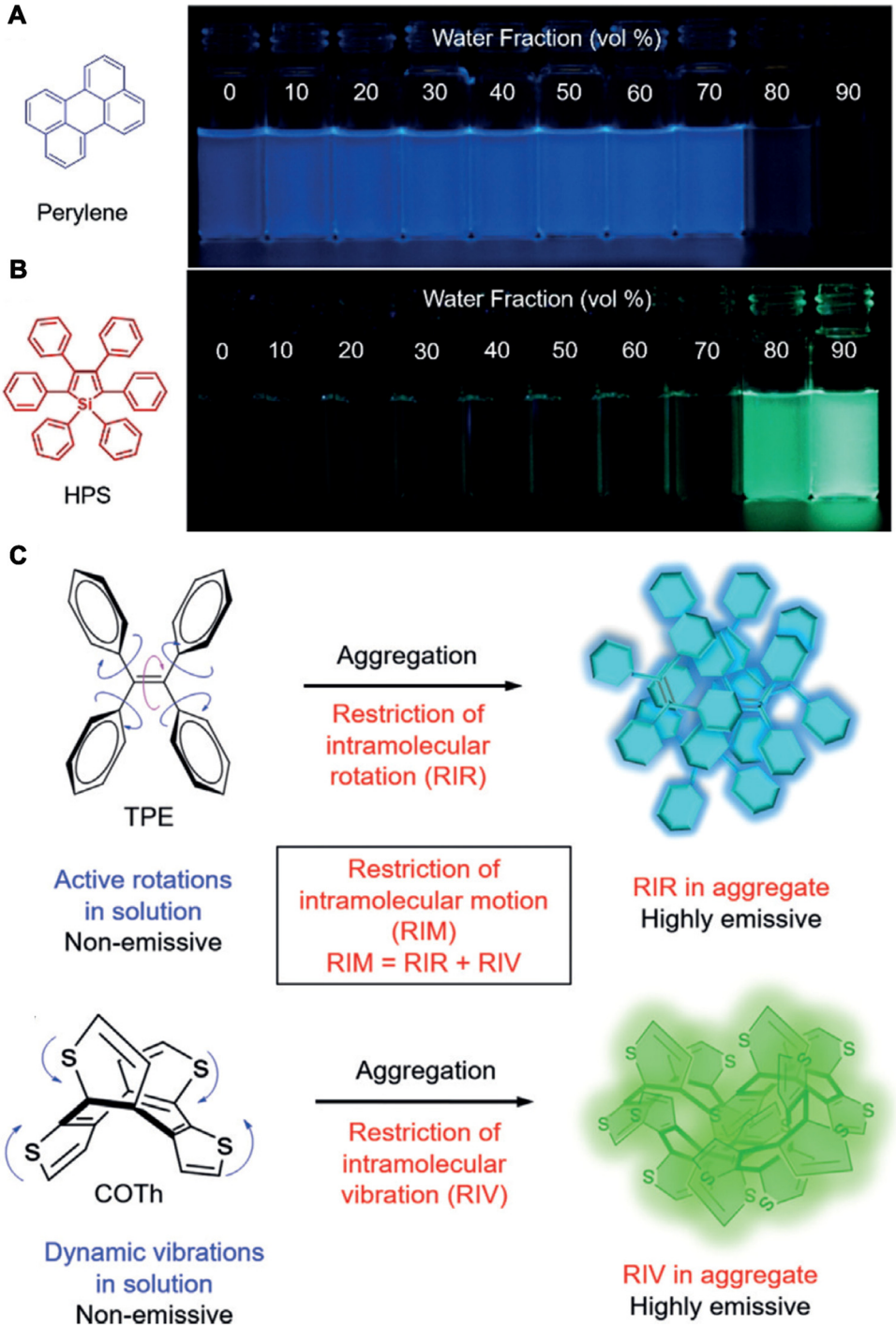

Fig. 1 Molecular mechanism of AIEgens. (A) Molecular structures and photographs of a typical ACQ molecule (perylene) and (B) an AIE molecule (hexaphenylsilole, HPS). (C) Schematic of the AIE mechanism of the restriction of intramolecular motion (RIM). Adapted with permission from ref. 14. Copyright 2020 Wiley-VCH Verlag GmbH & Co. KGaA, Weinheim.

effects—in molecules called AIE luminogens (AIEgens) (Fig. 1A and B).[13,14] Unlike other molecules, AIEgens show no light emission when present as individual molecules, when present in concentrated solution or solid states, resulting from reduced intramolecular motions (RIMs), and prevent radiative decay while enhancing nonradiative decay, which induces significant changes of the perception towards conventionally used photophysical phenomena of the scientific community and displays significant suppression of harmful π–π stacking in the limited space of nanoparticles (Fig. 1C).[14] Thus, AIEgens have been proven to be more advantageous than traditional fluorescent probes.[15]

Over the past 20 years, countless studies have proved that AIEgens possess high photostability, large Stokes shifts, high

signal-to-noise ratios (SNRs), high quantum yields (QYs), tunable emission properties and excellent biocompatibility. More importantly, they do not exhibit any ACQ effects.[16] Following the discovery of AIEgens, their applications as novel disease therapeutic agents have expanded, and industrial and other smart applications have expanded rapidly.[17–21] Importantly, AIEgens can be generated using chemical synthesis or be obtained from natural products, and they thus show high biosafety and biocompatibility.[22,23] Moreover, a database, named ASBase of AIEgens, has been built for public.[24] Recently, AIEgens have also been proven to be developed with a particular shape.[25] Until now, a variety of AIEgens have been synthesized and applied for the detection, diagnosis, bioimaging, and bioimaging-guided therapy of noncancerous diseases upon rational designs and functionalized strategies.[26–28] However, although several studies and reviews have focused on the AIEgen-based intelligent detection, imaging, or therapy of cancer,[26,29–32] a broad review of their value in noncancerous diseases has so far been lacking.[33–37]

In this review, we provide a comprehensive account of the detection, diagnosis, bioimaging and bioimaging-guided treatment of noncancerous diseases based on AIEgens (Scheme 1). This review is divided into four sections based on the classification of noncancerous diseases. AIEgen-based operation mechanisms and their rational design for detection and diagnosis are introduced first, followed by bioimaging application and the evaluation of pathological alterations in noncancerous diseases. Subsequently, the bioimaging-guided therapies for noncancerous diseases with various therapeutic modalities are demonstrated. In every section, the advantages and discussion are further elaborated based on the relevant applications. Finally, future outlooks and expected hurdles in this field of AIEgens are highlighted. Understanding and appropriately applying AIEgens could open up endless opportunities for diagnostic and disease management and promote the development of other kinds of bionanomedicines. This review seeks to offer fresh insights into the development of novel AIEgen-based multimodal therapeutic platforms for modern clinical applications.

2. Smart AIEgens for noncancerous disease detection and diagnosis

At present, diseases are primarily named based on the WHO International Classification of Diseases, 11th version (ICD-11), in which the definite names of diseases arise from their etiology,

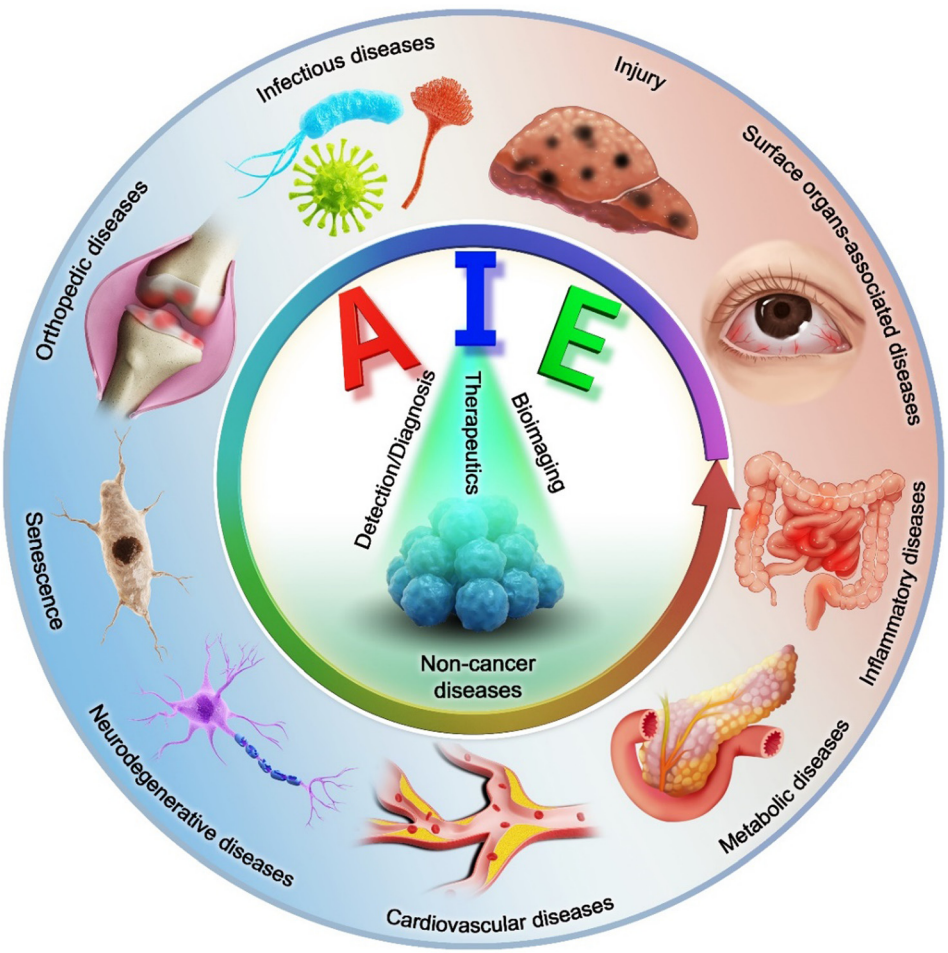

Scheme 1 The schematic diagram of noncancerous disease-targeting AIEgens.

pathology, parts of the body involved, clinical manifestations, *etc.* Therefore, there is a lack of unified criteria for disease classification. Here, in this review article, we classified noncancerous diseases into infectious diseases, wounds or injuries, metabolic diseases, CVDs, neurodegenerative diseases, orthopedic diseases, surface organ-associated diseases, inflammatory diseases, mental disorders, autoimmune diseases, and diseases of senescence. Each category contains a host of specific diseases.

During disease progression, there are biological alterations, including the changes in the phenotype and biological molecules. These alterations can thus be observed based on the identified biomarkers for the diagnosis and detection of certain diseases. In some cases, the biomarkers can also serve as therapeutic targets. For example, Alzheimer's disease (AD) is characterized by enhanced expression of the Tau protein and amyloid β-peptide, which is also the target for various therapeutic strategies.[38] Based on the current knowledge, detection and diagnosis not only help in diagnosing the diseases but also in monitoring the evaluation of disease courses and effectiveness of treatment. Thus, sensitive and specific tools for that are convenient to use and with high accuracy are urgently warranted for detection and diagnosis. Generally, the methods of disease detection and diagnosis involve the biopsy, imaging, and their combination. So far, fluorescent probes have been the most frequently used agents for disease diagnosis due to their high compatibility and ability to provide information on pathological processes instantly and non-invasively. However, owing to a poor SNR caused by high background signals, the sensitivity of fluorescent probes is still far from expectation. Moreover, the fluorescence is not present for a long-term, and when used in high concentrations, the probes exhibit light-off effects, thus not providing any target information. The previous described advantages of AIEgens have sparked a promise for applications in disease detection and diagnosis.[29,32,39,40] Moreover, AIEgens show no emission as single molecules and instead show strong emissions following aggregation, which guarantees a higher resistance to photobleaching and better photostability, higher signal reliability and low background signals. Thus, they can be used as ''light-up'' molecules for disease detection and diagnosis according to the alteration of their biological contents and reflected by the colour and intensity of fluorescence. Meanwhile, cationic and anionic AIEgens can identify the target molecules or cells with excellent selectivity and long term supervision upon rational design.[41–45] Furthermore, the light-up AIEgen probes are more attractive for the monitoring of biological alterations due to their wash-free operations.[46,47] Therefore, in this section, we summarize the detection and diagnosis of various noncancerous diseases using smart AIEgens.

2.1 Infectious disease detection and diagnosis

Infectious diseases, including malaria, pestis, severe acute respiratory syndrome (SARS), smallpox, dengue, H1N1 influenza, Middle East respiratory syndrome, Ebola, coronavirus disease 2019 (COVID-19), monkeypox and so on, are critical threats to populations of all ages.[48–50] Several factors have promoted the emergence of neo-pathogenic microorganisms and the re-emergence of infections. Infectious agents strongly inhibit the biological immune system, reducing the anti-infection capacity of the body and inducing a cascade of symptoms or even death,[51] which has created a great threat to human life and caused great losses owing to their rapid spread and high severity and several of these diseases have caused global social and economic disruptions.[52] Generally, most infectious diseases are caused by pathogenic microorganisms and viruses. Although effective strategies exist for curing the diseases, including drug treatment, actions that mitigate the spread of infection (for example, by cutting off the spreading route or transmission) are the most effective methods for nipping the infectious diseases in the bud. These steps are retrospective, however, and cannot prevent the deterioration at an early stage. In infectious diseases, the symptoms are non-isotropic and include the degeneration and necrosis of infected cells, formation of virions, exudative reactions, hemorrhagic lesisons, and increases in cytokine levels. Unfortunately, clear biomarkers and efficacious strategies for the early diagnosis and detection of infectious diseases are currently unavailable. To date, many methods and tools have been developed for the diagnosis and detection of pathogenic microorganisms causing specific infectious diseases,[53–56] these include bacterial culture, polymerase chain reaction (PCR), gene microarray, high-throughput sequencing (HTS), target-specific immunoassays, *etc.*[57,58] However, unfortunately, these methods are not very accurate, time-consuming and expensive. Up to now, the detection and diagnosis of infectious diseases have been the hottest fields of the AIEgen-based science community.[33,59]

2.1.1 Bacterial disease detection and diagnosis. Due to the abundant diversity of bacteria, the precise detection and diagnosis of bacteria are crucial and important in infectious diseases of many fields involved in clinics, food safety and so on. As mentioned above, fluorescent probes is an effective alternative method for the detection and diagnosis of bacterial diseases. With the advantages such as fast responses, superior sensitivity and simplicity, fluorescent probes are promising tools for pathogen detection and disease diagnosis. For instance, Xing and colleagues constructed a unique dual wavelength NIR cyanine-dyad molecular probe (HCy5-Cy7) for detecting bacterial infections since the infection is characterized by an increase in the content of reactive oxygen and nitrogen species (RONS), which leads to fluorescence at 660 nm due to the oxidation of the reduced HCy5 moiety to Cy5. Moreover, peroxynitrite ($ONOO^-$) and hypochlorous species (HClO) degraded Cy7 to turn on fluorescence emission at 800 nm.[60] However, similar to other fluorescent probes, this probe also suffers from key drawbacks such as the ACQ effects and the short wavelength that does not allow the examination of deeper tissues. Under these circumstances, AIEgens offer overwhelming advantages over traditional fluorescent probes owing to their high photostability, sensitivity, and selectivity in the detection of infections caused by pathogenic microorganisms, including bacteria, fungi and viruses.[33,61–65] Thus, the rapid detection and quantification of various bacteria are vital in many fields. To achieve this goal, Tang and Wu developed a series of sensor arrays based on tetraphenylethylene (TPE) derivatives. Each sensor array comprised three TPE-based AIEgens bearing a

cationic ammonium group and different hydrophobic substitutions to provide tunable log *P* (*n*-octanol/water partition coefficient) values, which ensured the different multivalent interactions with different pathogens and specific fluorescence signals (Fig. 2A). In the sensor array, seven TPE-ARs (TPE-AMe, TPE-AEt, TPE-APrA, TPE-ABu, TPE-ACH, TPE-ABn and TPE-AHex) were synthesized that showed a typical absorption peak at 313 or 314 nm and a typical emission at 476 nm. When these TPE-ARs were applied to seven targeted pathogen microorganisms, *S. aureus*, penicillin-resistant *S. aureus* (*S. aureus*^{R}), *E. faecalis*, *E. coli*, ampicillin-resistant *E. coli* (*E. coli*^{R}), *P. aeruginosa* and *C. albicans*, the TPE-Ars exhibited obvious changes of fluorescence intensity and fluorescence response speed due to the diverse self-assembly behavior of TPE-Ars that enriches the interactions of TPE-ARs with pathogens (*ClogP* values: 3.426 to 6.071), but only a little change on the maximum emission wavelength (Fig. 2B). Based on the diverse responses, the as-prepared seven TPE-ARs given 17 combinations that were constructed for sensor arrays and analyzed using the linear discriminant analysis (LDA), in which the fluorescence pattern of pathogens was transformed to a 2D canonical score (Fig. 2C). Furthermore, to enhance the compromised sensitivity and accuracy of TPE-ARs, three groups of different hydrophobilities were introduced to AIEgens for fabricating the competent sensor arrays that included TPE-AMe, TPE-ABn and TPE-AHex; TPE-AEt, TPE-ACH and TPE-ABn; and TPE-ACH, TPE-ABn and TPE-AHex, which augmented the diversity in the fluorescence response patterns to the high detection accuracy, even in a blends of pathogens (Fig. 2D). Collectively, the sensor arrays were capable to identify different kinds of pathogens with almost 100% accuracy and it also showed a rapid response (about 0.5 h), had a high-throughput nature, and was easy-to-operate without requiring interspersed washes.[40] In another study, based on the specific protein expression found in microorganisms, Ding *et al.* conjugated an AIEgen called AIE-DCM with Gram-negative bacterium-targeting peptides (polymyxinB) to obtain AIE-DCM-2polymyxinB. In this model, the polymyxinB bound to lipopolysaccharide (LPS) specifically enabled the selective and sensitive detection of Gram-negative bacteria.[66] Similarly, the other AIEgens also showed high efficacy as visual tools for detecting between live and dead bacteria as part of long-term bacterial detection assay based on the alteration of membrane permeability.[67,68] Metabolic biomolecular labelling technology in which synthetic sugars or amino acids are used to add chemical functional groups to cell membranes and enable the further conjugation of fluorescent dyes or drugs has become powerful tools for bacterial detection and precision therapy *in vivo*.[69] However, the lack of extreme specificity of delivering of these moieties to targeted cells hinders the improvement of outcomes. For addressing these obstacles, Liu and Kong developed a new bacterial metabolic labelling method using AIEgens (Fig. 3A–C),[70] wherein 3-azido-d-alanine (d-AzAla) was delivered with the help of MIL-100 (Fe) nanoparticles (NPs) by a simple absorbing process that was sensitive to a high H_2O_2 inflammatory environment. In these NPs, the d-AzAla was incorporated selectively into polymer Pluronic F-127 to form d-AzAla@MIL-100 (Fe) NPs that improve the dispersity of MOFs under physiological conditions. With the contribution of the EPR effect, the d-AzAla@MIL-100 (Fe) NPs preferentially accumulated within the infected region, where the frameworks of MIL-100 (Fe) were damaged by H_2O_2 to release d-AzAla that was specifically taken up by the bacteria. During the process, an ultrasmall AIEgen named US-TPETM NPs (2-(1-(5-(4-(1,2,2-tris(4-methoxyphenyl)vinyl)phenyl)thiophen-2-yl)ethylidene)malononitrile was adopted as the labelling reagent, where

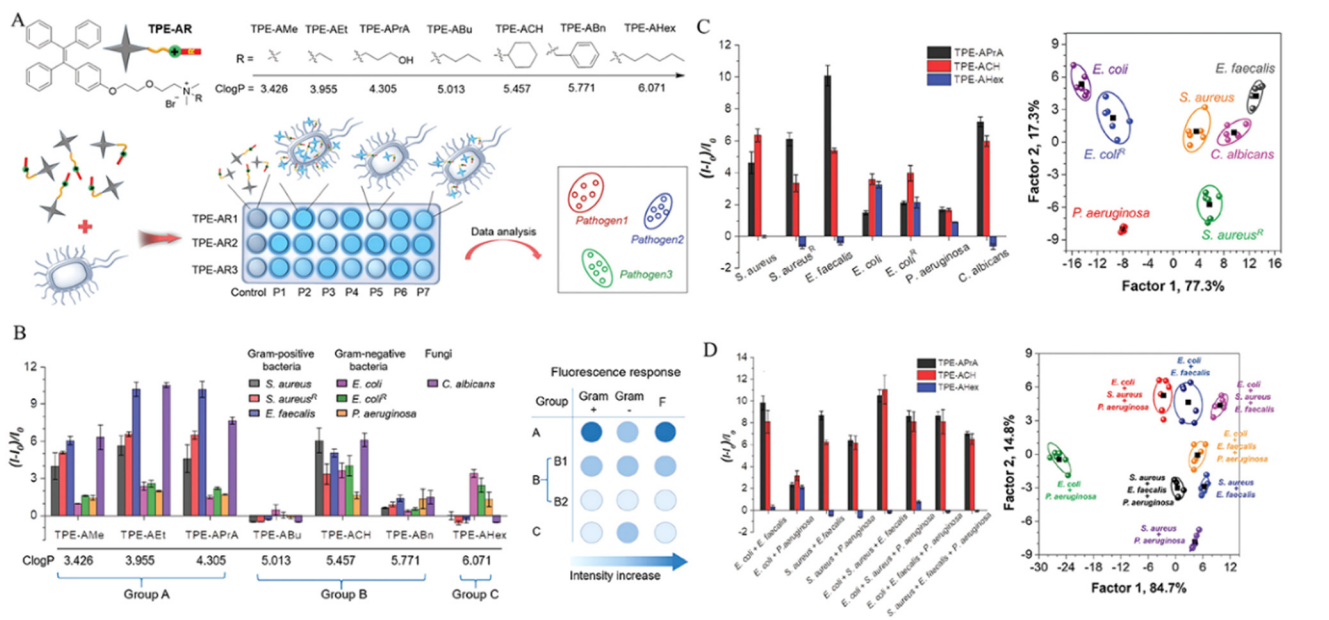

Fig. 2 Diagnosis of pathogenic microorganism with an AIEgen sensor array. (A) Structure of TPE-ARs and diagram of a sensor array. (B) Fluorescence responses to microbes (left) and the grouping criterion (right). (C) Fluorescence response patterns to microbes and canonical score plots. (D) Fluorescence response patterns (left) and canonical score plots. Adapted with permission from ref. 40. Copyright 2018 Wiley-VCH Verlag GmbH & Co. KGaA, Weinheim.

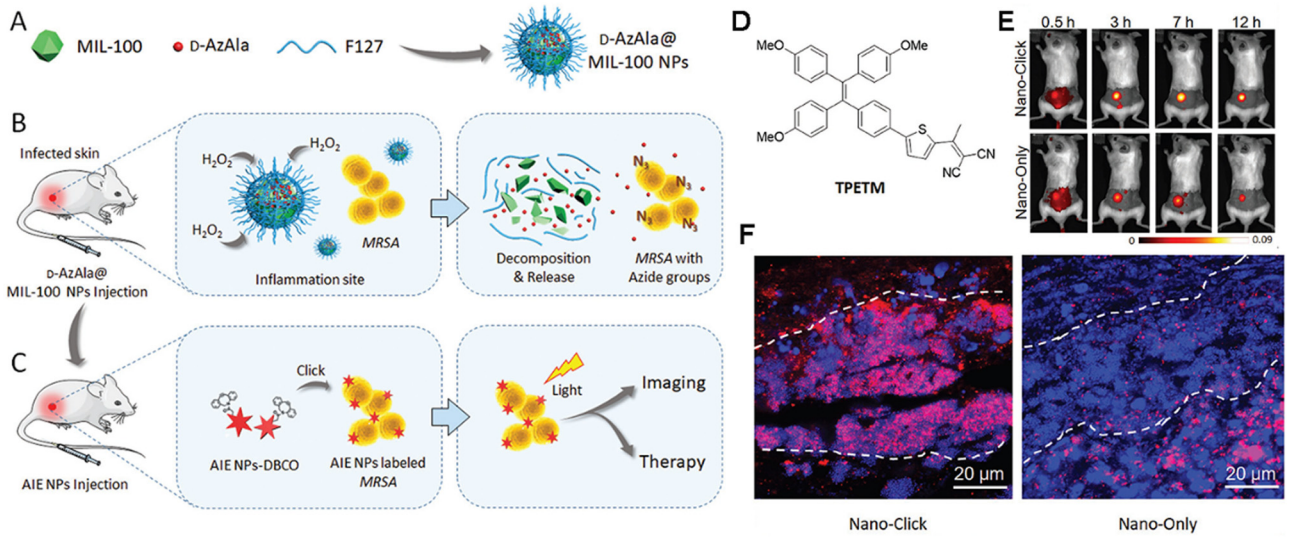

Fig. 3 Diagram of the proposed strategy. (A) Preparation of d-AzAla@MIL-100 (Fe) NPs. (B) Detection of bacteria internalized in the infected tissue. (C) Click reaction, specific tracking of bacteria. (D) Chemical structure of TPETM. E) The time-dependent *in vivo* fluorescence images. (F) The fluorescence images of the infected skin slices in (D). Adapted with permission from ref. 70. Copyright 2018 Wiley-VCH Verlag GmbH & Co. KGaA, Weinheim.

DBCO-DSPE-PEG$_{2000}$ formed an outer shell and promoted the accumulation around bacteria, where the clickable dibenzocyclooctyne-modified AIEgen (US-TPETM) anchored to the bacterial cell walls precisely and selectively by click reaction for bacterial detection (Fig. 3D–F).[70]

2.1.2 Fungal disease detection and diagnosis. Fungi, another main source of infectious diseases as bacteria, can cause diseases similar to bacterial infections.[50,71] More worryingly, the resistance to therapeutic drugs has become more serious due to the abuse of drugs.[72] Hence, effective detection of fungi is important not only in biomedicine but also in other fields. Early detection of fungi enables the eradication of these infections at an early stage. So far, many AIEgens have been synthesized for fungal detection.[73–76] For instance, Tang *et al.* synthesized a microenvironment-sensitive AIEgen named IQ-Cm through Suzuki coupling and a one-pot multiple component reaction (Fig. 4A–C), for the visual discrimination of Gram-negative bacteria, Gram-positive bacteria, and fungi by the naked-eye (Fig. 4D).[73] IQ-Cm had a twisted donor–acceptor and extended donor–π–acceptor (D–π–A) structure, retained its twisted intramolecular charge transfer (TICT) and AIE properties, while showed a sensitive fluorescence colour response to a pathogen-related microenvironment. IQ-Cm conjugated with a cationic isoquinolinium moiety and a membrane-active coumarin unit can selectively accumulate in three different regions in different types of microorganisms, providing different emission colours that can be discerned by the naked-eye. While IQ-Cm was suspended in the solution from dioxane to water, the emission colour of solution changed from blue (469 nm) to red (625 nm), and the three pathogens showed weak auto-fluorescence and induced a variation of emission intensity of IQ-Cm following the order of *C. albicans* > *S. aureus* > *E. coli*. In detail, *C. albicans* caused a large blue-shift from 650 nm to 575 nm and *S. aureus* caused a smaller blue shift to 610 nm (Fig. 4D–F), where the variation of emission intensity was attributed to the diverse interactions of three pathogens and different surrounding microenvironments. More, the IQ-Cm can also detect the pathogens from urine sample, persimmon, tomato, orange and bread in naked-eye observation (Fig. 4G–J).[73] Thus, the IQ-Cm can be applied for rapid fungal pathogen detection and point-of-care diagnosis *via* a simple visualization strategy based on one single AIEgen.

2.1.3 Viral disease detection and diagnosis. The high propagation speed, severity and mortality of viruses could lead to the crisis around the world, for instance, innumberable people have suffered due to the outbreak of COVID-19 since 2019.[77] The disease caused by COVID-19 is similar to other viruses that produce serious infectious diseases. Therefore, there is an urgent requirement to develop sensitive and accurate detection methods or tools to detect this virus and prevent further public health issues. Currently, PCR based on fluorescent probes is still the mainstream method for virus detection in clinical setting in the context of daily nucleic acid testing. As a booming and effective diagnostic tool, AIEgens are promising alternatives for ultrasensitive viral detection.[78–81] Li and colleagues developed a simple, rapid, and sensitive serological diagnostic protocol using AIEgen nanoparticles (AIE$_{810}$NPs, λ_{em} = 810 nm) in a lateral flow immunoassay, they used this assay for the early detection of immunoglobulin M (IgM) and immunoglobulin G (IgG) against SARS-CoV-2 in clinical serum samples. In the flow immunoassay, to avoid the interference caused by autofluorescence, an AIE dye with NIR emission, named BPBT, was selected as the fluorescent unit ($\Delta\lambda$ = 145 nm). Further, to further amplify the fluorescence signal, polystyrene (PS) nanoparticles of 300 nm size were loaded with a dye (AIE$_{810}$NP) (3.18×10^6) and used to label the detection ligand (Fig. 5). Under these conditions, the detection limit of this flow immunoassay was low with 0.236 and 0.125 μg mL^{-1} for IgM and IgG with high sensitivity (78 and 95%, respectively).

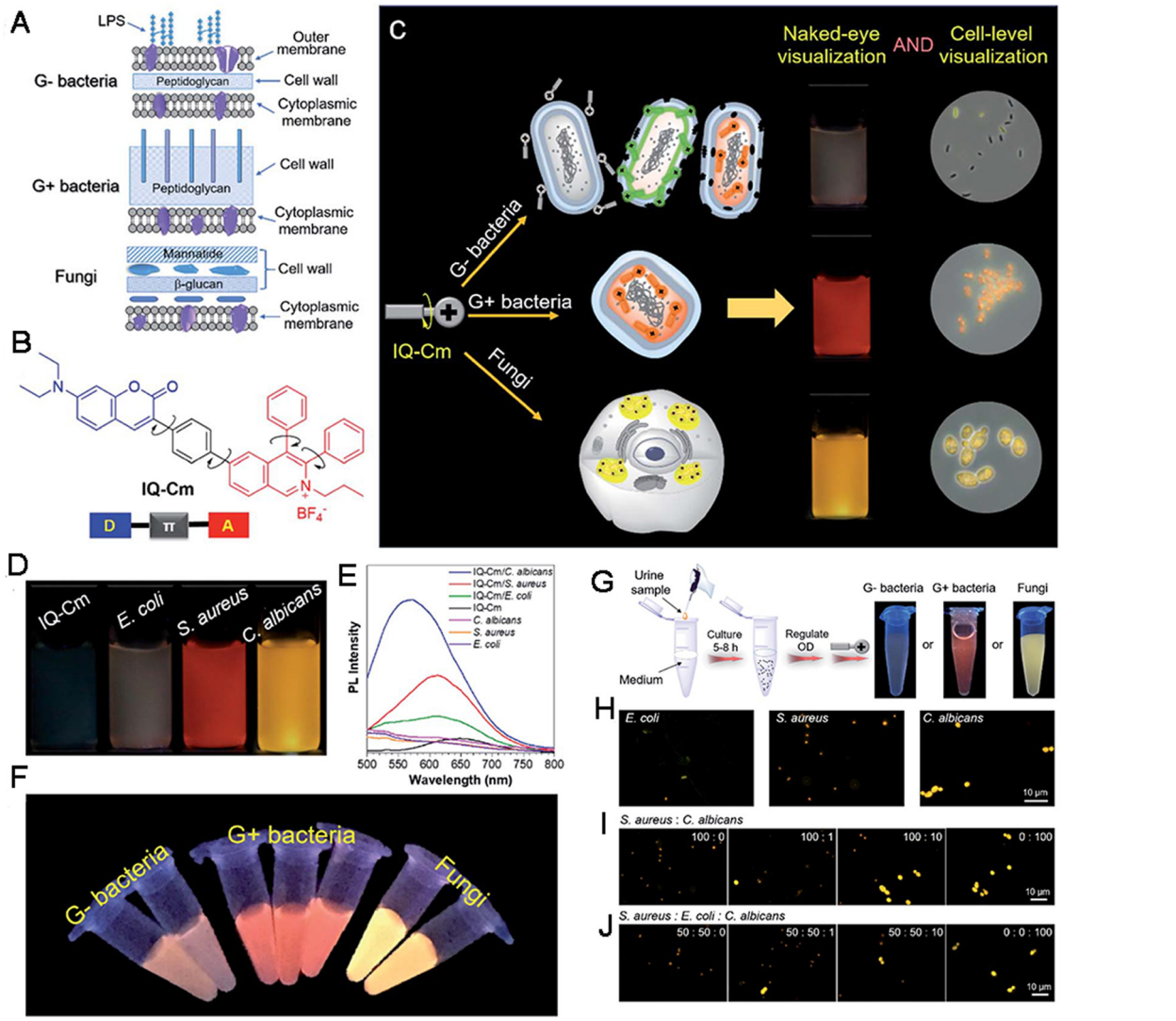

Fig. 4 (A) Schematic of cell envelope structures of Gram-negative bacteria, Gram-positive bacteria and fungi. (B) The chemical structure of IQ-Cm. (C) Diagram of IQ-Cm for visual discrimination of pathogens. (D) Photographs of IQ-Cm with different pathogens. (E) The Fluorescence spectra. (F) Photographs of IQ-Cm with different pathogens. (G) The procedures and results by naked-eye identification. (H) The fluorescence images of urine samples. (I and J) The fluorescence images of various samples with IQ-Cm. Adapted with permission from ref. 73. Copyright 2020 The Royal Society of Chemistry.

The performance was thus comparable to that of the enzyme-linked immunosorbent assay (ELISA) (detection limits of 0.040 and 0.039 μg mL^{-1} and sensitivity of 85% and 95%) and over AuNP-based test strip (41% and 85%). Importantly, the AIE_{810}NP-based test strip could detect IgM and IgG at 1–7 days after symptom onset, much before the AuNP-based test strip (8–15 days).[82] Overall, the AIE_{810}NP-based test strip was promising for the early detection of SARS-CoV-2 in clinical serum samples. A commercial 2019-nCoV Antigen Kit (AIE FICA) based on AIEgens was developed by Prof. Tang and its production was scaled up for routine COVID-19 testing. In another example, a multifunctional AIEgen (TPE-APP) was synthesized and served as an immunoassay platform for dual-modal detection of human enterovirus 71 (EV71 virus), H7N9 virus and Zika virus with high specificity and extreme low detection limit by simply changing the conjugated antibodies.[81]

Collectively, compared to conventional fluorescent probes, AIEgens show great advantages in detecting and diagnosing infectious diseases, including bacterial, fungal and viral infections. The advantages are as follows: (i) high SNR, sensitivity, rapid response speed and low detection limit; (ii) simple auxiliary tools for rapid and effective detection; and (iii) simple operation processes. Meanwhile, more rational designing is encouraged for infectious disease detection in order to achieve early-stage detection and infection control.

2.2 Metabolic disease detection and diagnosis

In biological cells, tissues and organs, metabolism always plays a fundamental role in supplying energy for each activity, including signal transduction, communication, proliferation, response to external stimuli, and so on. Therefore, there are significant differences in metabolic characteristics between

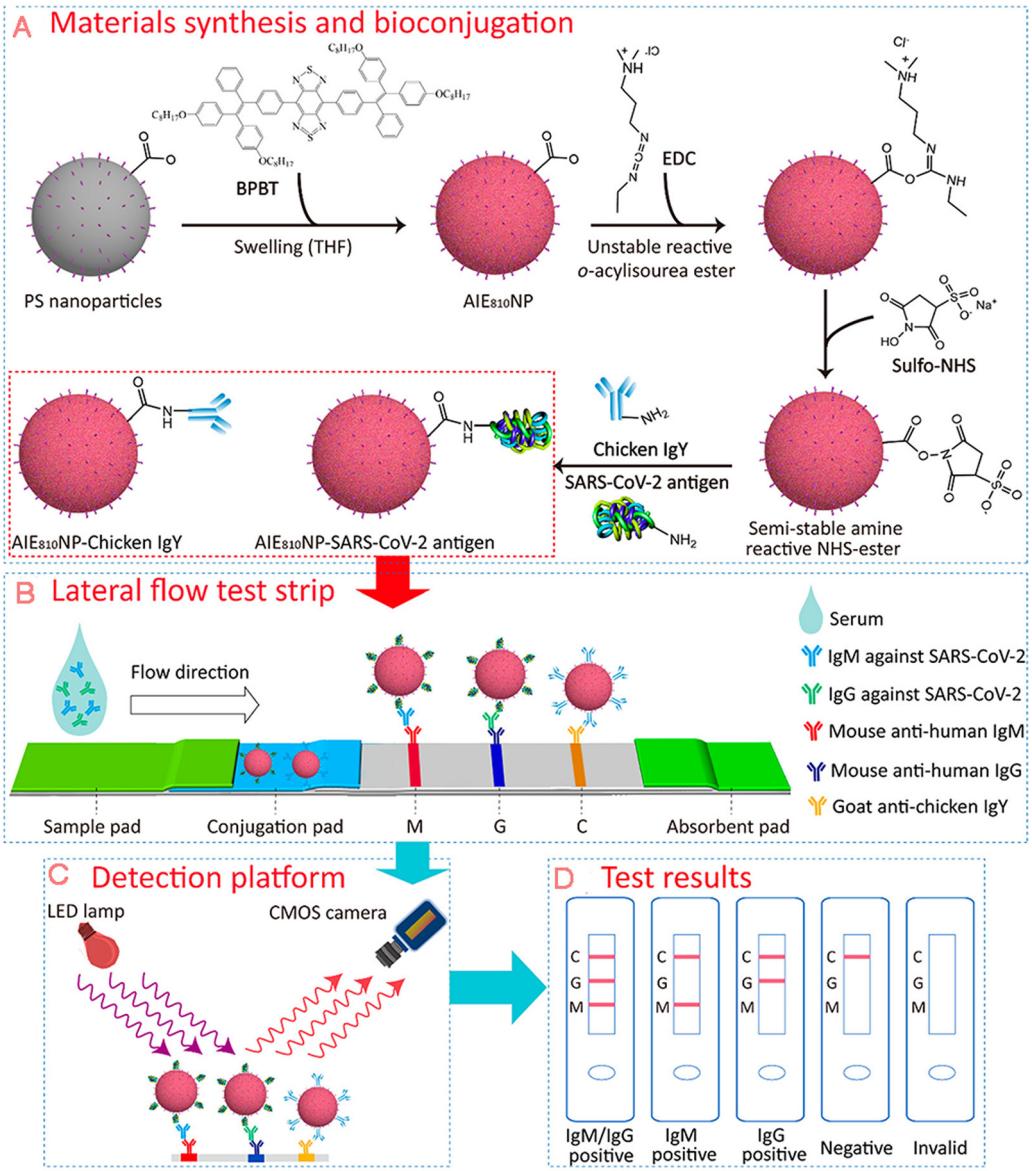

Fig. 5 Diagram of AIE nanoparticles-labelled lateral flow immunoassay for detection of virus. (A) Synthesis of AIE_{810}NPs and conjugation path of SARS-CoV-2 antigen and chicken IgY. (B) Schematic of test strip for the detection of IgM and IgG against SARS-CoV-2. (C) Schematic of the portable reader. (D) Interpretation of different test results. Adapted with permission from ref. 82. Copyright 2021 American Chemical Society.

normal and diseased states.[83] Moreover, metabolic imbalances can also induce various diseases.[84] In general, metabolic diseases include diabetes, gout, osteoporosis, fatty liver, vitamin D deficiency, hyperlipidemia, protein-capacity malnutrition, and so on. All of these are disorders involving an imbalance in cellular metabolism. However, the unclear molecular mechanisms have resulted in a lack of effective diagnostic and therapeutic target for metabolic diseases. For example, type 2 diabetes mellitus (T2DM) is one of the most common metabolic disorders across the world, it has two primary etiologies: (i) the impaired secretion of insulin from pancreatic β-cells and (ii) the resistance of normally insulin-sensitive tissues to insulin followed by a lack of appropriate responses to insulin stimuli. Hence, the release and action of insulin are essential for regulating the glucose homeostasis. Thus, insulin and glucose levels are important indicators of T2DM and the diagnosis could help in reducing the risks of diabetes comorbidities and enable individuals in maintaining the quality of life, while avoiding costly and lethal late-stage diabetic complications. Currently, the targeting of metabolic factors involved in metabolic diseases has been a hotspot in several studies.[85] The development of detection technologies has been re-evaluated in the past years, the methods to detect metabolic diseases include immunofluorescence staining, fluorescence sensing with small molecules, electrochemical sensors, ELISA, radioimmunoassays, mass spectrometry, chromatography techniques, and so on. Of these, the first two involve the use of fluorescent probes and are believed to be more sensitive, non-invasive and simple to perform compared

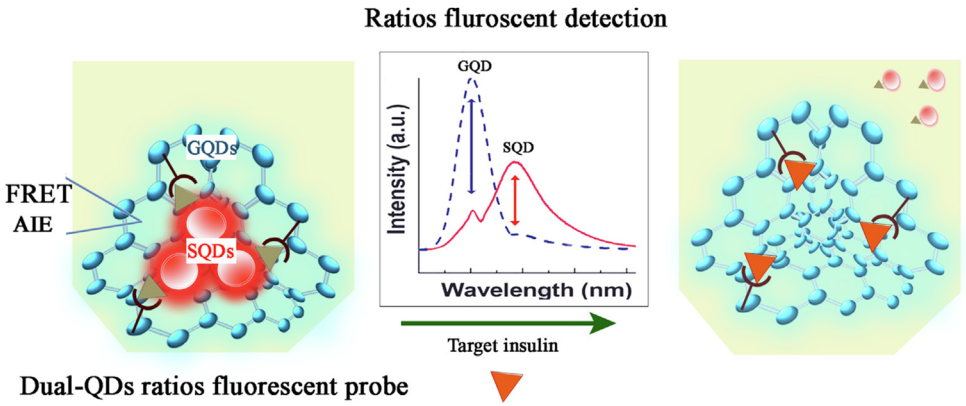

Fig. 6 The sensing mechanism of the dual-QDs ratios fluorescent probe. Adapted with permission from ref. 93. Copyright 2021 Elsevier B.V.

with other methods,[86,87] which leads to the evaluations of changes in fluorescence colour and intensity are the most effective methods for detecting the content alteration of metabolic diseases. However, as mentioned previously, the detection and diagnosis achieved based on fluorescent probes remain still far below expectations, especially at the extremely early stages of diseases with low concentration and sensitivity. Hence, better methods with higher accuracy and convenience are needed.

In the past few decades, the approaches for the detection and diagnosis of metabolic disease detection have become an attractive topic of the research. With the development of AIEgens and their biomedical applications, AIEgens have been proven to be an effective tool for the detection and diagnosis of metabolic diseases.[88–92] For example, Sai *et al.* constructed a dual-QDs ratiometric fluorescent probe by modifying immune-functionalized graphene quantum dots (GQDs) and semiconductor quantum dots (SQDs) such that they emitted blue and red emissions, respectively. In this system, the dynamic equilibrium of Förster resonance energy transfer (FRET) and AIEgen within the probe promoted the emission of special dual fluorescent light after exposure to insulin. Insulin promoted the cleavage of the probe, when the dual fluorescent light was altered according to the concentration of insulin such that GQD owned a bluer emission (450 nm, QY of 6.7%) and SQD owned a redder emission (625 nm, QY of 3.9%). As a result, the dual fluorescent light was altered according to the concentration of insulin. With this probe, an extremely low detection limit, as low as 0.045 ng mL^{-1} and rapid response time as short as 5 min were achieved, indicating that this method was superior to ELISA. Therefore, the dual-QDs system showed a great potential in the ratiometric sensing of insulin in biological samples (Fig. 6).[93] These excellent results suggested that AIEgens exhibit great advantages over traditional fluorescence methods.

Hyperlipidemia (HLP) is also a kind of metabolic disease that is characterized by the imbalance of various plasma lipids, it is typically caused by the altered contents and qualities of low-density lipoprotein (LDL) and high-density lipoprotein (HDL) cholesterol. The complicated plasma environment of HLP results in a high background interference and tests require large amounts of samples and are also cumbersome. Hence, practical *in vivo* detection for HLP has many disadvantages. To solve these problems, Tang *et al.* prepared a series of "smart aggregates", which was made up of AIEgens named SQBTTPE, SQBT-TPA and SQBT-DMA, for the early diagnosis of HLP. This approach was targeted at the alteration of LDL/HDL levels and ratios. All of these AIEgens had a typical D–A molecular structure that conferred both AIE and TICT effects and allowed accurate HLP detection. Notably, the AIEgens exhibited NIR-II and NIR-III luminescence with ultra-large Stokes shifts (>950 nm). In particular, the PL spectra of SQBTDMA were observed as far as 2100 nm with a high QY of 20%. Importantly, there was an exceptional linear association between fluorescence intensities and HLP-related pathological parameters and the testing of blood samples revealed high accuracy of SQBTDMA (96%).[94] Hence, AIEgens can collectively promote the rapid and convenient diagnosis of HLP.

So far, effective methods for the detection and diagnosis of metabolic diseases have remained far and few in between. However, AIEgens provide great promise in this field, AIEgen-based methods being less expensive and time-consuming than traditional methods. Hence, more endeavors should be dedicated to this area.

2.3 Cardiovascular disease detection and diagnosis

CVD is the largest and most lethal single contributor to global mortality,[95] it is also the leading cause of death in China accounting for 40% of the total deaths.[1,96] Due to the acute development of CVD, some necessary ambulance transports are often not acquired in time. As a result, the rates of CVD death have continuously and rapidly increased. In the classification of CVD, ischemic heart disease (IHD), hemorrhagic stroke (HS) and ischemic stroke (IS) are the three leading causes of CVD death. Meanwhile, other CVDs like rheumatic heart disease, hypertensive heart disease, myocarditis and myocardia disease, aortic aneurysm, and other circulatory diseases can also cause serious morbidity and mortality. Alarmingly, CVDs are related to other diseases, such as obesity and T2DM,[97] enhancing challenges of detection and prevention. However, early targeted treatment and prevention could be possible if populations at risk for CVDs are accurately identified. In the clinics,

electrocardiograms, ultrasonic cardiograms, coronary CT scans, coronary arteriography, *etc.*, are common methods for the diagnosis of CVDs. However, these previously mentioned methods are laborious and of low accuracy.

At present, the biopsy of biomarkers such as C-reactive protein (CRP), Lp-PLA2, and triglycerides with fluorescent probes capable of precise detection is the common approach for the detection of CVDs. Some other methods, including digital immunoassay technology[98] and computer-assisted technology,[99] have also been proved to be effective but still far away from expectation. Recently, AIEgens have shown great potentials in construction of advanced fluorescent bio-probes for CVD detection, diagnosis and disease theranostics. These potentials are linked to their high levels of fluorescence brightness, excellent photostability, low toxicity, and adaptability to a variety of biomedical tasks. Following incorporation into stimuli-responsive light-up probes and highly emissive fluorescent nanoparticles, AIEgen can help in detecting CVDs with a higher specificity and sensitivity than conventional probes.[100–103] For instance, atherosclerosis (ALS) is a type of CVD characterized by endothelial injury, progressive inflammation, and lipid deposition and can lead to the sudden occurrence of fatal plaque rupture, myocardial infarction, stroke, and even sudden death.[104] Under these conditions, Ding *et al.* developed a series of novel AIEgens (TPET-RO, TPE-T-RS and TPE-T-RCN), which were synthesized by McMurry reaction, Suzuki–Miyaura coupling reaction, and Knoevenagel condensation with high yields, by regulating the substituent of rhodamine for the early detection of atherosclerotic plaques and screening of anti-atherosclerosis drugs in a precise, sensitive, and rapid manner. These AIEgens had a typical D–π–A structure, In particular, twisted methoxy-substituted TPE served as the skeleton to obtain AIE properties and electron donor. Rhodamine derivatives with different substituents (O, S, or dicyanomethylene unit (CN)) served as the electron acceptor, respectively. Also, thiophene (T) was selected as both the second donor and for electronic π-conjugation to induce intramolecular charge transfer and increase conjugation length between the donor and acceptor. Among the prepared AIEgens, TPE-T-RCN showed the highest molar extinction coefficient (2.95×10^4 L mol^{-1} cm^{-1}), better charge transfer ability, the most largest PL QY (18.9%), and the absorption/emission spectra with the largest redshift (emission peak at 652 nm). Following encapsulation by DSPE-PEG_{2000}, the emission maxima of TPE-T-RCN NPs redshifted to 662 nm. Furthermore, after encapsulation by DSPE-PEG_{2000} and carboxyl-terminated DSPE-PEG_{2000}-COOH and surface functionalization with anti-CD47 antibody, TPE-T-RCN can bind to CD47 overexpressed cells in ALS plaques to efficiently recognize them at different stages peculiarly and rapidly. It can also recognize them at a very early stage (III) at which they cannot be detected clinically using CT nor MRI. These features indicated the value of using this AIEgen-based nanoprobe for monitoring the therapeutic effects of anti-ALS drugs during drug screening.[105]

Compared to conventional fluorescent probes, AIEgens have great advantages in the detection and diagnosis of CVDs, including: (i) high SNR, sensitivity and rapid response speed help in overcoming the background interference; (ii) NIR-II window wavelength, promotion of deep tissue penetration and visualization; (iii) feasibility of detection at the extremely early stage; and (iv) easy operation. Thus, one focus of the research on AIEgens should be their applications in CVD diagnosis.

2.4 Neurodegenerative disease detection and diagnosis

Neurodegenerative diseases are a type of deteriorative diseases and result from the gradual loss of the structure or function of neurons. They can be divided into acute neurodegenerative diseases, such as cerebral ischemia (CI), brain injury (BI), epilepsy, and chronic neurodegenerative diseases,[106] including Parkinson's disease (PD), AD, and Huntington's disease. Both types of neurodegenerative diseases seriously threaten the patient's quality of life. The occurrence of neurodegenerative diseases is associated with factors such as aging, stress, viral infections, genetic mutations, environmental effects, *etc.*[107] To date, the etiology of most neurodegenerative diseases is still unclear, and there is no effective method to cure them completely. During the progression of these diseases, the contents of some biomarkers, such as polyglutamine, FGF21, Tau protein, Lewy bodies, amyloid precursor protein, alpha-synuclein, TDP-43, and serum Vitamin D, are increased sharply.[108–111] Traditional diagnostic methods such as PET, CT, MRI, and biochemical assays,[112] used in clinical practice are expensive and time-intensive. On the contrary, fluorescent probes applied to detect or diagnose neurodegenerative diseases show high sensitivity and rapid response and are convenient to use.[113] Unfortunately, the application of conventional fluorescent dyes in the diagnosis of neurodegenerative diseases is limited by their ACQ effects, especially in cases of *in vivo* detection or diagnosis in deep tissues. Moreover, the blocking effect of the brain–blood barrier (BBB) and other biological barriers further inhibit the accumulation of fluorescent probes, lowering the final fluorescence intensity. Finally, given the structure of the brain, probes with a long wavelength near the NIR-II window are required. Thus, given their overwhelming advantages over traditional fluorescent probes, AIEgen probes are more suitable and effective for the detection and diagnosis of neurodegenerative diseases.[114–121] For instance, AD is a progressive neurodegenerative brain disorder and is considered to be untreatable.[122] The formation and accumulation of amyloid-β (Aβ) plaques in the brain are believed to be the primary pathological hallmark for the early diagnosis of AD. Commercial thioflavin derivatives (ThT or ThS) are the well-known gold standard probes for *in vitro* detection of amyloid fibrils *via* histological staining. However, problems such as the ACQ effect, background interference, and low SNR hinder improved detection outcomes, especially in cases of *in vivo* detection. Further, commercial probes are limited in their ability to detect oligomeric species. For the sensitive and effective detection of Aβ, Zhu *et al.* developed an NIR AIE-active probe (QM-FN-SO_3), this probe could map Aβ plaques and thereby detect AD upon a rational design strategy (Fig. 7A–C). In QM-FN-SO_3, a lipophilic π-conjugated thiophene-bridge for an extension to the NIR wavelength range and enhancement of BBB penetrability was introduced. The substituted position of the sulfonate group was tuned to achieve specific hydrophilicity and retained the "fluorescence-off" state

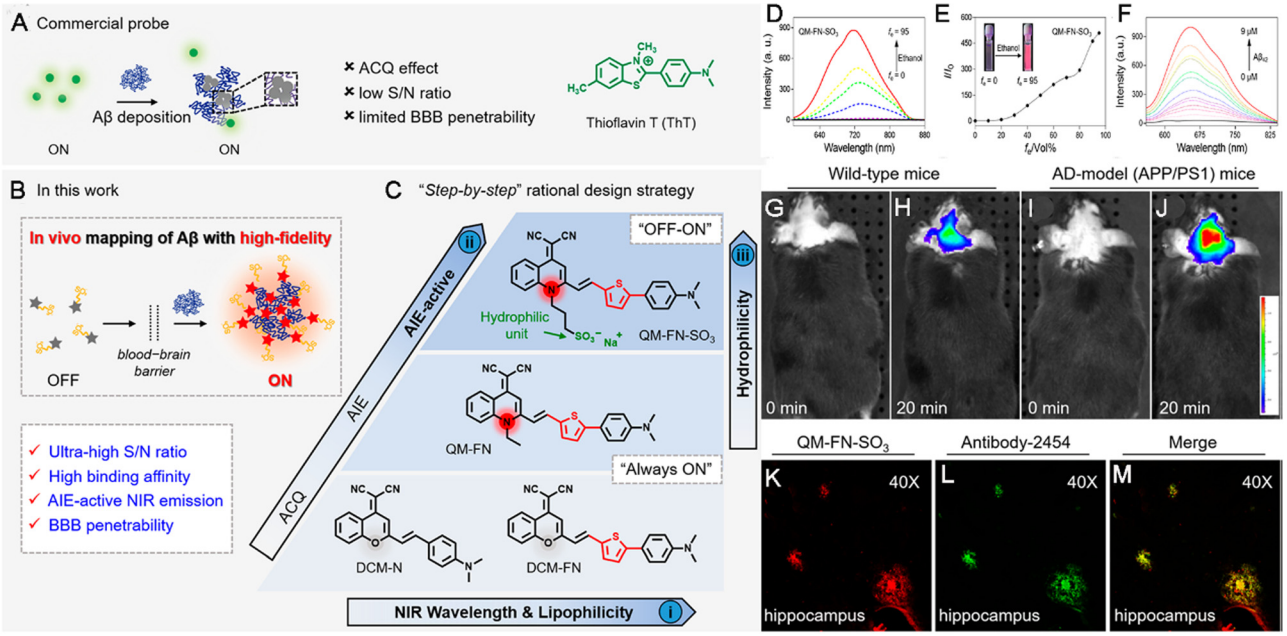

Fig. 7 Diagram of NIR AIE-active probes for Aβ deposition. (A) Commercial probe ThT. (B and C) The "step-by-step" strategy to address the defects of ThT and create ultrasensitive off–on NIR probes. (D) The emission spectra of QM-FN-SO_3. (E) Variations in I/I_0. (F) The fluorescence spectroscopic titration of QM-FNSO_3 by $Aβ_{42}$ aggregates. (G–J) *In vivo* mapping of Aβ deposition. (K–M) *Ex vivo* fluorescence of brain slices. Adapted with permission from ref. 123. Copyright 2019 American Chemical Society.

before binding to Aβ deposits. As a result, the QM-FN-SO_3 probe became non-emissive in aqueous solution and its NIR fluorescence at 720 nm continuously intensified until the volume fraction of ethanol was up to 95%, achieved excellent capability for mapping protein fibrillogenesis (Fig. 7D and E). When bound to $Aβ_{42}$ aggregates, QM-FN-SO_3 exhibited remarkable enhancement of fluorescence intensity-dependence on the concentration, where the conformational freedom and rotational restriction of the QM fluorophore of QM-FN-SO_3 were restricted after entering into the hydrophobic pockets and bound to the aggregated amyloid fibrils with the help of *N*,*N*′-dimethylamine (Fig. 7F). Also, QM-FN-SO_3 exhibited remarkably higher binding affinity and specificity to Aβ plaques to initiate the off–on response of fluorescence. The *in vitro* and *in vivo* examination indicated that the QM-FN-SO_3 can exhibit a big breakthrough in high-fidelity feedback on detection of Aβ plaques than the commercial probe ThT or ThS (Fig. 7G–M).[123]

Compared to commercial probes applied for the detection of neurodegenerative diseases, AIEgen probes show benefits as follows: (i) they can cross the BBB, enhancing targeted accumulation in the region of interest after rational design; (ii) they have a tunable wavelength that can be expanded to the NIR-II window, guaranteeing detection in deep tissues; and (iii) they allow the long-term monitoring of dynamic disease progression. More rational design strategies should be developed for the precise detection of neurodegenerative diseases and AIEgens can help in this regard.

2.5 Orthopedic disease detection and diagnosis

The skeletal system plays a fundamental role in supporting the basic shape and motion of the body and the different bones are connected by joints made up of constituents of various osteocytes.[124] In the past few decades, orthopedic diseases other than fracture, including cervical spondylosis, frozen shoulder, ankylosing spondylitis, lumbar disc herniation, femoral head necrosis, rheumatoid arthritis (RA), osteoarthritis (OA) and so on, have created a significant health burden and hindered social development. The incidence of these conditions have increased with increased rates of aging and obesity, both of which lead to long-term disability.[125] More concerningly, the lack of effective diagnostic indicators and therapeutic targets has resulted in a shortage of effective treatment modalities. Orthopedic diseases are classified as chronic degenerative joint disorders and inflammatory diseases caused by excessive ROS and inflammation.[126,127] Moreover, the diagnosis of orthopedic diseases is usually performed using bioimaging techniques, such as CT, MRI, radiography, and ultrasound.[128] When compared with *in vivo* bioimaging and ELISA, biopsy detection using fluorescent probes is more cost-friendly, rapid, and operationally simple. AIEgens are better candidates than conventional fluorescent probes in this regard. For example, for detecting the enhanced expression protein in OA in a sensitive and specific manner and facilitating early diagnosis and timely treatment, Bian, Tang and Li synthesized a new AIEgen named Cy–Py–N_3 for detecting OA based on the overexpressed matrix metallopeptidase 13 (MMP-13). An MMP-13-responsive probe (AIEgen–Pro–Leu–Gly–Val–Arg–Gly–Lys–Gly–Gly–Ac, or AIEgen–PLGVRGKGG–Ac) was synthesized *via* the "click chemistry" conjugation of an azide-functionalized AIEgen with an alkyne-functionalized MMP-13 sensitive peptide. This peptide was sensitive to MMP13 and cleaved by activated MMP-13, made the probe water-soluble and

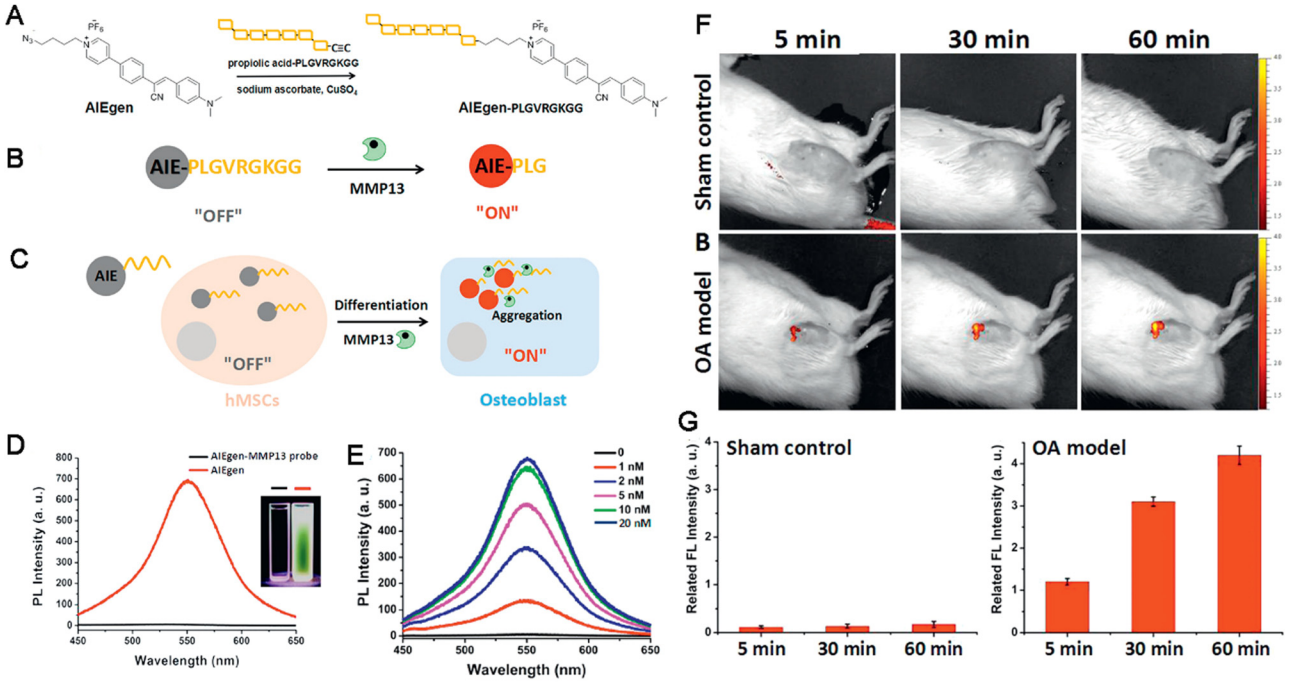

Fig. 8 (A–C) Diagram of the AIEgen-based probe for detection of the enhanced expression protein in OA. (D) The PL spectra, inset: photographs of AIEgen probe in DMSO/water under UV illumination. (E) The PL intensity of the AIEgen probe. (F and G) Detection of MMP-13 by the AIEgen probe *in vivo*. Adapted with permission from ref. 129. Copyright 2018 Wiley-VCH Verlag GmbH & Co. KGaA, Weinheim.

produced an off–on fluorescence (Fig. 8A–C). The AIEgen–PLGVRGKGG–Ac exhibited maximum emission at about 550 nm (Fig. 8D) and high sensitivity to MMP-13 with enhanced fluorescence intensity (Fig. 8E). When exposed to increased activity of MMP-13, promoting easy and semi-quantitative assessment of the extent of stem cell differentiation (hBMSCs). This probe also detected the activity of MMP-13 in osteoarthritic knee joints of living animals in real-time. Thus, AIEgen–PLGVRGKGG–Ac demonstrated the effective detection ability of the AIEgen for orthopedic diseases *in vitro* and *in vivo* (Fig. 8F and G).[129]

Up to now, although many elevated biomarkers, including proteins and cytokines, have been found to be elevated in orthopedic diseases,[130–132] key biomarkers for detection, diagnosis, and treatment are still lacking. Thus, there is an urgent need for collaboration across different fields for the better application of our current knowledge in the field of orthopedic diseases.

2.6 Inflammatory disease detection and diagnosis

Inflammatory responses constitute a reaction in which the body exerts autonomic defensive actions against various stimuli (inflammatory agents) in order to provide protection from adverse factors. The goal is to maintain homeostasis and the functional and structural integrity of the biological system. Inflammatory reactions are characterized by redness, swelling, heat, pain, and dysfunction and can occur due to various causes, such as infection (most common cause) and autoimmune regulation.[133] In general, slight inflammation is beneficial for the body. However, the excessive inflammation can induce a series of life-threatening conditions. Inflammation is usually accompanied by the elevated expression of inflammatory factors or cytokines, including TNF-α, IL-1β, IL-6, TGF-β and other small molecules; these cytokines are considered to be biomarkers of inflammatory diseases and are capable of inducing various biological cascades, including cytokine storms that become fatal to life. Thus, the detection of inflammatory diseases can allow interventions aimed at preventing further deterioration. At present, the diagnostic methods for inflammatory diseases include ELISA, PET, CT, MRI and so on. Although ELISA has the advantages of good specificity, moderate sensitivity ($\sim$510 pg mL^{-1}), and reliability, it also has disadvantages such as cumbersome and time-consuming operation, the requirement of large sample volumes, detection limits (endocrine inflammatory factors), and the lack of real-time, dynamical monitoring. Thus, a method with characteristics such as a rapid response rate, high accuracy and detection limit, convenient operation, and small volume requirement is needed. Based on previous studies and commercial applications, fluorescent probe-based detection appears to be the hotspot of interest.

As described previously, AIEgens exhibit great advantages in detection and diagnosis of inflammatory diseases.[134] Inflammatory bowel diseases (IBDs) refer to a class of chronic, progressive, and immunity-mediated intestinal tract diseases, which create a heavy burden for patients, which can be partly attributed to lack of clear methods for early diagnosis and appropriate management. Therefore, it is important to find ways to detect IBD at the early stage using a precise, sensitive and convenient method. For example, Liu and Gong collaboratively developed a new far-red-emissive AIEgen-active fluorescent probe named TZB-FR with a D–π–A structure to detect IBD.

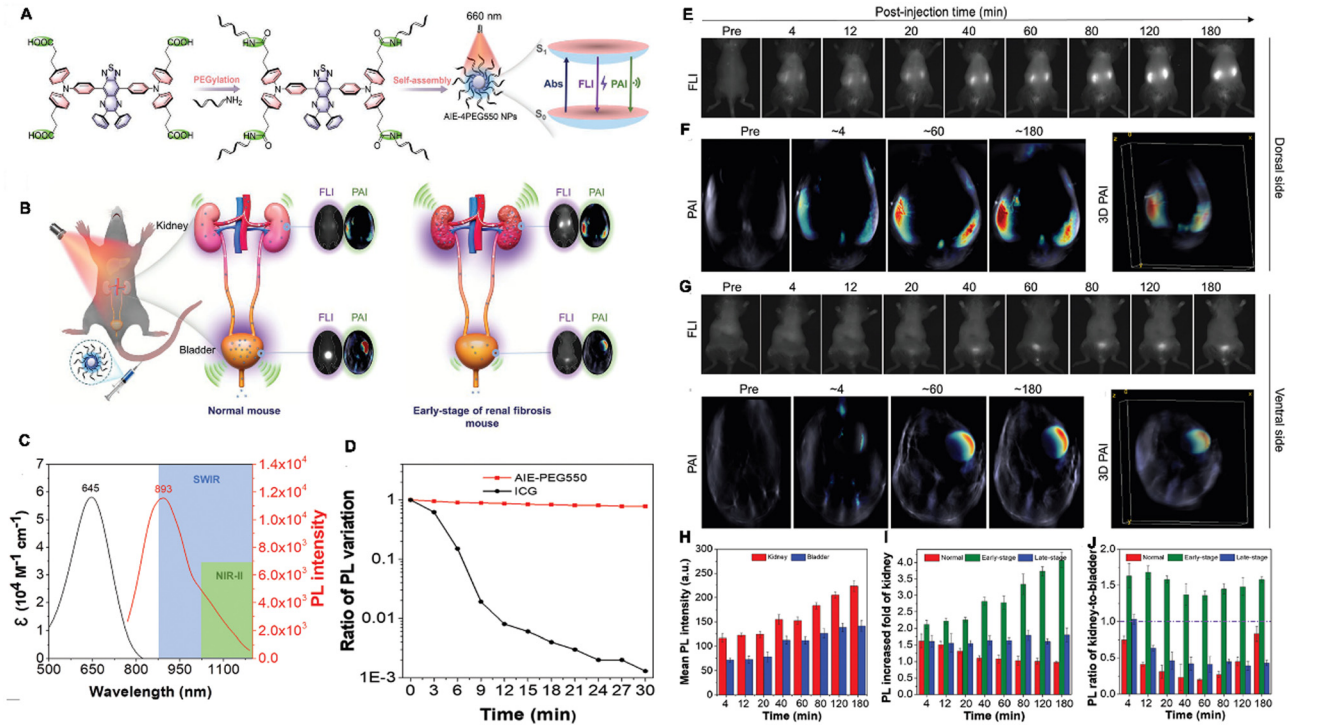

Fig. 9 (A) Molecular design philosophy of AIE-4PEG550 NPs and the reconciled photophysical processes. (B) Illustration of AIE-4PEG550 NPs using the SWIR FLI/PAI bimodal imaging. (C) The absorption and emission spectra. (D) Photostability of AIE-4PEG550 NPs. (E–J) The optical images in a renal fibrosis mouse model with AIE-4PEG550 NPs. Adapted with permission from ref. 138. Copyright 2022 Wiley-VCH GmbH.

TZB-FR showed far-red-emissive emission (624 nm) and a large Stokes shift (~184 nm). Upon incubation with LS174T and HT-29 cells, this AIEgen was found to be photostable and non-cytotoxic, which was also capable to provide excellent imaging capabilities to assess intestinal barrier function in animal models of DSS-induced colitis.[135] In another study, Lin *et al.* also developed AIEgen nanoprobes (BPN-BBTD NPs) by encapsulating BPN-BBTD within the amphiphilic polymer Pluronic F-127, where the BPN (*N*,*N*-diphenylnaphthalen-1-amine) served as the donor, and BBTD (benzo[1,2-*c*:4,5-*c*′]bis[1,2,5]-thiadiazole) served as the acceptor. The D–A structure conferred the intense NIR-II fluorescence property of the BPN-BBTD molecule with peak emission located at ≈930 nm. BPN-BBTD enables NIR-II fluorescence imaging that could be utilized to accurately detect inflammatory lesions, monitor inflammation severity and detect the response to drug interventions in an IBD mouse model directly.[136]

Fibrosis is a chronic inflammatory disease associated with persistent inflammation, including renal fibrosis, liver fibrosis.[137] Biopsy is the present "gold standard" for the detection and diagnosis of fibrosis and the invasive procedure might induce high bleeding risk. Hence, the noninvasive methods are urgently needed. Under these conditions, Tang *et al.* developed a water-soluble AIEgen-based nanoplatform named AIE-4PEG550 NPs for diagnosing kidney fibrosis *via* the SWIR fluorescence and photoacoustic imaging (Fig. 9A and B). AIE-4COOH was prepared using Wittig reaction and Suzuki coupling reaction with a typical D (triphenylamine derivative)-A (DPTQ) structure. Then, AIE-4PEG550 was synthesized *via* a facile condensation reaction in which 0.55 kDa PEG-NH_2 was PEGylated to the carboxylic acid groups of AIE-4COOH. AIE-4PEG550 dissolved well in water and exhibited a maximum emission peak in the SWIR region with a tail stretching to a second near-infrared window (NIR-II, 1000–1700 nm) with acceptable photostability (Fig. 9C and D) with a QY of 1.26%. After administrated intravenously, AIE-4PEG550 NPs showed high renal clearance efficiency (93.1 ± 1.7%) within 24 h and high targeting capability rapidly (4 min), providing a distant and rapid discrimination through SWIR FLI/PAI with a neglectable liver retention signal for detection of fibrosis using a 1000 nm long pass filter in nephropathy mouse model induced by folic acid. Furthermore, kidneys were visualized clearly with high definition in the NIR-II region. By evaluating the alteration of FL/PA intensities responsive to urinary excretion, the severity of renal fibrosis can be evaluated effectively, indicated by the alteration of fluorescent intensity (Fig. 9E–J). More importantly, AIE-4PEG550 NPs distinguished the progressive renal fibrosis at an early stage clearly than H&E staining, Masson's trichrome staining, and blood biochemistry test.[138] Hence, the literature indicated that the AIEgen exhibits great advantages over traditional methods and hold great potentials in the multimodal detection of inflammatory diseases.

2.7 Senescence detection and diagnosis

Senescence, a state involving permanent inhibition of cell proliferation, is a natural process in biological systems wherein senescent and dead cells are replaced by new and young cells to maintain tissue function.[139] Typically, the senescence phenotype is characterized by altered cellular morphology, increased

activity of senescence-associated-beta-galactosidase (SA-β-GAL), increased formation of senescence-associated heterochromatin foci (SAHF), the presence of promyelocytic leukemia protein nuclear bodies (PML NBs), permanent DNA damage, chromosomal instability, cell-cycle arrest, metabolic dysfunction, and the development of inflammatory secretome, among other factors.[140] In general, there exists a sophisticated balance between senescent and newborn cells, ensuring tissue homeostasis and organismal health. However, increased rates of senescence lead to pathological processes promoting disease development. For instance, aged immune cells are believed to be the most dangerous of all senescent cells, as they also accelerate the aging of other organs, leading to organismal aging,[141] and diseases like cancer. On the other hand, the above-mentioned characteristics can also be identified in cells from patients with age-related pathologies. In addition replicative senescence can occur depending on telomere erosion or dysfunction, while stress-induced premature senescence (SIPS) is telomere-independent, and also includes oncogene-induced senescence (OIS). These two processes are believed to be the two major mechanisms of cellular senescence.[142,143] Thus, the diagnosis and detection of senescence can help in preventing the occurrence of the associated diseases.[143] However, senescence detection cannot be detected by identification of a single biomarker but instead requires joint detection.

Nowadays, β-gal, SAHF, SASP, lipofuscin, Lamin B1, P53, P21, RB, and Ki67, are considered the main indicators of senescence and are examined using different diagnostic and detection methods.[144] When compared with previous co-staining, methods and optical microscopy, the fluorescent probes consisting of AIEgens offer several obvious advantages as with other diseases. More importantly, AIEgens could detect the contents in a real-time and dynamic manner.[145–152] Thus, AIEgen-based fluorescence detection allows the elucidation of senescence levels in biological systems. For example, based on the properties of the AIE-active nature and ESIPT of salicylaldehyde azines (SAs), a β-galactosidase probe, called SA-βGal, was synthesized by blocking the hydroxyl groups at the *ortho*-position on the benzene ring of salicylaldehyde azine (SA) with β-galactopyranoside by Liu *et al.* (Fig. 10A). The β-galactopyranoside group when reacted with β-galactosidase released the fluorescent probe salicylaldehyde azine to generate increased fluorescence emission at 545 nm. The fluorescence intensity was positively connected with the concentration of β-galactosidase (R^2 = 0.99). Hence, SA-βGal showed a broad range of β-galactosidase activity *in vitro* from 0 to 0.1 U mL^{-1} and the detection limit could be lowered to 0.014 U mL^{-1} (Fig. 10B–E). To validate this system, β-galactosidase activity was also detected in C6/LacZ cells and HeLa cells with high specific detection sensitivity (Fig. 10F and G).[145]

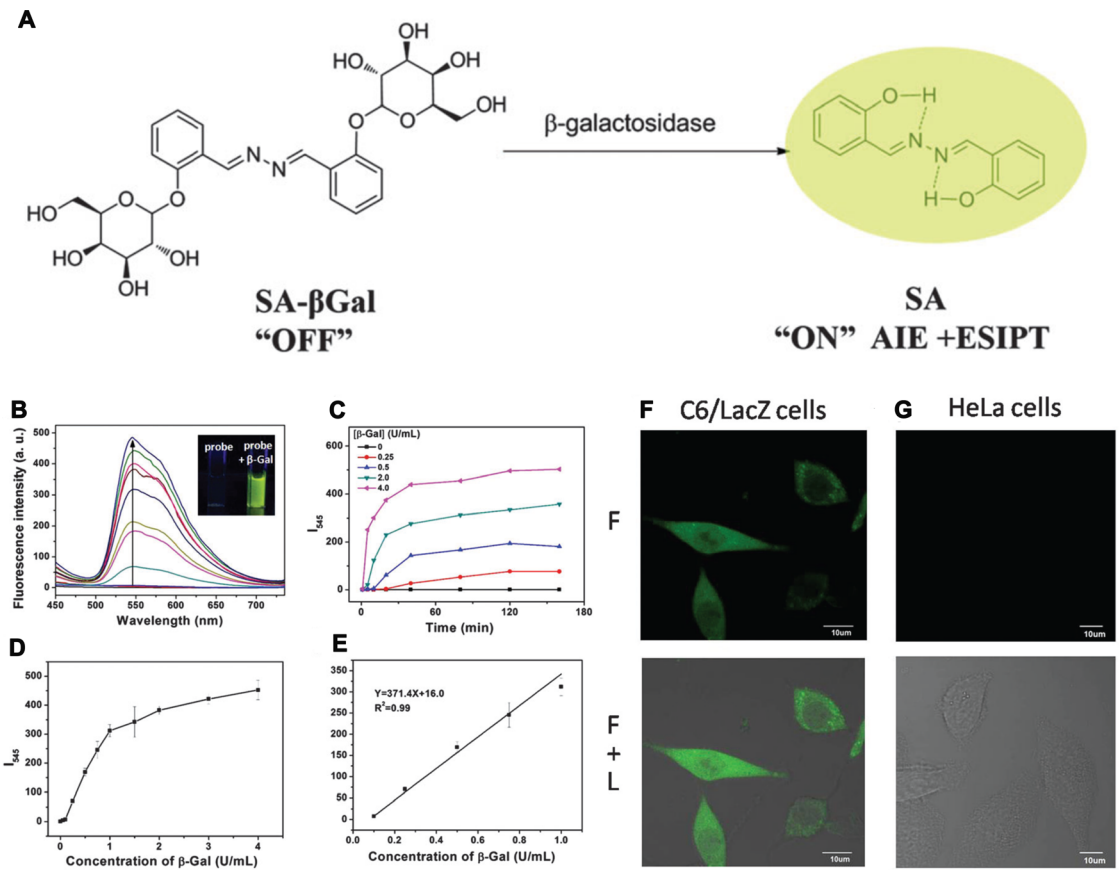

Fig. 10 (A) The fluorescent light-up probe of SA-βGal. (B) The FL spectra of SA-βGal, inset: photographs of SA-βGal without (left) or with β-Gal (right). (C and D) The fluorescence intensity changes (C) and concentrations (D). (E) The calibration curve of the fluorescence intensities. (F and G) Imaging of β-galactosidase activity in cells. Adapted with permission from ref. 145. Copyright 2015 The Royal Society of Chemistry.

Hence, AIEgen-based probes demonstrate the prospects of applying AIEgens over using traditional methods.

Beyond the above-mentioned non-cancer diseases, AIEgens have also been applied to detect other biological processes, such as the detection of human germ cell quality,[153] monitoring transplant immune response,[34] and the detection of damage of BBB.[154] Importantly, the detection and diagnosis of specific diseases are of great interest and AIEgens appear to be more effective tools for disease detection according to the literature. However, much attention should be still placed to achieve better outcomes using these agents in a range of other non-cancer diseases.

3. Noncancerous disease bioimaging with smart AIEgens

Currently, various biomedical technologies, such as MRI, PET, digitized radiography (DR), CT, single photon emission computed tomography (SPECT), ultrasonic imaging (UI), radionuclide imaging and so on have been used to image for the diagnosis and surveillance of diseases successfully. These methods own by themselves advantages and are applied in specific ranges of diseases when compared to each other. They also have their separate and collective weaknesses, including low resolution and contrast with high background signals, tissue damages induced by radiation, biotoxicity, invasive injury, and high expense. Moreover, these methods often fail to achieve the monitoring of pathogens in-depth dynamically. On the contrary, fluorescence imaging is capable of achieving better imaging results with excellent spatial resolution, high sensitivity and specificity, low biotoxicity, multimodal imaging capability, optical bioimaging, which show better potential for precisely and living imaging. Along with the development of optical bioimaging, a lot of fluorescent materials, such as fluorescent proteins, organic dyes, inorganic semiconductors, quantum dots (QDs) and so on, have been designated and developed rapidly.

For clinical applications, bioimaging agents must have characteristics such as a high SNR, penetration depth and photostability and excellent biocompatibility. As described in the introduction section, as imaging agents, AIEgens are superior to conventional fluorescence agents. Several AIEgens with tunable wavelengths from the infrared (extended to NIR-IIb, 1500–1700 nm) to the visible and UV spectrum and good biocompatibility and photo-/physical-stability have been developed, these agents are more suitable for super-resolution bioimaging approaches at the cellular and tissue levels. More importantly, AIEgens can intravitally visualize dynamic changes of diseases-associated biological processes *in vivo*, allowing long-term disease monitoring. Thus, they help both diagnostic imaging and treatment. Meanwhile, the occurrence of diseases is accompanied with the aberrant expression of small molecules, cytokines, enzymes and proteins, which can be effectively targeted for bioimaging.[36,45,155–158] Therefore, in this section, we summarize the latest advances in bioimaging for non-cancer diseases by using smart AIEgens. The advantages of AIEgens in the visualization of noncancerous diseases, when compared with conventional fluorescent probes are also discussed.

3.1 Bioimaging of infectious diseases

Bacteria, fungi, and viruses are the main pathogens that cause infectious diseases, serious infectious diseases are responsible for widespread death and panic across the world.[48,50] Meanwhile, microorganisms also play multiple essential roles in biological defense mechanisms by boosting the immune system and testing its protective features. Therefore, the selective and sensitive bioimaging of pathogens is vital in clinical medicine and could guide the use of antibiotics, preventing the occurrence of concomitant diseases and allowing the monitoring of the disease process in long term. At present, traditional methods for bacterial identification, such as the BacT/Alert blood culture system, biochemical staining, and PCR, are quite complex in terms of operation, and labor-intensive. Moreover, they rarely allow *in situ* bioimaging of living pathogens. Under these circumstances, fluorescence techniques have attracted attention owing to their high sensitivity and simplicity and distinct resolution. However, their ACQ effects and photobleaching during dynamic visualization and long-term monitoring greatly hinder their practical applications. In contrast, AIEgens do not have these disadvantages during the simultaneous discrimination, bioimaging, and monitoring of the infectious diseases. For example, Gram-positive bacteria are significant contributors to infections associated with high morbidity and mortality. Hence, their discrimination and monitoring of their biological processes from other microbes are important. To validate the capability of AIEgens in discriminating Gram-positive bacteria from other bacteria or fungi, Tang, Qin and Wang developed a new (2-{[(diphenylmethylene)hydrazono]methylphenol}) derivatives (DPAS)-based AIEgen, namely M1-DPAN, containing morpholine and naphthyl units to selectively discriminate Gram-positive bacteria even in the presence of Gram-negative bacteria and fungi, owing to the interaction between the outer wall of the microbes and the probe. It could label *S. aureus* and exhibit good tracing ability, tracking the translocation of the bacteria with high contrast and allowing dynamic monitoring of the infection process (Fig. 11A). Firstly, three DPAN-based AIEgens (M1-DPAN, M2-DPAN, and M3-DPAN) were synthesized (Fig. 11B). In details, DPAN was selected as the skeleton and the alkaline morpholine was introduced because it could interact with the macromolecules in acidic outer wall of pathogens *via* electrostatic interactions and the introduction of hexyloxyl group between morpholine and DPAN based on the flexibility and the insertion in cell membranes with appropriate thickness and structure of probe to achieve the turn off–on imaging effect (Fig. 11C). M1-DPAN exhibited maximum absorption and emission at around 391 and 525 nm with a high QY of 10.6% and photostability. Upon application in imaging the pathogens, M1-DPAN can discriminate Gram-positive bacteria from other microbes selectively (Fig. 11D). Moreover, M1-DPAN was also utilized to visualize the processes *via* which Gram-positive bacteria infect mammalian cells using fluorescence imaging.[159] In another study, to gain insights into the processes of bacterial phagocytosis, Chen *et al.* developed an environment-sensitive

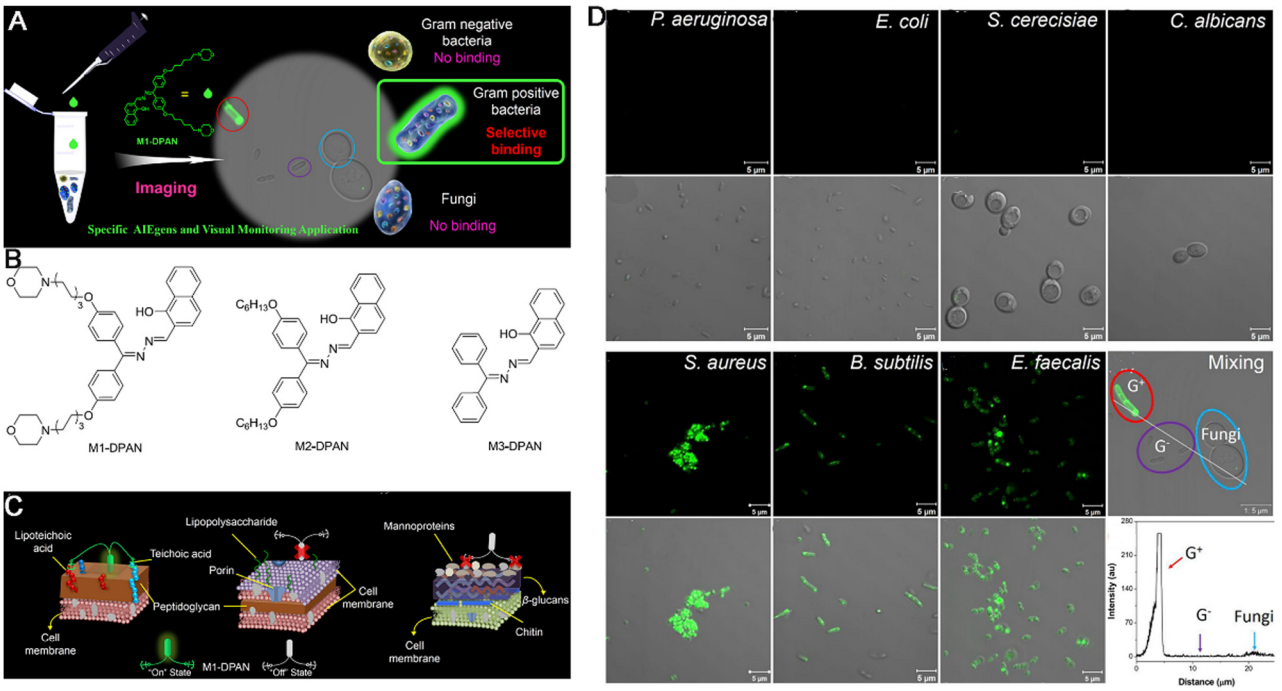

Fig. 11 (A) Illumination of bacteria-specific discrimination by M1-DPAN. (B) Chemical structures of DPAN. (C) Illustration of the interaction model between M1-DPAN and the outer cell walls of the Gram-positive bacteria (left), Gram-negative bacteria (center) or fungi (right). (D) The representative images of pathogen identification with M1-DPAN. Adapted with permission from ref. 159. Copyright 2018 Elsevier Ltd.

(pH value) AIEgen named TPE-Cy to label and image bacteria for visualizing the process of phagocytosis by macrophages. The bacterium labelled with TPE-Cy fluorescence served as pathogens that induced phagocytosis in macrophages and the fluorescent probe helped in visualizing the position and morphology of the bacteria, while also indicated the pH changes in the microenvironment during phagocytosis.[160] More, Gendelman's group also constructed a novel AIEgen nanoplatform, named RPV-NC, which was fabricated with L-α-phosphatidylcholine and DSPE-PEG_{2000}, where RPV-NC showed a blue fluorescence with maximum emission at 385 nm and high fluorescence stability in a range of pH values from 2 to 14. RPV-NC can target to $CD4^+$ T cell and macrophage specifically for imaging HIV virus and tracking the behavior of antiviral drugs in cell and subcellular organelles.[161] Thus, AIEgen-based bioimaging could be utilized for tracking various biological processes involved in infectious diseases.

3.2 Injury bioimaging

Injuries are sometimes inevitable parts of daily life and their damage can be unpredictable. In cancer treatment, radiotherapy is mainstay of treatment methods. However, there are obvious adverse effects. For example, approximately 95% of patients receiving irradiation in radiotherapy experience skin injuries. Moreover, the treatment of noncancerous diseases with chemotherapy and other treatments can also cause injury. Thus, the bioimaging of injuries and repair features are crucial for the improved reduction of adverse effects and for elucidating the molecular mechanisms of repair, which lead to the necessity of long-term imaging and tracking, and fluorescence imaging is particularly suitable for studying the occurrence and development of injuries and the underlying recovery mechanisms. This is because this imaging technique is considerably sensitive and of low-cost and can provide plentiful information at different levels owing to the advantages of AIEgens.[162–165]

To monitor the effects of stem cell therapy for the treatment of ionizing radiation-induced skin injury *via* bioimaging, Liu *et al.* constructed NIR-activated organic AIEgen nanodots with a high QY of 33%, prominent retention in adipose-derived stem cells (ADSCs), and good biocompatibility. The AIEgen nanodots exhibited excellent performance in examining the fate and regenerative mechanism of ADSCs after radiation-induced skin injury. At the molecular level, the AIEgen dots served as effective fluorescent cell trackers, precisely tracking the activity of transplanted ADSCs over a 1 month period.[166]

Acute liver injury, another type of serious and common clinical injury, can be triggered by various endogenous and exogenous factors, including alcohol consumption and inappropriate drug use. Therefore, accurately evaluating the hepatotoxicity of drugs or treatment methods is crucial. To visualize acute liver injury precisely and clearly, Wu and colleagues developed a nitric oxide (NO)-activatable AIEgen probe named QY-N, this probe could be used for diagnosing and visualizing liver injury caused by herbal medicine. It detected *in situ* NO levels in the liver based on NIR-II fluorescence and multispectral optoacoustic tomography (MSOT) imaging. QY-N contained a D–A structure in which bismethoxyphenyl-amine containing dihydroxanthene served as an electron donor, while quinolinium served as an electron acceptor, the butylamine served as the recognition group and fluorescence quencher. When the NO in hepatic tissues reacted with butylamine, the

activated probe QY-NO was generated, leading to an obvious red-shifted absorption band (700–850 nm) for optoacoustic (PA) imaging. The strong emission at 910–1110 nm allowed NIR-II fluorescence imaging. In a triptolide-induced liver injury model, QY-N was activated by *in situ* hepatic NO to detect and image liver injuries. The 3D MSOT bioimaging results indicated that the QY-N nanodots could accurately identify the location and size of the liver injury. Moreover, QY-N was found to be effective in the long-term tracking of the subsequent recovery.[167]

Compared to conventional fluorescent probes used for injury bioimaging, AIEgens have many advantages, including: (i) tunable emission wavelengths into the NIR-IIa and NIR-IIb regions, allowing deep tissue bioimaging at a high spatial resolution; (ii) high targeting capability and selectivity for precise bioimaging; (iii) multimodal bioimaging capability; and (iv) capacity for long-term monitoring and tracking. Thus, greater efforts should be put forward for injury bioimaging based on AIEgen probes.

3.3 Metabolic disease bioimaging

Metabolic diseases are chronic diseases that are characterized by abnormal metabolism that induces the dysfunction of cells and tissues. In metabolic diseases, the levels of biological molecules change dynamically and aberrantly. Thus, the targeted imaging of these biological molecules is an effective way for supervising the status of the disease and guiding treatment. However, although current bioimaging approaches, such as MRI, PET, mass spectrometry imaging, Raman microscopy, and fluorescence imaging are capable of mapping *in situ* metabolic activities,[168–170] they possess several disadvantages, including low spatial resolution, low labeling capability, high time-expenditure, low imaging sensitivity, slow imaging speed, strong biological interference, and limited spectral coverage. However, fluorescence imaging is most suitable for the imaging of metabolic diseases due to its rapid response rate and non-invasive nature, among other advantages. Compared with conventional fluorescent probes, AIEgens show great advantages in the imaging of metabolic diseases.[91,171,172]

To overcome the strong hydrophobicity that limits the efficiency of lipid-specific fluorophores for *in vivo* labeling in metabolic diseases, Liu *et al.* synthesized two AIEgens (TPACN and TPAPhCN) with a typical D–A structure. Triphenylamine (TPA) served as the electron donor, while the dicyanovinyl group served as the electron acceptor. Both AIEgens showed maximum emissions in the red and far-red/NIR region (620 nm and 684 nm, respectively) and high fluorescence QYs (40% ± 2% and 26% ± 1%, respectively). The AIEgen dots (TPACN dots and TPAPhCN dots) were prepared by fabricating with DSPE-PEG using a nanoprecipitation method, they could also be applied for *in vivo* labeling and the three-photon fluorescence imaging of lipid-rich tissues, such as fatty livers and atherosclerotic plaques in the brain vasculature and carotid arteries with a high targeting specificity. Thus, they provided better imaging results than commercial lipid-specific fluorophores.[173]

Alcoholic liver disease (ALD) is caused by the excess consumption of alcohol and is becoming a significant threat to human health around the world,[174] which has been identified as a chronic disease resulting from acute alcoholic liver injury (AALI). However, due to a lack of clinical symptoms and biomarkers, such liver injury is usually ignored and appropriate prevention or treatment is not performed. Moreover, previous studies have revealed that ALD leads to variations in the intracellular microenvironment, thus altering mitochondrial

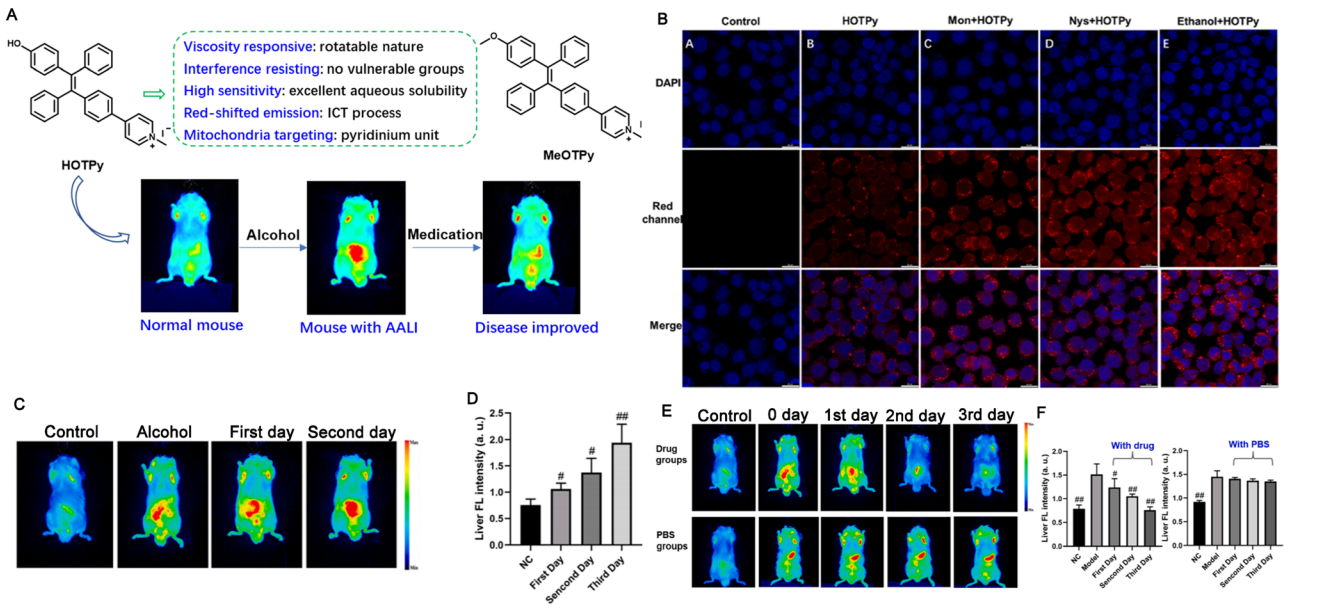

Fig. 12 (A) Structures of HOTPy and its counterpart MeOTPy and the diagram of AALI imaging. (B) The confocal images of HOTPy for imaging the mitochondrial viscosity. (C) The *in vivo* imaging. (D) Quantification of fluorescent intensity of (C). (E) The *in vivo* imaging of AALI mice under drug treatment. (F) Quantification of fluorescent intensity of (E). Adapted with permission from ref. 176. Copyright 2021 Elsevier B.V.

viscosity.[175] To diagnose AALI and monitor its progression in a timely manner based on the change in mitochondrial viscosity, Chen *et al.* constructed a robust fluorescent AIEgen probe named HOTPy for imaging ALD, which was soluble in water, showed prominent chemical stability, and could resist interference (Fig. 12A). Within the HOTPy, the D–A structure and interaction lead to red-shifted emission upon aggregation to benefit bioimaging with less light scattering, lower background fluorescence and deeper penetration. The increase of solvent viscosity induced the absorption peaks of HOTPy and MeOTPy (contrast probe) red-shifted from 379 nm and 376 nm to 396 and 392 nm, respectively, and the fluorescence showed large a redshift from 548 nm to 614 nm of MeOTPy, while HOTPy exhibited a constant emission peak at 611 nm with steady increase of the fluorescence intensity, also both exhibited increased QYs. When applied for the imaging of mitochondrial viscosity alteration, the examination results revealed that HOTPy could respond to the changes of mitochondrial viscosity *in vitro* (Fig. 12B) and *in vivo* (Fig. 12C and D), allowing the tracking of liver recovery based on changes in mitochondrial viscosity *in situ* (Fig. 12E and F).[176] Thus, owing to their high compatibility, high fluorescence QYs, and large emission wavelengths, among other advantages, AIEgen probes are obviously beneficial as candidates for the bioimaging of metabolic diseases and disease monitoring.

3.4 Cardiovascular disease bioimaging

Alterations in the structure and function of the cardiovascular system lead to a plethora of serious diseases or even death because of blood vessels that provide the necessary nutrition to cells and transport the waste from cells. Hence, the bioimaging of cardiovascular system not only provides diagnostic evidence for diseases but also guides the treatment and the monitoring of treatment effectiveness. At present, bioimaging methods for CVDs can be classified into methods based on morphology (CT, MRI, and US), physiology (US, MRI, PET, and SPECT), and biochemistry (PET, SPECT, and CSI). Although these methods have a high resolution and can provide adequate information, some drawbacks persist and must be addressed; these include the high cost, complex operation, slow speed, labor-intensive nature and so on. Thus, more effective, low-cost, and convenient bioimaging methods are urgently warranted. Similar to the bioimaging of other diseases, fluorescent probes are also better options for CVD bioimaging. Given the presence of biological barriers, these fluorescent probes must possess strong excitation and fluorescence emission capabilities in the NIR spectral range and be resistant to the impact of biological components. Some fluorescent compounds, including cyanine dyes, lanthanide chelates, tetrapyrrole-based dyes, and quantum dots,[177] are used for CVD imaging. However, the results of these traditional agents are still far below expectations. Owing to their properties and promising results from previous studies, AIEgens appear to be more suitable for CVD imaging and they have been a hot topic of AIEgen-based science community.[103,178–186]

At present, many fluorescent probes applied for the bioimaging of CVDs have mainly been tested in small animals such as mice, the testing of these probes in larger-size animals such as rats, dogs, and monkeys are still rare. Tang *et al.* thus synthesized a novel AIEgen (BPN-BBT) with a D–A structure to visualize the vasculature in large-size animals. In this probe, bisphenylnaphthalen-1-amine (BPN) served as an electron-donating moiety, while benzobisthiadiazole (BBT) served as an *o*-quinoid type acceptor. BPN-BBT exhibited long wavelength absorption (713 nm) and fluorescence emission (954 nm, the QY was 6.1%) and an intense emission tail extended to 1400 nm. BPN-BBT showed high luminosity, excellent stability, and good biocompatibility. Given the tail extension to 1400 nm, NIR-II fluorescence imaging with BPN-BBT dots beyond 1200 nm allowed the visualization of the rat brain vasculature with a high spatial resolution ($\sim$4 μm) and deep penetration (700 μm). Small vascular blockages could be observed in real-time at the early stage of cerebral thrombosis. Further, the gastrointestinal tract and bladder could also be observed with high contrast.[187] In another study, Tang and Qian also developed a novel AIEgen, named 2TT-*o*C26B NPs for vascular imaging collaboratively (Fig. 13A). Within 2TT-*o*C26B, BBTD, the quinoidal structure served as the strong electron acceptor accompanied with lower band gap, alkyl thiophene served as the donor unit and π-conjugation bridge, TPA with twisted structure served as the molecular rotor to assure the formation of the TICT state, while acting as a second donor unit to facilitate the charge transfer (Fig. 13B). The 2TT-*o*C26B NPs could emit light up to 1600 nm with a QY of 11.5% at the peak emission at about 1000 nm (Fig. 13C), with a high SNR in the NIR-II region. *In vitro*, the SNR and Gaussian-fitted full width at half maximum (FWHM) of 2TT-*o*C26B NPs were 3.1 and 0.32 cm, respectively. During whole-body imaging, the SNR values at 1100, 1200, and 1500 nm LP were 1.1, 1.2, and 2.0, respectively, and the apparent widths of similar vessels were 0.41, 0.56, and 0.58, respectively. This study demonstrated that NIR-IIb imaging with 2TT-*o*C26B NPs provided a high spatial resolution (Fig. 13D). Meanwhile, the blood vessels close to the liver cannot be clearly imaged using 1100 and 1200 nm LP but clearly in 1500 nm LP (Fig. 13D). In cerebral vasculature imaging, high magnification through-skull microscopic vessel imaging with 2TT-*o*C26B NPs revealed the small vessel with an apparent width of only 10 μm (Fig. 13E). In bowel imaging, the results at 1100 and 1200 nm LP were blurry and the resolution was low, but 1500 nm LP provided a high spatial resolution ($\sim$4 mm) and deep penetration (5 mm) (Fig. 13F).[188]

Recently, with the development of the microscope technologies, many molecular designs and structural optimization of AIEgens also emerged rapidly. For instance, Tang, Qian and Liang constructed a novel AIEgen with excellent three-photon absorption for vasculature imaging in normal and disease cells. In this AIEgen, triphenylamine fragment was introduced to BTF for enhancing the D–A strength, to endow BTF exhibiting a large red-shift of about 230 nm to reach NIR region and multi-photon absorption than the BTF analogue without the triphenylamine moiety with high QYs in solid (42.6%) and aggregated states (36.1%) (Fig. 14A–D). Encapsulated by Pluronic F-127 to yield BTF dots, it can image cerebrovascular in real-time with a

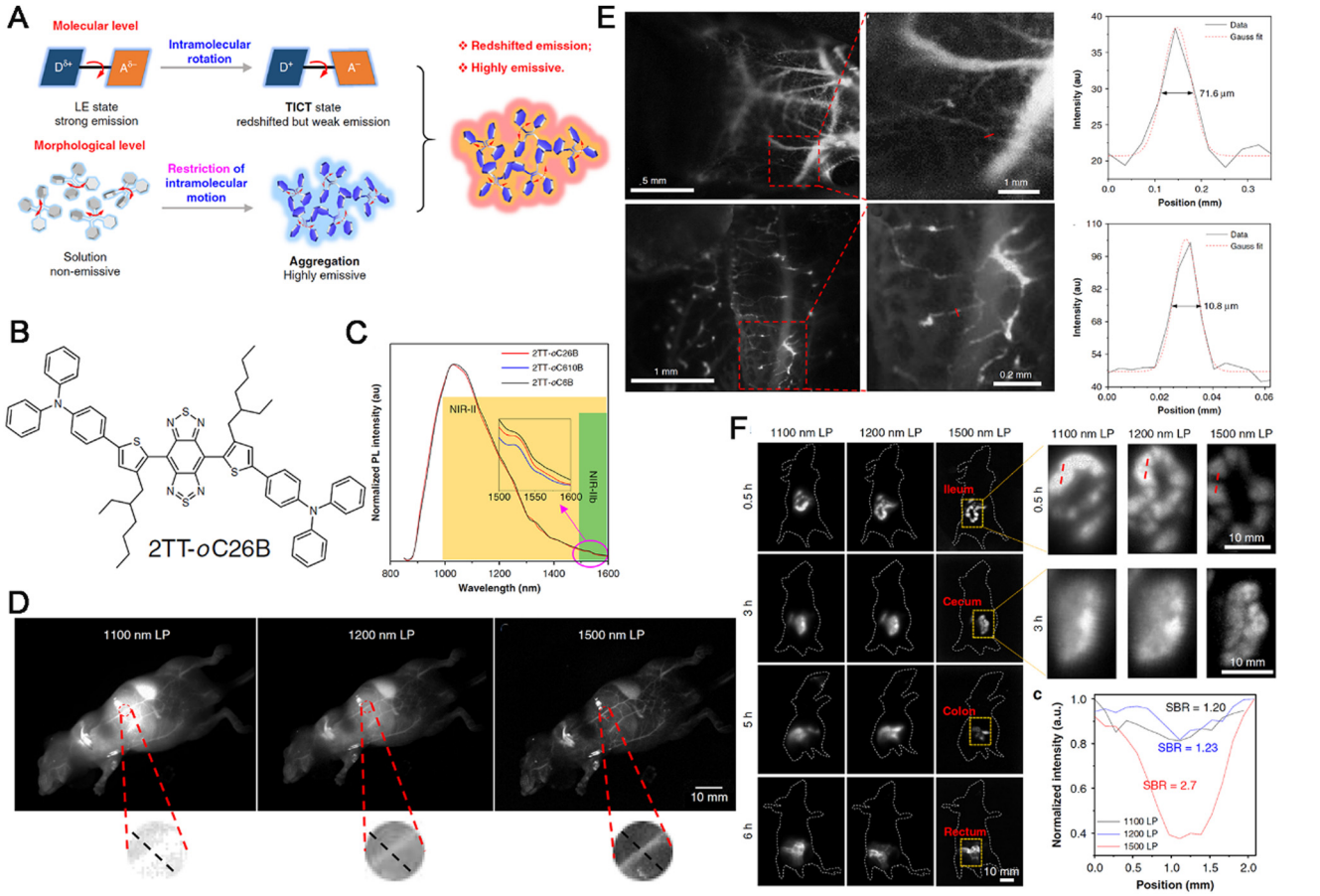

Fig. 13 (A) Diagram of emission mechanism of AIEgens. (B) Chemical structure of 2TT-*o*C26B. (C) The PL spectra of NPs. (D) Wholebody imaging, zoom-in images of the red circle areas. (E) Cerebral vasculature imaging, inset: zoom-in images of the red rectangle areas. (F) Bowel imaging, inset: zoom-in images of the yellow rectangle areas. Adapted with permission from ref. 188. Copyright 2020 Springer Nature.

higher depth of up to 900 nm (Fig. 14E–G). More importantly, the visualization of cerebral thrombosis process with this AIEgen probe through the intact skull of mouse was reported combined with multi-photon fluorescence imaging technology (Fig. 14H and I).[180]

Compared to conventional fluorescent compounds, AIEgens show great advantages in the imaging of CVDs, including the long wavelength emission in the NIR-IIb region that promotes the bioimaging of deep tissues, high QYs that promote fluorescence intensity, high clarity, and enhanced SNRs, especially in cerebral angiography,[189–195] expand the progresses of CVDs. Hence, they should be applied for bioimaging in more animal and non-cancer disease models.

3.5 Neurodegenerative disease imaging

As stated above, neurodegenerative diseases result from the chronic or acute but progressive and selective loss of functions and structures in anatomically or physiologically associated neuronal systems. At present, the process of neurodegeneration is not fully understood and therapeutic targets are largely unavailable. As a result, effective diagnosis, bioimaging, and therapeutic strategies have not been developed. The nervous system has a central regulatory function in the body. Hence, neurodegenerative diseases are often associated with language impairments, personality changes, dementia, and progressive muscle weakness, creating a heavy long-term burden for patients. Thus, the bioimaging of neurodegenerative diseases is not only beneficial for diagnosis but can also provide guidance for treatment and effective monitoring. At present, the main modern bioimaging technologies for the evaluation of neurodegenerative disease pathology include PET, SPECT, and MRI, among others.[196,197] However, these applications are limited by the hindrance caused by the BBB, high cost, involvement of hazardous radiolabeled compounds, need for high-tech instruments, relatively low spatial resolution and sensitivity, and application of complex data acquisition and analysis protocols. Hence, more effective methods need to be developed. Due to their multifold advantages, including the ability to cross the BBB and through skull and provide high-resolution fluorescence imaging, many fluorescent probes have been constructed for the imaging of neurodegenerative diseases. However, recent studies have demonstrated that AIEgens exhibit multifold advantages over fluorescent probes for the bioimaging of neurodegenerative diseases owing to their advantageous properties.[115,117,119,198–201]

PD is a typical chronic and progressive neurodegenerative disease that usually occurs in people aged 60 years and above, it

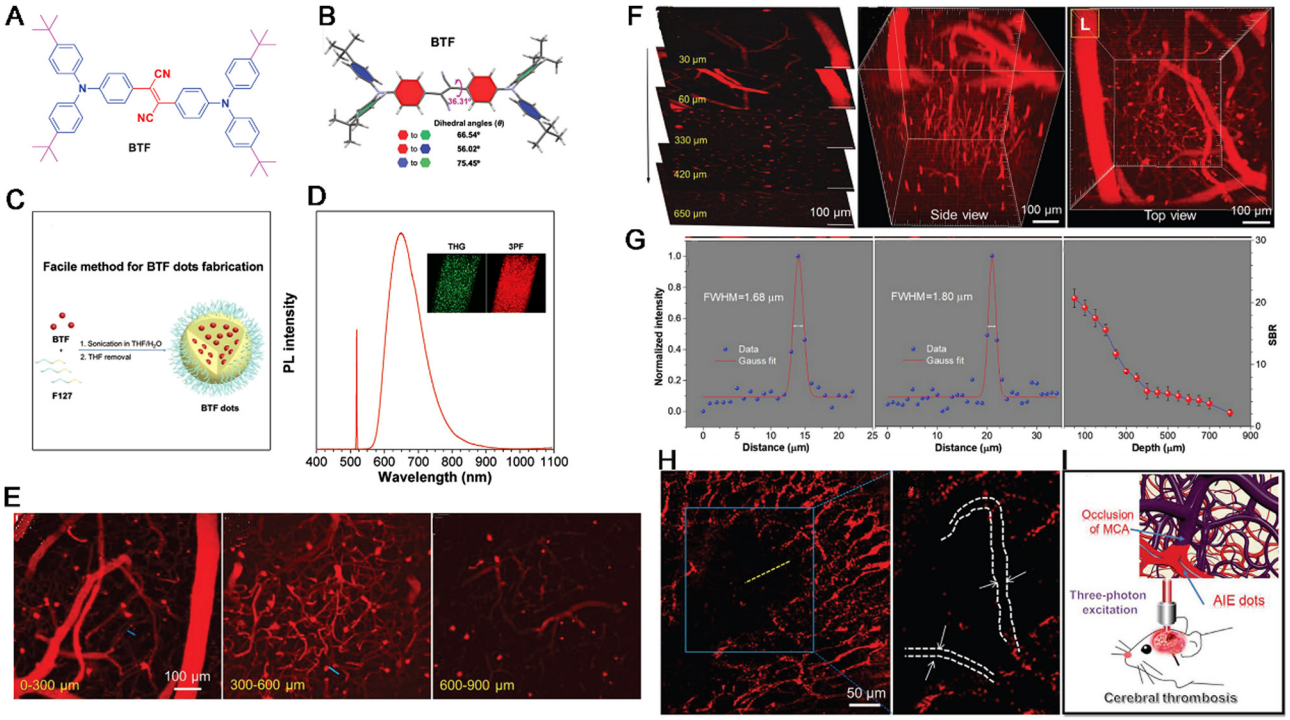

Fig. 14 (A) Chemical structure of BTF. (B) Single crystal structure of BTF. (C) Illustration of BTF dots. (D) Diagram of two-photon fluorescence imaging, three-photon fluorescence imaging, and third-harmonic generation processes. (E–G) *In vivo* 3D high resolution images, cross-sectional intensity profiles. (H) Brain thrombosis imaging. (I) Diagram of the visualization of brain thrombosis. Adapted with permission from ref. 180. Copyright 2020 Wiley-VCH Verlag GmbH & Co. KGaA, Weinhe.

is characterized by resting tremor, slowness of movements, rigidity, gait disturbance, and postural instability.[202] In a previous study, mitochondrial lipid droplets (LDs) were proven to be central players in PD progression, excessive LD accumulation due to metabolic production was found to cause neuronal death.[203] Commercial agents, Nile Red and BODIPY, show the shortcoming of low photostability, photobleaching, and ACQ, which limits their applications in the long-term tracing of disease progression. With AIEgen-based probes for LDs, their detection becomes easier and long-term monitoring becomes possible. Tang *et al.* prepared an AIEgen LD probe named 2-DPAN by inserting a 2-naphthalene group instead of phenyl group for enhancing luminous efficiency. 2-DPAN could target cellular LDs and accumulate selectively inside these cells, emitting bright green fluorescence accompanied with high photostability and excellent biocompatibility. Thus, the real-time dynamic alteration of LDs after 6-OHDA stimulation could be monitored (Fig. 15A and B). 2-DPAN exhibited a maximum emission peak at approximately 550 nm without significant shift in the aggregated state and a large Stokes shift (139 nm), both beneficial for long-term monitoring that was not affected by external environmental changes (Fig. 15C and D). Upon incubation with SH-SY5Y cells, 2-DPAN could target LDs specifically and in the PD model induced by 6-OHDA, 2-DPAN can target to LDs of mitochondria only (Fig. 15E and F). In molecular mechanism, following 6-OHDA stimulation, LDs first showed rapid accumulation, however, the LDs were finally released from damaged cells. In addition, 2-DPAN staining for LDs and mitochondria identified a negative relationship between LDs and mitochondrial activity in the first two phases. Thus, 2-DPAN exhibited good effectiveness in LD-based imaging in PD models and could protect mitochondria and rescue the effects of PD.[204]

Myelin, a special structure that surrounds and insulates neuronal axons, is a vital component of the central nervous system. The pathological changes in myelin alter motor, sensory, and cognitive abilities, thus inducing a series of neurodegenerative diseases, including multiple sclerosis[205] and AD.[206] Owing to the important role of myelin in the central nervous system, its visualization in brain tissues can facilitate the diagnosis and monitoring of myelin-related diseases. However, current fluorescent probes such as Vybrant DiD and FluoroMyelin exert ACQ effects and low accumulation efficiency; as a result, they produce a high background signal, provide low staining contrast, and have low brightness, leading to a low resolution and poor bioimaging results. To solve these problems, Chen *et al.* developed a novel AIEgen named PM-ML for high-performance myelin imaging, which originated from the advantages of AIEgen probes. PM-ML (Fig. 16A) showed a blue-shifted maximum emission from 705 to 670 nm when suspended in over 80% PhMe/DMSO fraction, strong emission (in 99.9% PhMe solution was 214-fold higher than that in pure DMSO) and the QY increased to 8.5% from 0.05% (Fig. 16B and C). PM-ML can target to plasma membrane with excellent targetability (Fig. 16D) and could specifically label myelinated fibers in teased sciatic nerves and mouse brain tissues specifically with

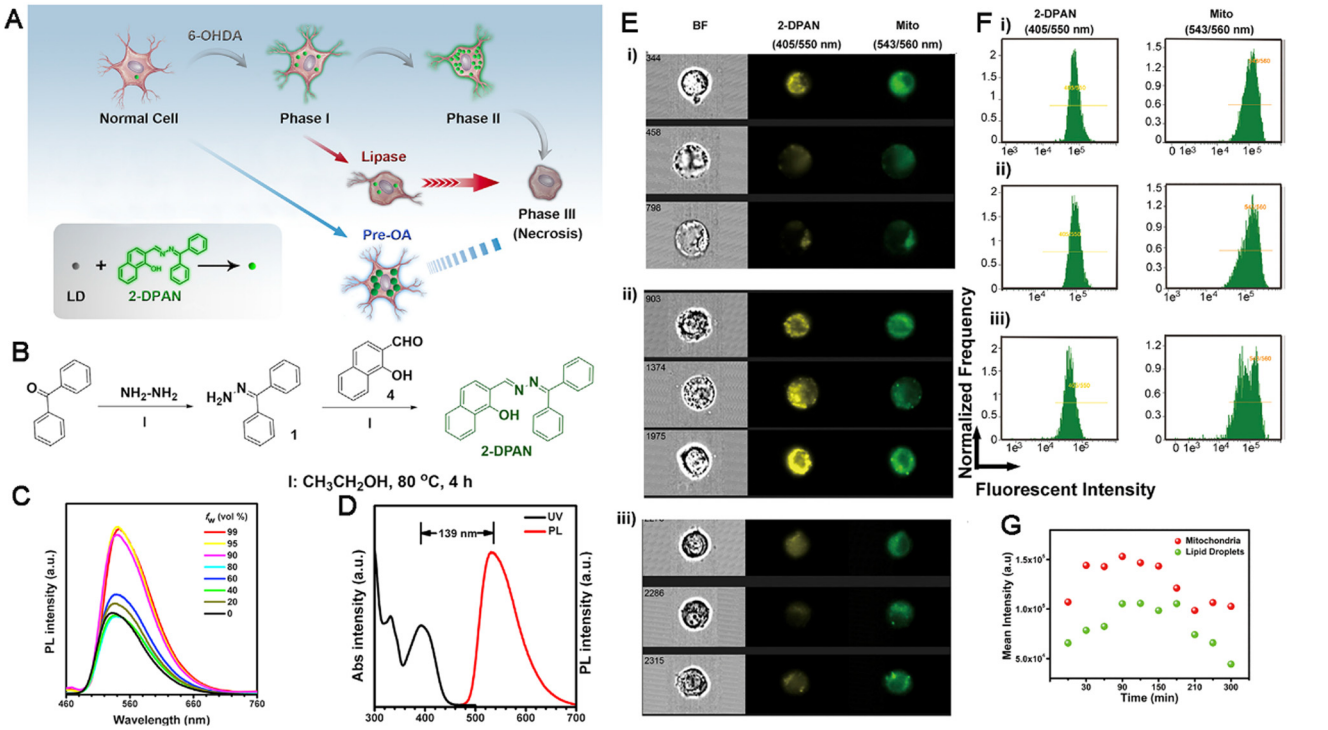

Fig. 15 (A) Diagram of real-time monitoring of LD behavior. (B) Synthetic route of 2-DPAN. (C) The PL spectra of 2-DPAN. (D) The absorption and PL spectra. (E) The imaging of LDs in PD. (F) Fluorescence diagram of flow cytometry responses to (E). (G) Quantitative mean fluorescent intensity. Adapted with permission from ref. 204. Copyright 2019 Elsevier.

a high SNR over FMR and DiD (Fig. 16E and F). Moreover, PM-ML was also capable of providing a 3D visualization of myelin sheaths, myelinated fibers, and fascicles at a high penetration depth (30 μm) (Fig. 16G). With the help of two-photon microscopy, the depth of imaging could increase to more than 900 μm. PM-ML was compatible with Clear^{T} and Clear^{T2} brain tissue-clearing methods and showed excellent bioimaging performance in a mouse model of multiple sclerosis (Fig. 16H).[207]

Compared with conventional fluorescent probes, AIEgens exhibit overwhelming advantages for better bioimaging outcomes as follows: (i) the high BBB-crossing rate enhances the results of fluorescence imaging; (ii) the high specificity of AIEgens promotes precise and accurate bioimaging of disease sites; and (iii) the high SNR enhances the resolution of bioimaging findings. In future, more rational design for the application of AIEgens in the bioimaging of neurodegenerative diseases is required.

3.6 Orthopedic disease bioimaging

Orthopedic diseases can arise from chronic or acute damage and can create a heavy burden to patients in the long term. Imaging plays an increasingly important role in understanding the process of orthopedic disease progression and monitoring any alterations that occur following different treatments. In the clinics, radiography, CT, MRI, NMR, and ultrasound imaging are usually applied for diagnosis and supervision. However, these methods are time-consuming, expensive and do not provide ideal results. Given the pathological alterations observed in orthopedic disorders dynamicly,[131,132] compared with these methods, fluorescence imaging for detecting these alterations is more convenient and less expensive. Moreover, it also provides a high spatial resolution.[208,209] Similar to other diseases, AIEgens also provide great advantages in the imaging of bones and orthopedic diseases.[210,211] For example, Zhang *et al.* developed a novel AIEgen probe named PTB-EDTA for monitoring the process of osteogenic differentiation following efficient chelation with Ca^{2+}. PTB-EDTA was synthesized with an AIE-active TPE and benzothiadiazole-conjugated polymer and ethylenediaminetetraacetic acid moieties (PTBEDTA) that served as side chains. PTB-EDTA showed a Stokes shift as large as 165 nm, with maximal absorption and emission at 429 and 594 nm, respectively. PTB-EDTA could target osteogenic differentiated cells and the intracellular fluorescence gradually increased with the long-term enhancement of osteogenic differentiation over 14 days, it did not cause any obvious effects on the survival and differentiation of osteoblasts. Thus, PTB-EDTA could overcome the shortcomings of typical methods such as Alizarin Red S staining in which cell growth needs to be halted.[211] Thus, more AIEgens need to be designed for the bioimaging of orthopedic diseases.

3.7 Inflammatory disease bioimaging

Inflammatory diseases are often induced by various ROS and are also accompanied by sustained elevation of the ROS and various kinds of cytokines. Consequently, the specific imaging of elevated ROS production and cytokines at the inflammatory

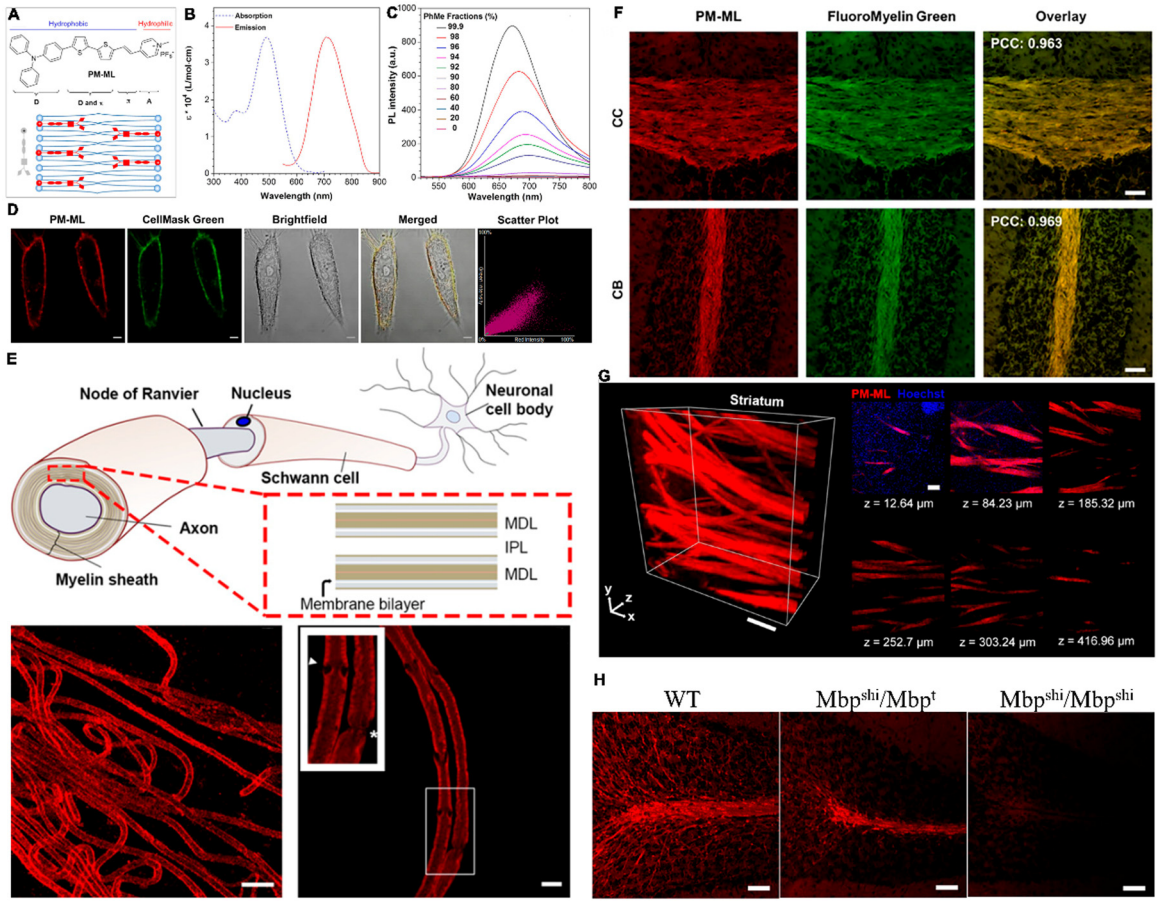

Fig. 16 (A) The chemical structure, diagram of PM-ML structural characteristics and its interaction with membrane structure. (B) The molar absorption coefficient and emission spectrum of PM-ML. (C) The PL spectra of PM-ML. (D) PM-ML-labelled plasma membrane. (E) Labelling of myelin sheath in teased sciatic nerve fibers. (F) Brain regions rich in myelinated fibers (CC and CB). (G) 3D rendered Z-stack of the STR. (H) PM-ML staining in cleared brain sagittal sections. Adapted with permission from ref. 207. Copyright 2021 PNAS.

level is undoubtedly beneficial for obtaining valuable information on the pathological process of inflammatory diseases. It can also help in optimizing therapeutic interventions. Among the different versatile imaging modalities, fluorescence imaging offers the advantages of high sensitivity, excellent temporal resolution, high safety, and low cost. At present, various fluorescent probes have been applied for detecting the content of ROS and imaging inflammatory diseases. However, the presence of ACQ effects in these conventional fluorescent probes leads to a "blinking" effect, preventing long-term imaging and causing high cytotoxicity, which limits their further applications. On the contrary, AIEgens do not have photobleaching thresholds, show stable fluorescence without "blinking" and provide low cytotoxicity and the additional property of a "fluorescence turn-on mode", which makes them perfect for the evaluation of inflammatory diseases at a high resolution with long-term bioimaging.[212–217]

Some inflammatory diseases are characterized and caused by the elevated generation of $ONOO^-$.[218] To image the region of inflammation, Tang *et al.* designed and synthesized a fluorescence light-up nanoprobe based on a new and distinctive imine-functionalized TPE derivative, which was called TPE-IPB (*N*-(2-((4-(4,4,5,5-tetramethyl-1,3,2-dioxaborolan-2-yl)benzyl)oxy)-benzylidene)-4-(1,2,2-triphenylvinyl)aniline). TPE-IPB was prepared *via* a condensation reaction between TPE-NH_2 and phenylboronate-modified benzaldehyde under mild conditions (Fig. 17A). The TPE moiety served as the AIEgen, the imine group served as the emission mediator, and the phenylboronate served as the recognition site for $ONOO^-$. Then, the TPE-IPB-PEG probe was formulated within a lipid-PEG matrix, it was non-fluorescent in an aqueous solution and emitted intense yellow fluorescence after reacting with $ONOO^-$ at pH 7.4 (Fig. 17B). The TPE-IPB-PEG probe showed emission with a maximum at 538 nm and the fluorescence gradually increased with an increase in the concentration of $ONOO^-$. The fluorescence accumulation occurs within the region of inflammation due to the enhanced permeability and retention (EPR) effect because the blood vessels within this region are permeable (Fig. 17C). Thus, the TPE-IPB-PEG fluorescence intensity was elevated with enhanced $ONOO^-$ generation, allowing the high-contrast imaging of the inflammatory site over a long period (14 days) and promoting the imaging that was achieved both *in vitro* and *in vivo* with good biocompatibility.[219] In another study, Tang *et al.* developed an AIEgen probe to image the regions of inflammation within the brain.[220] The AIEgen named 2TT-*o*C6B was synthesized and contained both backbone

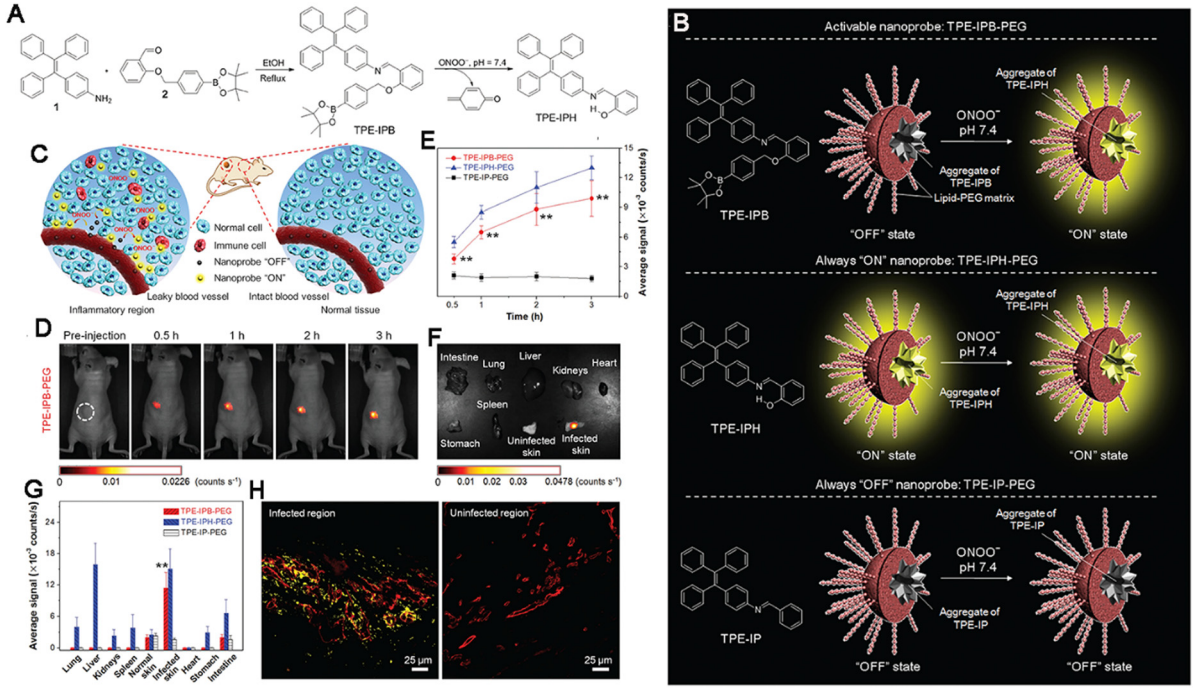

Fig. 17 (A) Synthetic route to TPE-IPB and design rationale for $ONOO^-$ detection. (B) Diagram of AIEgens and their performance. (C) Inflammation region imaging. (D) The time-dependent fluorescent images of an inflammation-bearing mouse. (E) The average fluorescence signals. (F) The *ex vivo* fluorescence images. (G) The average fluorescence signals. (H) The representative confocal images of slices of infected and uninfected skin tissues. Adapted with permission from ref. 219. Copyright 2016 Wiley-VCH Verlag GmbH & Co. KGaA, Weinheim.

distortion and rotor twisting characteristics. 2TT-*o*C6B exhibited NIR-II emission at 1030 nm with a QY of 11%. To enhance the targeting ability towards deeply located brain tissues, neutrophils (NEs) were used as carriers, which allowed the penetration of brain tissues and accumulation at the site of inflammation. Thus, NEs carrying 2TT-*o*C6B nanoparticles penetrated the BBB and the deep-seated inflammation (front thickness of 8 mm and back thickness of 0.5 mm) could be visualized across an intact scalp and skull with a significantly enhanced SNR (30.6). The SNR, speed, and depth of imaging were significantly superior to those of the conventional ICG probes.[220] Therefore, AIEgen probes are more suitable for the bioimaging of inflammatory diseases.

3.8 Senescence bioimaging

As described above, senescence is characterized by the altered expression of β-gal, SAHF, SASP, and other molecules. The increased accumulation of β-gal is especially notable in senescent cells. Beyond conventional methods like MRI and PET, which have several limitations, fluorescent probes have become a powerful tool for imaging senescent cells. Several fluorescent probes have been developed for β-gal imaging,[143,146,221] but they are vulnerable to ACQ effects, which reduces the quality of imaging results. Given their AIE effects that are in contrast to the ACQ effect, AIEgens have attracted much interest in the imaging of senescent cells and excellent results have been achieved.[151,152] For instance, Jia *et al.* synthesized a new fluorescent AIEgen probe named TPh-PyBz-β-gal that contained a novel AIE fluorophore and a receptor unit, a D-galactose residue connected by glycosidic bond to enhance β-gal targeting. TPh-PyBz-β-gal showed a peaked emission at 605 nm and can visualize β-gal-expressing cells after the cleavage of the glycosidic bond, increasing the fluorescence signal at 605 nm, which provided a high resolution obviously.[150] In another study, Kim *et al.* reported the development of an α-L-fucosidase (α-fuc)-responsive AIEgen named QM-Nhαfuc for *in vivo* cellular senescence detection and imaging. When the proportion of water in the water/tetrahydrofuran solution exceeded 80%, the fluorescence of QM-NH_2 increased sharply with an emission maximum centered at 586 nm and remained stable even in 100% water solution. Within QM-Nhαfuc, the α-fucopyranoside unit provided the formation of loosely packed nanostructures with large internal free volumes and α-fuc led to the release of QM-NH_2 from QM-NHαfuc promoting the formation of tightly packed QM-NH_2 nano-aggregates, characterized by an intense AIE fluorescence. QM-NHαfuc could be used to effectively evaluate the onset of replicative and ROS-, ultraviolet A (UVA)-, and drug-induced senescence. Moreover, QM-Nhαfuc could also help in identifying senescent cells that lacked β-gal expression and enabled *in vivo* non-invasive real-time senescence tracking (Fig. 18).[222] These findings show that the high bioimaging capability and selectivity of AIEgen probes support their applications for *in vitro* and *in vivo* senescence bioimaging over traditional fluorescent probes.

In other diseases or biological processes beyond the above-mentioned diseases, the novel AIEgens were also developed for imaging *in vivo*, such as the OTPA-BBT dots that were synthesized for non-invasive fluorescence hysterography in near-

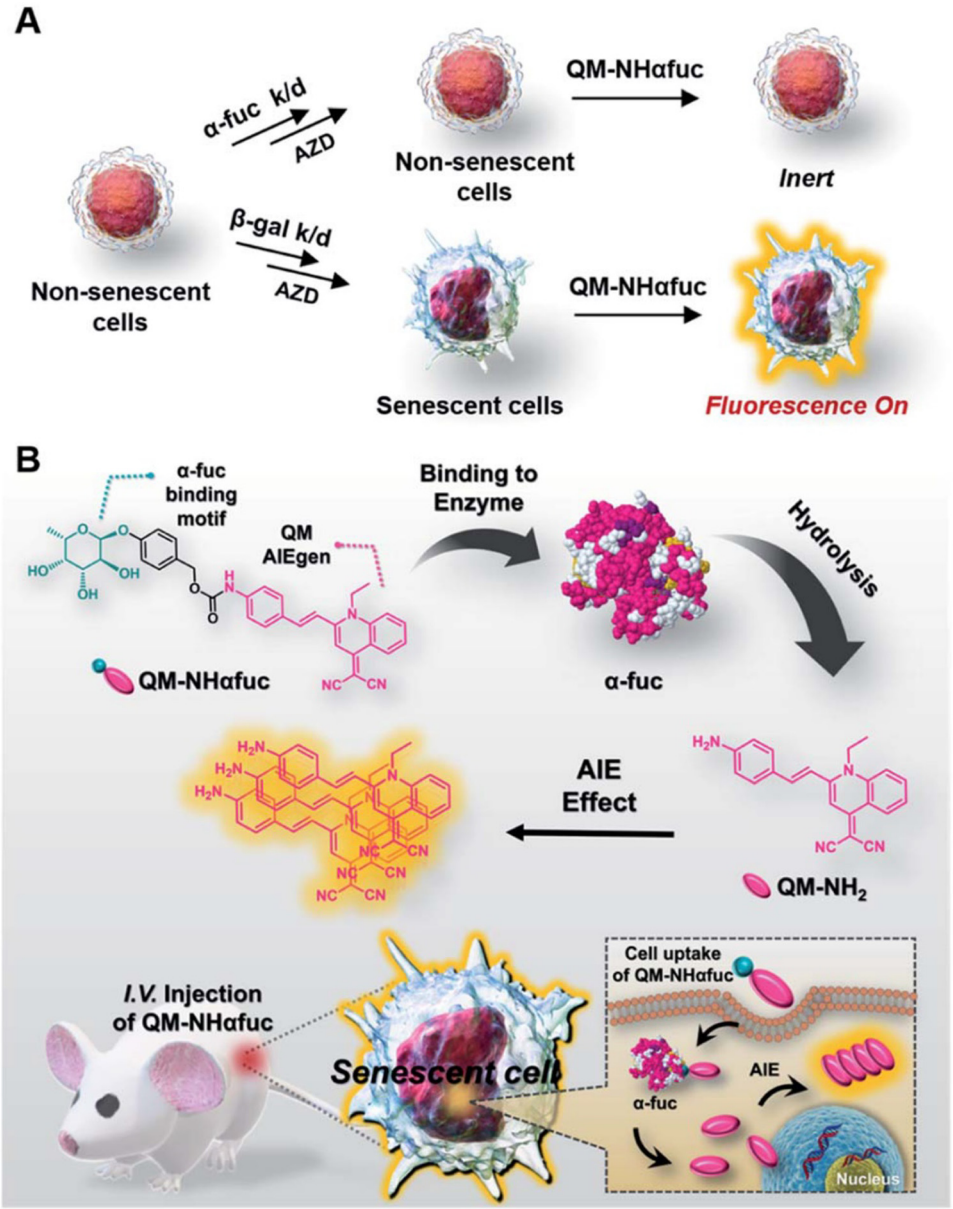

Fig. 18 Rational design of QM-Nhαfuc for senescent cell detection and imaging. Adapted with permission from ref. 222. Copyright 2021 Royal Society of Chemistry.

infrared IIb window,[223] CSMPP with lysosome targeting capability for monitoring tissue regeneration.[224] On the other hand, more attention is valuable to put into the field of rare diseases.

4. Bioimaging guided treatment of noncancerous diseases with smart AIEgens

Similar to cancer, which is characterized by various abnormal features such as a low pH value, hypoxia, high content of ROS, aberrant metabolism, and altered gene expression and modifications, noncancerous diseases can also be identified based on typical features that differentiate affected tissues from normal tissues at the molecular and tissue levels. From the viewpoint of therapeutics, simple and effective strategies are valuable pursuits in the fundamental and clinical research. Traditional probes and therapeutic agents usually have a single function – they help with only detection, bioimaging, or treatment. However, they can rarely be incorporated into theranostic platforms and multi-step rational design becomes necessary. However, AIEgens possess multiple properties that confer them with great advantages over traditional probes and therapeutic agents, these properties allow not only imaging but also endow them with the potential for applications in therapeutic modalities. They can be used as drug delivery platforms[225] for photothermal therapy (PTT),[226,227] photodynamic therapy (PDT),[228] radiotherapy (RT),[229] sonodynamic therapy (SDT),[230] immunotherapy,[231] and

synergistic therapy.[232–234] Accordingly, AIEgens are regarded as "all-in-one athletes" for disease detection, diagnosis, bioimaging, and therapeutics. More importantly, AIEgens show good biocompatibility and biosafety that are prerequisites for biological applications. Until now, a lot of AIEgens have been proven to serve as excellent therapeutic platforms for the bioimaging-guided treatment of non-cancer diseases with extreme specificity and effectiveness. Therefore, the latest advances in AIEgen-based bioimaging-guided therapeutic applications for non-cancer diseases are summarized in this section.

4.1 Infectious disease therapeutics

As described in the previous section, bacteria, fungi, and viruses are the three main pathogens causing infectious diseases and several infectious diseases show high transmission speeds and multiple transmission routes and cause severe acute damages. For example, COVID-19 continues to threaten public health around the world even 3 years after it was first detected. The effective ways of stopping infectious diseases include the inhibition of pathogen multiplication, cutting off of routes of transmission to prevent broad transmission, and so on. Thus, greater efforts are needed urgently. Compared with chemotherapy for infectious diseases, treatment with AIEgen-based modalities has shown prominent outcomes in terms of protection[235,236] and therapeutics.[237,238]

The most effective method to cure an infectious disease is to kill the pathogen completely. PDT has received great interest owing to its high-precision treatment of infectious diseases. In the article published in Nature Photonic, Dr Nicholas Kipshidze proposed PDT as an effective method for combating COVD-19.[239,240] In PDT, photosensitizers (PSs) and light irradiation are employed to induce the generation of various ROS. The ROS, in turn, induce oxidative damages in biological molecules, including nucleic acids, proteins, and lipids, which induce an irreversible death cascade to kill the virus, this technique has a lot of advantages, including its minimally invasive nature and low systemic toxicity.

The outcomes of PDT are directly linked to the PS employed during treatment. However, owing to their coplanar structures, most PSs show an extensive decrease in fluorescence intensity and ROS-sensitizing efficiency with time. Under these circumstances, agents such as AIEgen with excellent ROS generation capabilities that help in overcoming these shortcomings and achieve good treatment outcomes can be immensely valuable.[241] For example, Chen *et al.* developed a new AIEgen (DTTPB) to efficiently inactivate the human coronavirus (Fig. 19A). DTTPB was made up by constituents of a hydrophilic head and two hydrophobic tails, thus, mimicking the structure of phospholipids on biological membrane phospholipids (Fig. 19B). It had a broad absorption band covering the complete visible light range (maximum at 505 nm) and also showed fluorescence emission (606 nm) and high molar absorptivity (5.4×10^4 L mol^{-1} cm^{-1}) *in vitro*, these effects were accompanied with its superior ROS-sensitizing ability (Fig. 19C and D). Based on the hydrophilic head and hydrophobic tails, DTTPB could target the membrane and bind to the envelope of human coronaviruses (Fig. 19E), following NIR laser irradiation, it exhibited excellent antiviral effects *via* generating high levels of

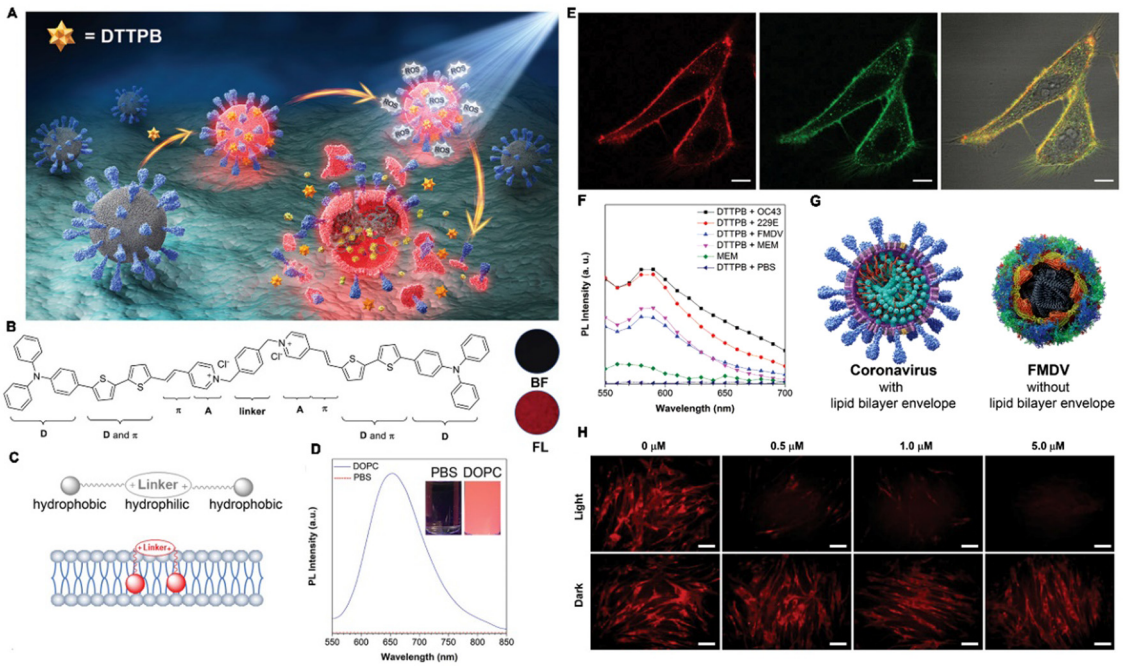

Fig. 19 (A) Diagram of the PDI process of coronaviruses with DTTPB. (B) The chemical structure of DTTPB. (C) Diagram of DTTPB structure and the interaction with membrane structure. (D) The PL spectra of DTTPB, inset: photograph of DTTPB in PBS solution with or without DOPC under UV lamp. (E) Co-localization of DTTPB in HeLa cells. (F) The PL spectra of DTTPB. (G) Structural characteristics of (left) COVID-19 and (right) foot-and-mouth disease virus. (H) Immunofluorescent staining of PDT against virus. Adapted with permission from ref. 242. Copyright 2019 American Chemical Society.

ROS and inducing a complete loss of infectivity (Fig. 19F–G).[242] Other AIEgens, including PSGMR, were also shown to fight SARS-CoV-2, the virus causing COVID-19, *via* the disruption of cellular mitochondria,[243] 2TPE-2NDTA was also applied for PTT,[244] aimed at fighting against SARS-CoV-2 and achieved good outcomes.

Fungi are another pathogens that cause severe infectious diseases. To treat a fungal infection, Tang *et al.* developed a novel AIEgen platform named DPNAP to selectively combat fungi (Fig. 20A). A salicylaldehyde Schiff-base with hydroxyl groups was introduced into DPNAP, it not only endowed the ability of strong ROS generation capability and AIE activity *via* extending conjugation and the restriction of intramolecular rotation, but also endowed the good selectivity towards Gram-positive bacteria and fungi and acid-responsiveness (Fig. 20B). The nanoplatform showed strong fluorescence emission at about 560 nm (Fig. 20C and D) and excellent PDT efficiency (Fig. 20E). DPNAP could recognize fungi and label them with bright fluorescence, which was not observed for bacteria and it exerted PDT effects against multiple microbes (Fig. 20F–I). Moreover, DPNAP was capable of eradicating a supergerm of drug resistant fungi (methicillin-resistant *S. aureus*) (Fig. 20J–L).[245]

In the past years, tuberculosis (TB) represents a large public health burden worldwide. It is a disease caused by *Mycobacterium tuberculosis* (M.tb) infection. At present, there are no effective methods for completely curing TB. For achieving excellent PTT and PDT effects, red/near-infrared (NIR) emissions that can penetrate the deep tissue affected by TB are required. Under these circumstances, Huang *et al.* performed anti-TB treatment using an AIEgen as a drug (rifampicin) carrier. The AIEgen (TTD) fluorophore, (2,6-bis((*E*)-4-(phenyl(4′-(1,2,2-triphenylvinyl)-[1,1′-biphenyl]-4-yl)amino)styryl)-4*H*-pyran-4-ylidene)malononitrile, possessed photosensitizer characteristics. The RIF-loaded AIE carrier (TTD + RIF NPs) was synthesized using a modified bottom-up approach (Fig. 21A). TTD showed strong fluorescence intensity at 633 nm. The TTD + RIF NPs could target preliminary granulomas formed at the early stage of infection in zebrafish embryos and a mouse tail mode and tracked the granuloma in zebrafish granuloma mode (Fig. 21B and C). Following white-light irradiation, they could release the loaded rifampicin (RIF), achieving chemotherapy and induce the generation of ROS for PDT, as a result, they could achieve the fluorescence imaging-guided synergistic treatment of persistent bacteria that were capable to induce TB (Fig. 21D–G). Moreover, TTD + RIF NPs also exerted robust antibacterial effects against clinical drug-resistant bacterial strains causing TB.[246] In another study, the AIEgens (TTD NPs) were applied as the fluorophore for imaging and imaging-guided PDT (UCNP@pyrolipid) against TB.[247]

The treatment of bacterial diseases using AIEgens is a hot-spot of the research at present. Many studies have revealed that AIEgens can serve as photosensitizers for phototherapy in PTT and PDT and effectively kill bacteria, thus curing infectious diseases, even in drug-resistant cases.[59,248–256] For instance, to expose bacteria hiding within host phagocytes and thus prevent

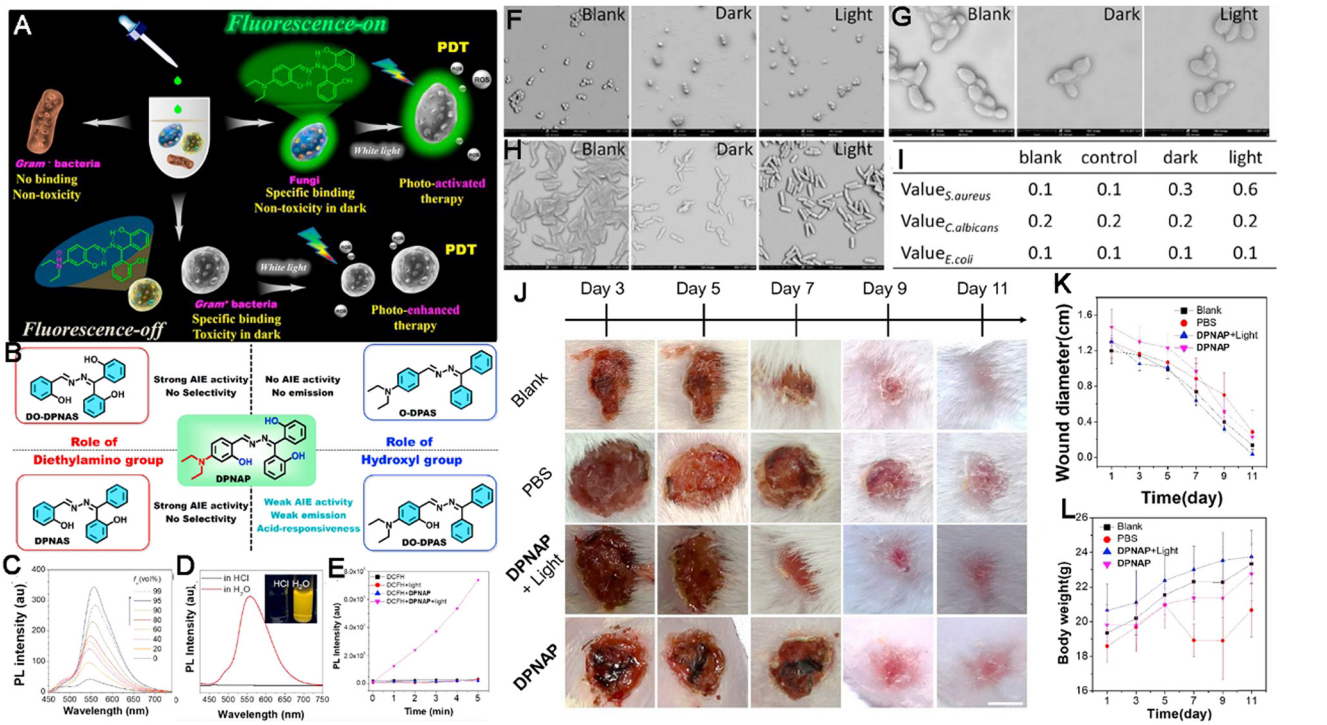

Fig. 20 (A) Diagram of DPNAP antimicrobe. (B) Structures of DPNAP. (C) The fluorescence spectra. (D) The fluorescence spectra under different conditions, inset: photograph of DPNAP in water and acid aqueous. (E) *In vitro* PDT. (F–H) The SEM images of *S. aureus* (F), *C. albicans* (G) and *E. coli* (H) after treatment. (I) Nucleic acid detection. (J) Photographs of infected skin, (K) the sizes of the infected areas and (L) body weights. Adapted with permission from ref. 245. Copyright 2021 Elsevier Ltd.

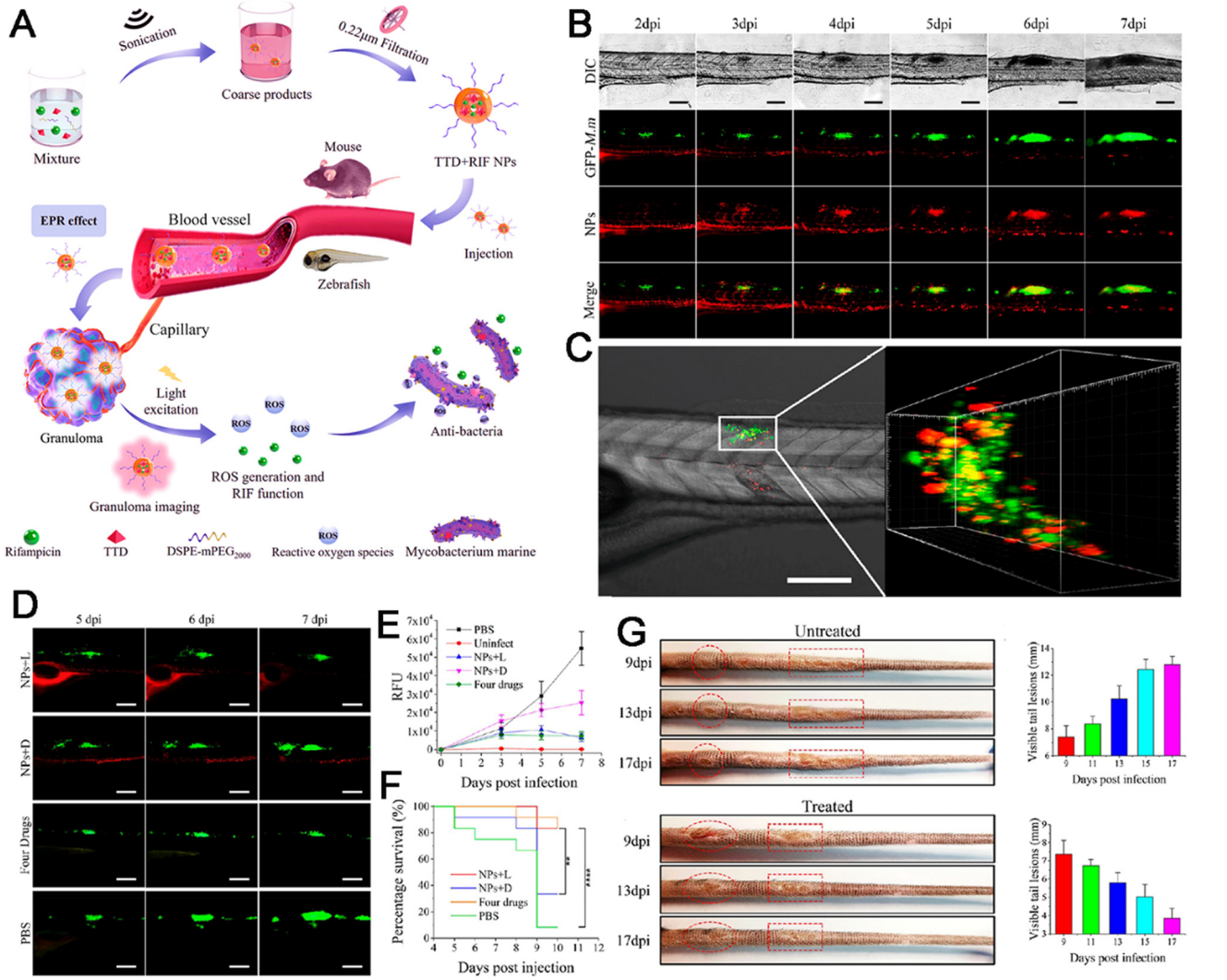

Fig. 21 (A) Diagram of TTD + RIF NPs anti-TB therapy. (B) Granuloma tracking in zebrafish. (C) The CLSM imaging (left) and 3D CLSM imaging (right) of granulomas. (D) The fluorescence images of GFP-M.m. (E) The Fluorescence intensities of GFP-M.m shown in (D). (F) Survival analysis. (G) Photographic images of tail lesions. Adapted with permission from ref. 246. Copyright 2020 American Chemical Society.

phagocyte disorders and subsequent local and systemic tissue damages, Liu *et al.* developed a HClO-activatable AIEgen nanoplatform in which an AIEgen served as a theranostic nanoprobe, named DTF-FFP NPs, to achieve bioimaging-guided bacterial ablation in phagocytes (Fig. 22B). DTF-FFP NPs were synthesized by the nanoprecipitation of an HClO-responsive FFP, an efficient PS DTF. The encapsulation matrix was Pluronic F-127 (Fig. 22A). By serving as energy acceptor, FFP quenched both fluorescence and the production of ROS of DTF, eliminating the phototoxicity of DTF-FFP NPs in normal cells and tissues. The DTF NPs without FFP exhibited brilliant fluorescence emission around 660 nm under the excitation at 488 nm (Fig. 22C). When DTF NPs were added to different concentrations of HClO, they emitted red fluorescence intensity (near 800 nm) constantly (Fig. 22D) and with the addition of HClO combined with light irradiation, the ROS generation was increased effectively (Fig. 22E). DTF-FFP NPs targeted to *S. aureus* hiding within the lumen of RAW264.7 cells *in vitro* (Fig. 22F), upon light irradiation, *S. aureus* was killed effectively *via* PDT effects (Fig. 22G). Delivered to the infection sites *in vivo*, DTF-FFP NPs also emitted red fluorescence and efficiently generated ROS owing to the degradation of FFP by the high content of HClO in phagocytes for fluorescence imaging-guided precise PDT against bacteria (Fig. 22H).[248] Thus, this study confirmed the selective activation of fluorescence and photosensitization *via* AIEgens owning high effectiveness and theranostic potentials in precise bacterial therapy.

Compared to chemotherapy, AIEgen-based therapeutic strategies such as PDT and PTT show higher therapeutic efficacy in the treatment of infectious diseases, these strategies help in completely and directly killing pathogens and overcoming obstacles caused by drug resistance. More importantly, the high targeting capability of these techniques guarantees precise ablation and decreases any potential adverse effects. Therefore, more applications should be developed.

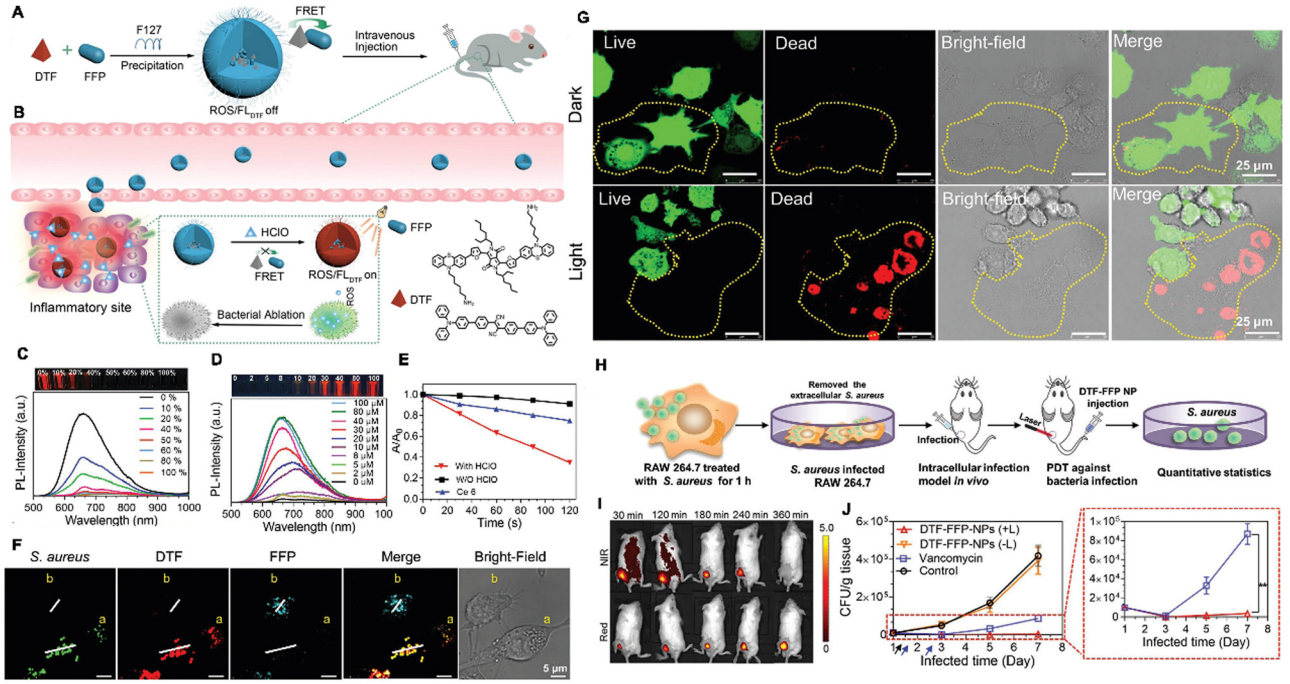

Fig. 22 (A and B) Diagrams of DTF-FFP NP preparation and anti-bacteria inside the invaded phagocytes. (C) PL detection. (D) The fluorescence of turn-on effect. (E) Decomposition rates of ABDA. (F) The confocal fluorescence images of RAW264.7. (G) Representative images of live and dead staining. (H) *In vivo* model of *S. aureus*-intracellular infection. (I) The *in vivo* fluorescence images. (J) Antibacterial activities *in vivo*. Adapted with permission from ref. 248. Copyright 2020 Wiley-VCH GmbH.

4.2 Injury therapeutics

Injury can occur in daily life due to trauma, burns, surgeries, traffic accidents, and toxin consumption. Hence, the rapid and appropriate treatment of injuries is required to prevent concomitant deterioration and disease development or even substantial morbidity and mortality. Notably, infectious injuries caused by microbes are difficult to heal fully. An ideal injury dressing that enables immediate wound closure and patient-specific treatment and shows effective antibacterial action is highly anticipated. However, conventional injury dressings can only provide wound closure and slowly promote the injury-healing process. Because of their excellent imaging capabilities and feasible therapeutic applications, AIEgens have been applied in the imaging-guided treatment of injuries.[257] Tang and Zhao developed a novel AIEgen therapeutic nanoplatform for dressing long-term antibacterial activity during the wound healing process (Fig. 23A and B) based on a typical AIEgen (TBP). The UV-vis spectra showed that TBP owned a wide absorption arrange from 400 to 600 nm, absorption peaks at 500 nm and the peak emissions of TBP and TBP/TCL occurred at about 737 nm (Fig. 23C and D). When *S. aureus* and MRSA were irradiated by white-light illumination after incubation with TBP/PCL nanofibers, significant ROS generation and enhanced bacterial killing efficacy *via* PDT were observed (Fig. 23F and G), which kept the excellent biocompatibility and promoted the induction of inflammation effectively, acceleration of wound healing significantly (Fig. 23H–L). More importantly, TBP/PCL demonstrating its potential in the management of emergencies.[258] Another novel AIEgen, triphenylethylene-naphthalimide triazole (TriPE-NT), was also synthesized by Tang and colleagues for staining and killing multidrug-resistant (MDR) Gram-positive and Gram-negative bacteria *via* efficient PDT effects, thereby promoting the healing of MDR bacteria-infected wounds.[259] With the exception of infectious injuries, the treatment of other injuries such as liver injury can be developed further with more rational designs.

4.3 Cardiovascular disease therapeutics

CVDs are serious causes of death around the world and often show sudden onset. Although drugs have proven effective in treating CVDs to a certain degree, the demand for better therapeutic strategies persists. Previous studies indicate that the biogenesis of various CVDs is complicated. Hence, synergistic therapeutic strategies for all-in-one treatment appear to be the future trend of the fundamental research and clinical applications. For example, in ALS, it is important to target plaques, reduce local inflammation, and remove lipid bodies in order to achieve comprehensive ALS therapy.[104] By exploiting ROS overexpression as a marker and stimulus for ALS therapy, Wang and Li developed a novel therapeutic platform for achieving ALS detection and imaging-guided therapy. In this platform, a two-photon AIEgen (TP) was linked to β-cyclodextrin (CD) *via* an ROS-responsive bond and loaded with prednisolone (Pred) in the entocoele *via* supramolecular interaction. Accordingly, a two-photon fluorophore–cyclodextrin/prednisolone complex (TPCDP) was prepared. Then, TPCDP was packaged into nano-sized micelles based on an ROS-sensitive copolymer poly (2-methylthio ethanol methacrylate)-poly(2-methacryloyloxyethyl

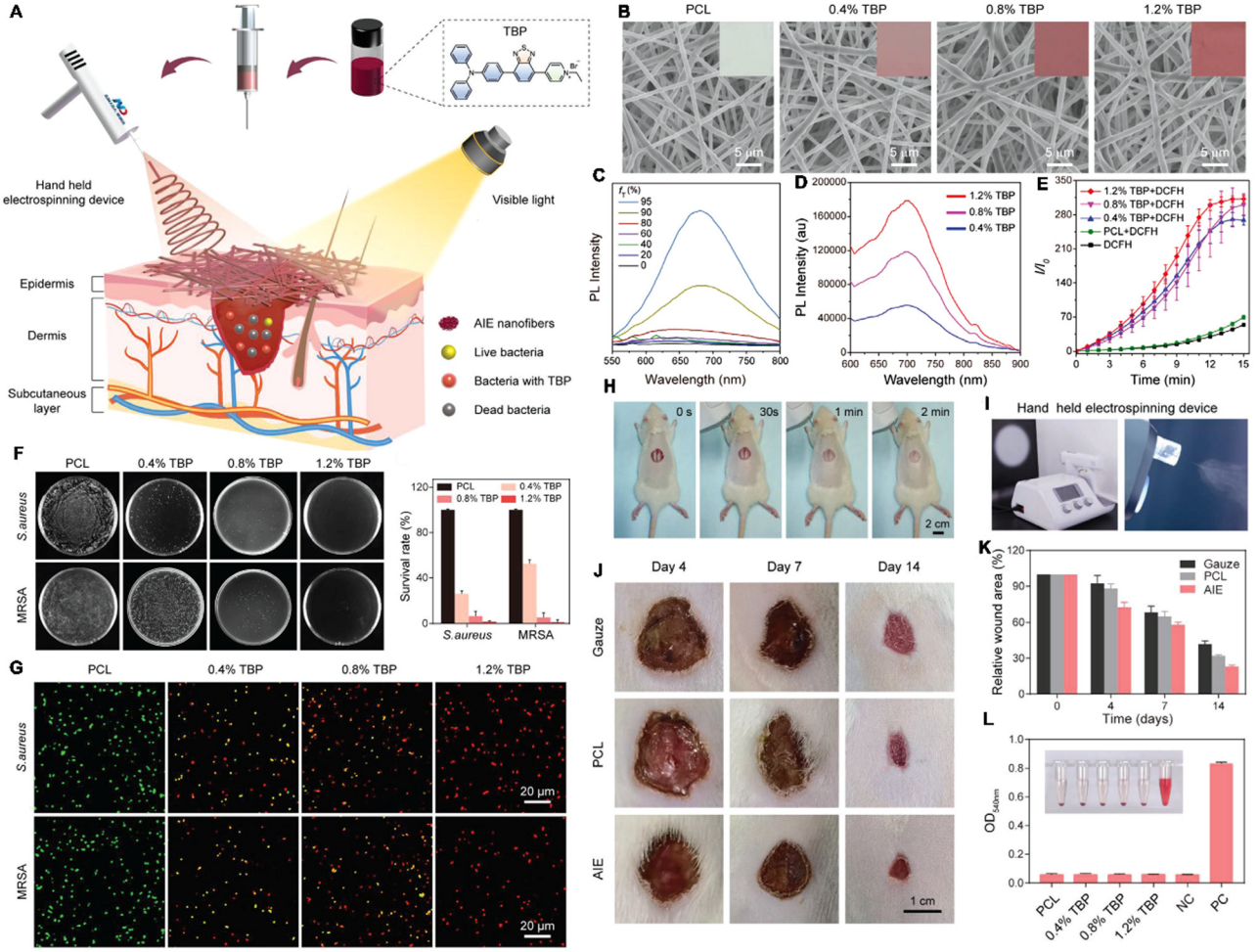

Fig. 23 (A) Diagram of electrospinning AIEgen-incorporated antibacterial dressing in treating surface wounds. (B) The SEM images of PCL nanofibers. (C) The PL spectra of TBP. (D) The PL spectra of PCL nanofibers. (E) The spectra of DCFH. (F) Photos and survival rates of *S. aureus* and MRSA treated with TBP/PCL nanofibers. (G) The confocal images after treatment with TBP/PCL nanofibers. (H) *In situ* deposition of AIE nanofibers on the wounds. (I) Photos of the hand-held electrospinning device. (J) Photographs of the wounds. (K) The ratios of MRSA-infected wound area. (L) Hemolysis test, inset: photograph of hemolysis incubated with PCL nanofibers. Adapted with permission from ref. 258. Copyright 2022 Wiley-VCH GmbH.

phosphorylcholine) to obtain TPCDP@PMM for ALS diagnosis (Fig. 24A and B). Based on the aggregation in water solution and the reconstituted aggregation of TP by the hydrophobic interaction, the fluorescent spectra revealed that TPCDP@PMM showed a strong fluorescence emission in pure water and H_2O_2 solution at about 580 nm (Fig. 24C), indicating the wonderful adaptation for the bioimaging of TPCDP@PMM at the atherosclerotic site and the Pred was released from TPCDP@PMM responsive to increase of H_2O_2 content (Fig. 24D). After accumulation in atherosclerotic tissues through the damaged vascular endothelium, TPCDP@PMM responded to local ROS overproduction and the lipid-rich environment, TPCDP was disintegrated and the Pred was released. The TP within TPCDP@PMM allowed a distinct two-photon AIE imaging (Fig. 24E–G) for ALS recognition for ALS detection, and the Prep exerted anti-inflammatory and lipid removal effects for two-photo fluorescence imaging-guided ALS inhibition by downregulating the expression of inflammatory proteins and cytokines (Fig. 24H–J).[260] In another study, a novel AIEgen, DPA-SCP, acted as the fluorescent probe and allowed the tracking of extracellular vesicles from mesenchymal stem cells, it helped in rescuing the function of mitochondria to treat renal ischemia-reperfusion injury.[261] With regard to the treatment of CVDs, the therapeutic capacity of AIEgens has not been fully utilized beyond their excellent imaging of drug delivery capabilities. Therefore, more endeavors are needed to put forth additional effective modalities for CVD treatment based on novel AIEgens.

4.4 Neurodegenerative disease bioimaging-guided therapeutics

With aging population, the burden of neurodegenerative diseases is expected to increase sharply. A complete understanding of the molecular mechanisms causing these diseases is currently lacking, due to which effective treatments have not been developed successfully. Meanwhile, due to the complex structure of the brain, imaging is important for guiding the therapy. Unlike in theranostics in the field of cancer, which combines various therapeutic modalities, AIEgens are seldom applied for the

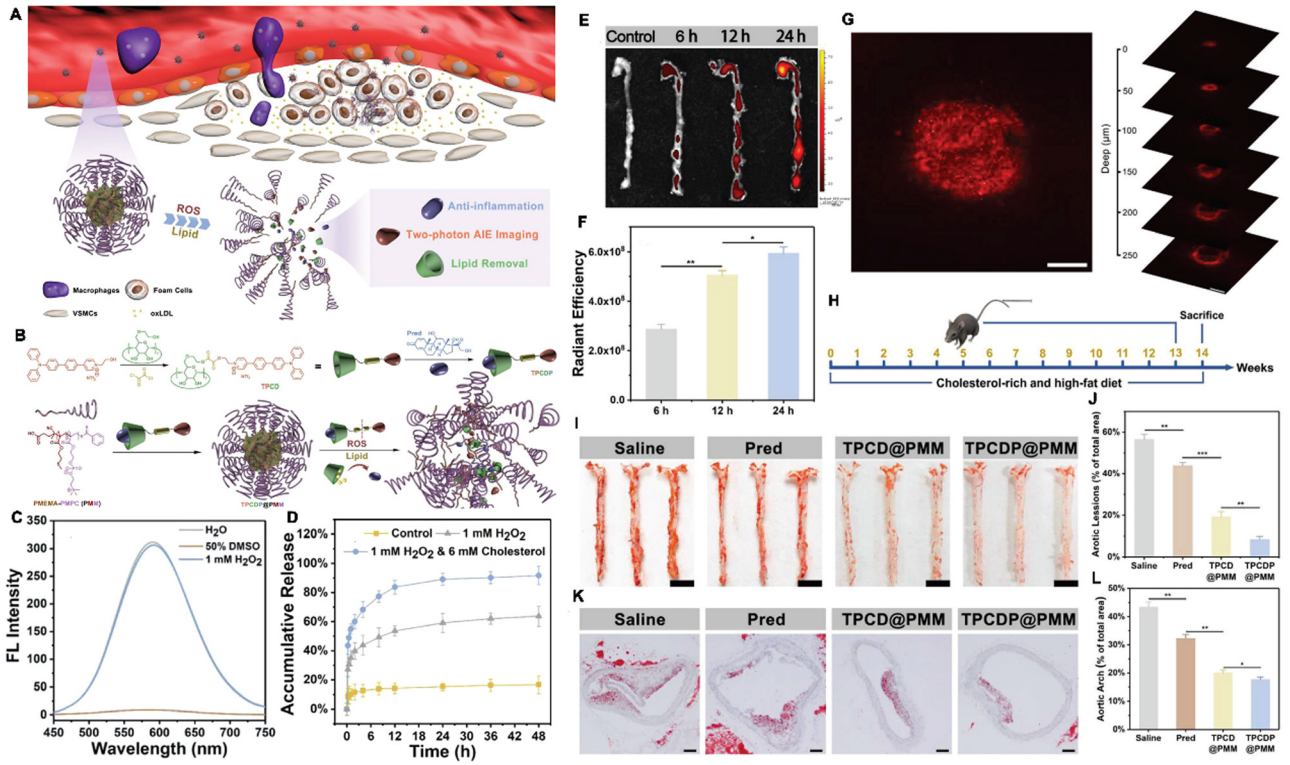

Fig. 24 (A) Diagram of TPCDP@PMM for atherosclerosis plaque recognition and inhibition. (B) Illustration of TPCDP@PMM preparation and its responsive behavior. (C) The fluorescence spectra. (D) Accumulative Pred release. (E) The *ex vivo* fluorescence images and (F) quantitative results of TPCDP@PMM. (G) The projection image of atherosclerotic plaques. (H) Treatment protocol. (I) Photographs of ORO-stained en face aortas and (J) quantitative results of the ORO positive areas. (K) Sections of aortic arch stained with ORO and (L) quantitative analysis. Adapted with permission from ref. 260. Copyright 2020 Wiley-VCH GmbH.

treatment of neurodegenerative diseases. Based on the pathological characteristics of AD, *i.e.*, excessive Aβ accumulation (fibrils and plaques) and the subsequent activation of neurotoxic cascades, under these conditions, Tang, Li and Gao collaboratively developed two new AIEgens named Cur-N-BF_2 and Cur-O-BF_2 with strong D–A structural features and TICT effects, for the detection and treatment of AD under the guidance of fluorescence imaging (Fig. 25A), which was especially important because Aβ itself causes the quenching of some fluorescent probes. The maximum fluorescence emissions of Cur-N-BF_2 and Cur-O-BF_2 were observed at 572 and 655 nm and the QYs were 14.0% and 1.2%, respectively (Fig. 25B–E). In HT22 cells, Cur-N-BF_2 – but not Cur-O-BF_2 – exhibited excellent biosafety, its fluorescence intensity was even higher in the presence of $A\beta_{1-42}$ fibrils *in vitro* and selectively stained these fibrils *in vivo* (Fig. 25F–H). More important, Cur-N-BF_2 inhibited the fibrillation of Aβ and promoted the disassembly of Aβ fibrils, protecting the neuronal cells from the toxicity of Aβ (Fig. 25I).[116] More, DNTPH was also developed for detection and imaging-guided therapy against AD[262] and a UCNP–peptide–AIEgen nanoprobe loading siMMP3 was constructed for detection and imaging-guided therapy against PD.[263] Meanwhile, Liu *et al.* developed a novel AIEgen-based amyloid inhibitor probe named AIE@amyloid by site-specific conjugation of an AIEgen with amyloid proteins, Aβ and α-synuclein (αSN) to help the screening of drug. The AIE-amyloid probe alone exhibited strong fluorescence emission at ~480 nm due to amyloid-like aggregation, but showed no fluorescence in the presence of amyloid inhibitors that prevented amyloid aggregation. By combining the AIE@-amyloid probes with computational virtual screening, a drug named tolcapone was screened out. Tolcapone could inhibit both the aggregation and cytotoxicity of Aβ and αSN and its administration led to significant improvements in spatial cognition and recognition in Aβ-treated mice.[264] Up till now, few studies have reported the capability of AIEgens in combination with different modalities for the treatment of neurodegenerative diseases. Since there are great advantages of AIEgens in terms of the detection and bioimaging of neurodegenerative diseases, therapeutic strategies are urgently needed.

4.5 Surface organ-associated disease therapeutics

Surface organs, including the skin, mouth, nose, ears, and eyes, play different functions and provide primary protection from external agents. The rapid treatment of any damage to these organs can help in preventing further internal deterioration and concomitant disease development, especially in the case of infection with drug-resistant microbes. Among these organs, the eye is the most vulnerable. Thus, more methods are needed to effectively treat any eye damage. Due to their high targeting capability and multi-functional effects in simultaneous bioimaging-guided therapy, AIEgens show great potentials in the treatment of surface organ-associated diseases.[265,266]

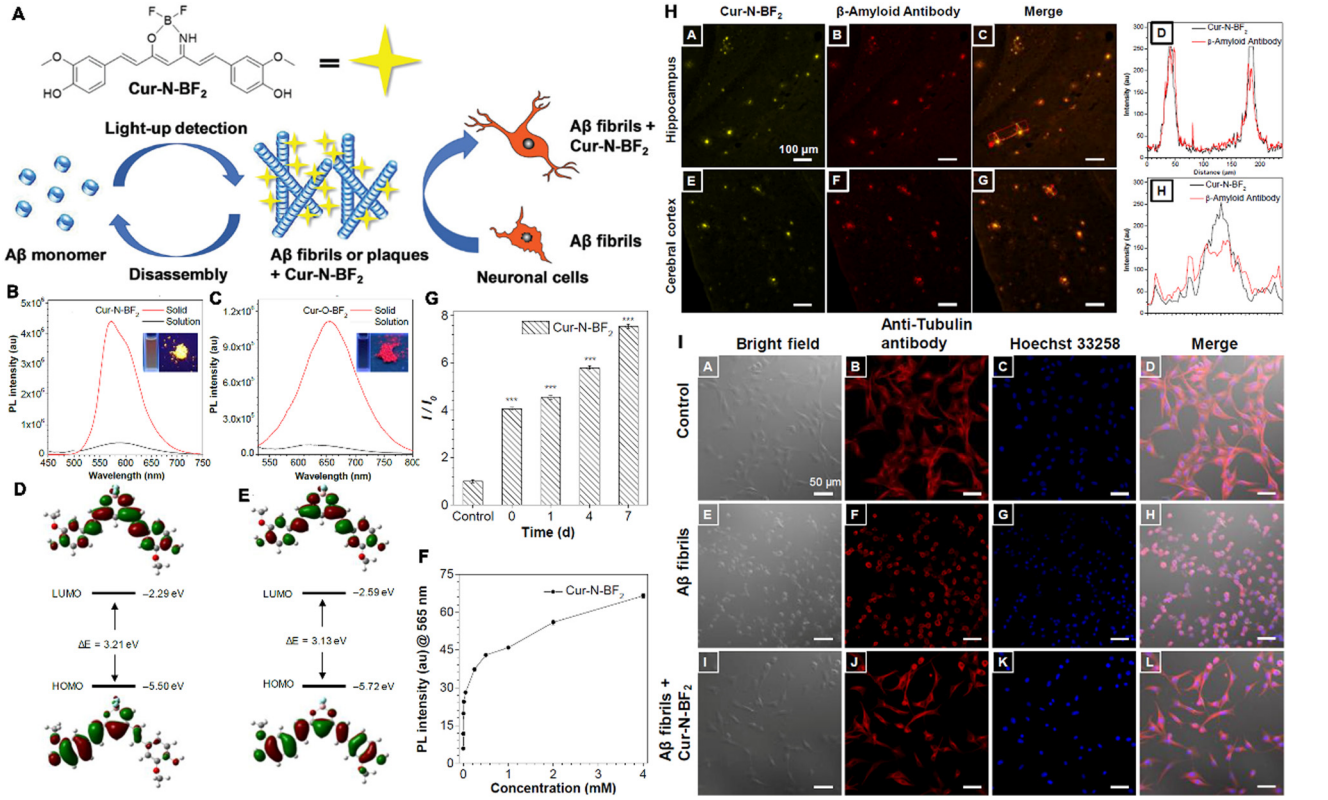

Fig. 25 (A) Diagram of Cur-N-BF_2 for detection, imaging and therapeutics of AD. The PL spectra of (B) Cur-N-BF_2 and (C) Cur-O-BF_2, inset: the photographs of Cur-N-BF_2 and Cur-O-BF_2 in aqueous solution (left) and the solid state (right) under UV irradiation. The optimized molecular orbital amplitude plots of (D) Cur-N-BF_2 and (E) Cur-O-BF_2. (F) The PL of Cur-N-BF_2 response to $A\beta_{1-42}$ fibrils. (G) PL intensity of Cur-N-BF_2 response to $A\beta_{1-42}$ fibrils. (H) The CLSM images of slices. (I) Protection action of HT22 cells. Adapted with permission from ref. 116. Copyright 2019 The Royal Society of Chemistry.

Keratitis is a serious ocular disease caused by microorganisms, it represents a major treatment challenge and often results in ocular morbidity and blindness.[267] Tang and Shi developed three AIEgens, named IQTPE-2O, IQ-Cm, and IQ-TPA (Fig. 26A), all three AIEgens had a cationic isoquinolinium (IQ) moiety and appropriate hydrophobicity, for selective photodynamic killing of fungi and efficacious treatment of keratitis (Fig. 26B). These three AIEgens showed the absorption maximum wavelengths at around 430, 440, and 450 nm, respectively, with extinction coefficients of about 104 M^{-1} cm^{-1}, and emission peaks at about 600, 650, and 610 nm with high QYs (5.1%, 14.1% and 19%, respectively) (Fig. 26C). Upon incubation with bacteria and cells, the three AIEgens can target to the mitochondria of *C. albicans* only but not normal mammalian cells (Fig. 26D), following white light irradiation, the irreversible damage to fungal mitochondria and further death were induced by effective generation of ROS ($^1O_2$), thus killing the bacteria effectively (Fig. 26E). Among the three AIEgens, IQ-TPA showed the most superior PDT efficiency against fungi and also produced negligible toxicity in mammalian cells. Thus, it can achieve the selective and highly efficient killing of keratitis-causing fungi. This PDT strategy showed better therapeutic outcomes in treating fungal infections in a rabbit model than the clinical standard, rose bengal (Fig. 26F–I).[268] This AIEgen was the first trail, which was applied for the detection, imaging-guided therapeutics of keratitis. Meanwhile, many diseases affecting the surface organs require better therapeutic strategies. Therefore, based on the excellent advantages of AIEgens, attention should be drawn to their applications in this regard.

4.6 Bioimaging-guided therapeutics of orthopedic diseases

Compared with cancer and other diseases, orthopedic diseases lack effective methods for imaging and treatment. The development of therapeutic AIEgens for other diseases brings hope for overcoming these existing problems. In orthopedic diseases, inflammation and the overgeneration of ROS are often present. Wang *et al.* developed a theranostic nanoplatform (TPP@PMM) with ROS-responsive behavior for two-photon AIE bioimaging. They used this platform for the diagnosis and treatment of acute lung injury, arthritis, and atherosclerosis (Fig. 27A and B). TPP@PMM was generated by attaching Pred to a two-photon fluorophore (TP) *via* an ROS-sensitive bond to obtain TPP, which was encapsulated within the amphipathic polymer PMPC–PMEMA (PMM) through self-assembly into core–shell micelles (Fig. 27C). The TPP@PMM platform showed a maximum emission at about 600 nm (Fig. 27D) and the Pred was responsive to the higher ROS (H_2O_2) content to release the Prep (Fig. 27E). Upon incubation with RAW264.7 cells, TPP@PMM was internalized rapidly to inhibit the generation of inflammatory cytokines, including TNF-α, IL-1β and

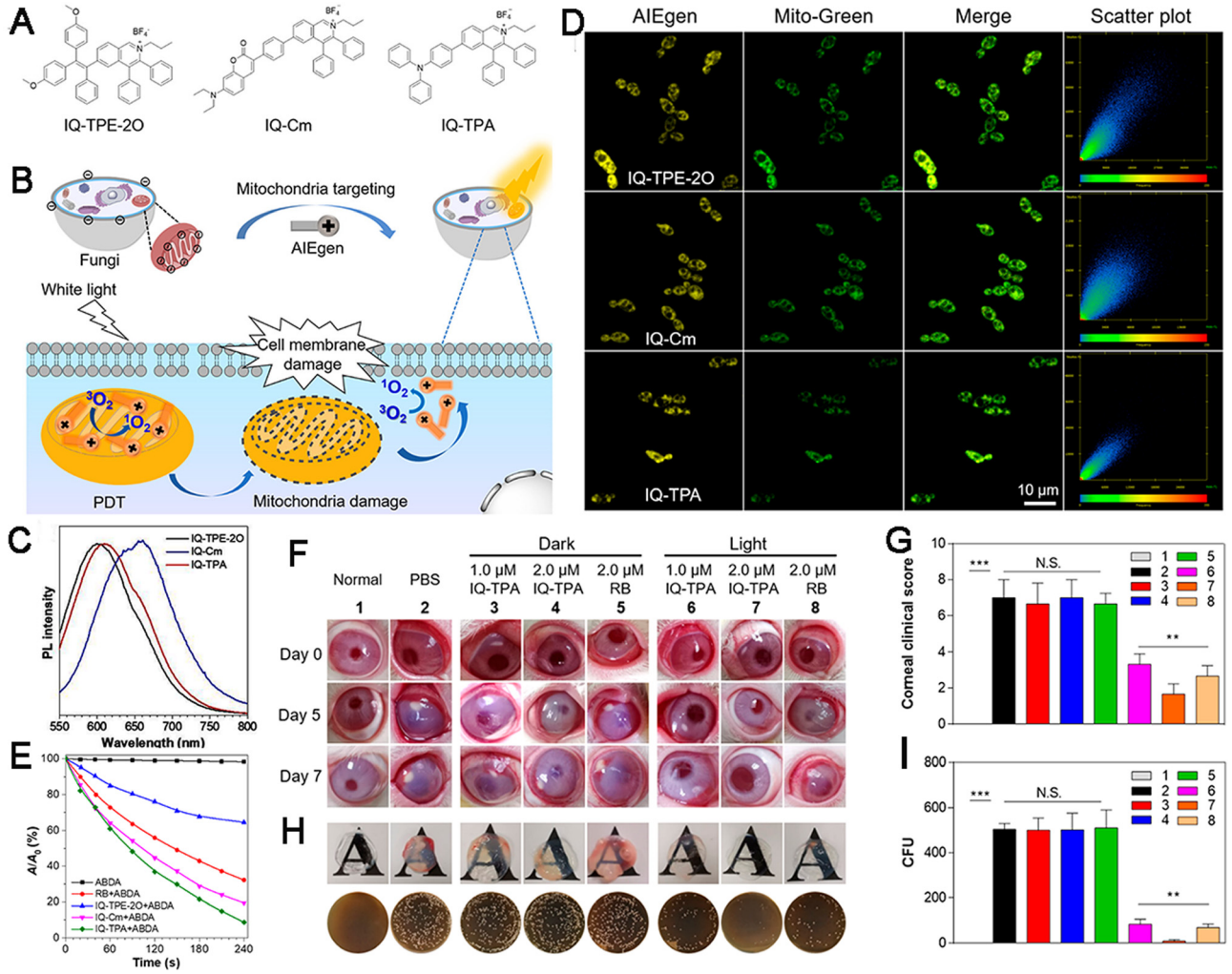

Fig. 26 Molecular structures (A) and diagram (B) of an AIEgen against fungi of keratitis. (C) The normalized PL spectra. (D) Colocalization imaging of *C. albicans*. (E) Absorbance of ABDA. (F–I) Disease progression of fungal keratitis. (F) Photographs of rabbit eyes. (G) Clinical score. (H) The macroscopic views of corneas and fungal cultures on YPD agar plates and (I) the number of surviving. Adapted with permission from ref. 268. Copyright 2021 American Chemical Society.

MPO. TPP@PMM also exhibited distinct single-photon and two-photon florescence emissions, which enabled a distinct dimensional bioimaging of inflammation location with minimum autofluorescence interference and deeper imaging penetration. The vasculature at inflammatory tissue in the joint from arthritic mice induced by type II collagen is leaky, which attributed to the extravasation of TPP@PMM that promoted the targeting to joint with inflammation significantly (Fig. 27F–H). Then, the excessive ROS triggered micelle disassembly, the drug was delivered accurately, and reversed the deterioration of rheumatoid arthritis (Fig. 27I). Accordingly, the theranostics of the TPP@PMM platform achieved a high-resolution inflammation diagnosis and two-photo fluorescence imaging-guided efficient anti-inflammatory action.[269] This above study revealed the excellent bioimaging potentials of AIEgens in orthopedic diseases and their advantages over traditional probes, combined with their ability to provide chemotherapy and imaging-guided treatment. However, the complete applications of AIEgens in therapy have not been achieved yet and much attention must be drawn to this area.

4.7 Inflammatory disease therapeutics

Inflammatory diseases are refractory diseases that often result from infection by various pathogens and they contribute to the pathogenesis of various other diseases. At present, the induction of oxidative stress is a common and effective approach for the elimination of pathogens and imaging can promote improved therapeutic outcomes in clinical practice. Unlike conventional fluorescent dyes and therapeutic agents, AIEgens do not need to be incorporated into multicomponent systems, thus providing significant advantages.[212] For example, Wu *et al.* developed a nanosystem (QM@EP) for oral administration and the detection of colitis, followed by targeted drug delivery to the colon (Fig. 28A). QY–SN–H_2O_2 was based on an AIE-active chromophore QY–SN–OH with pentafluorobenzenesulfonate moieties, which could recognize the inflammatory biomarker

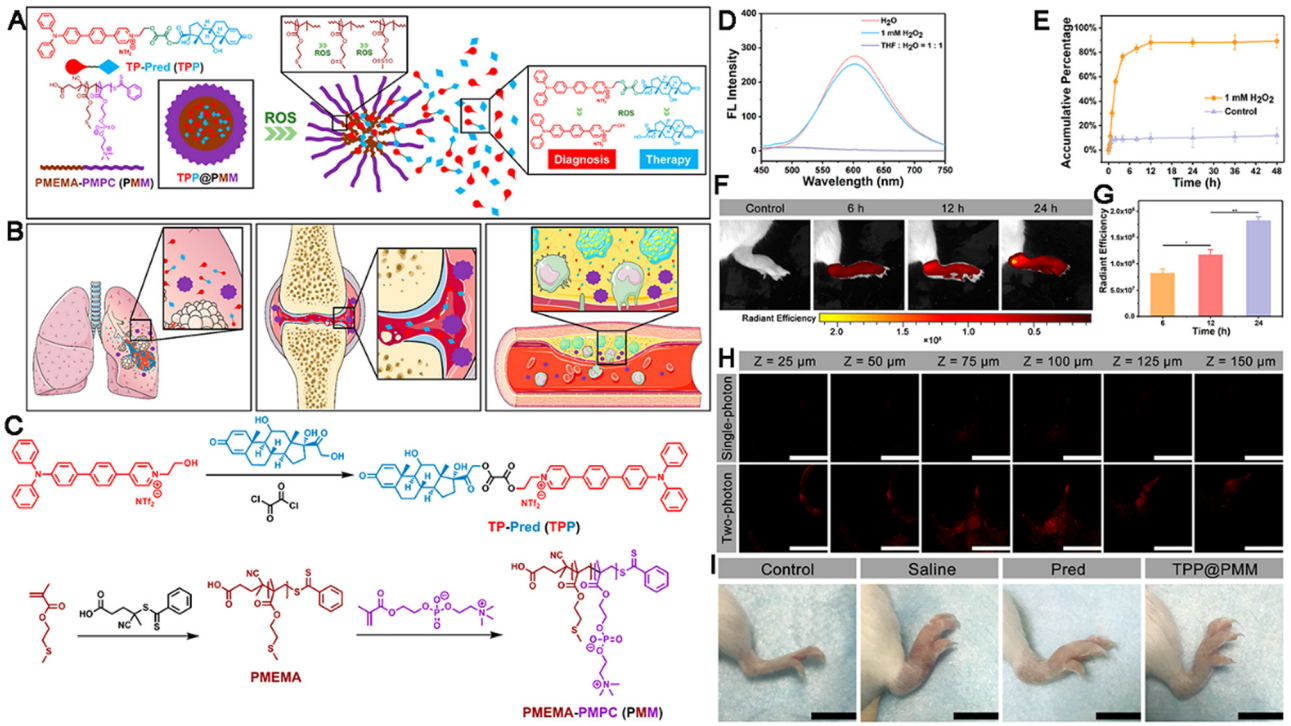

Fig. 27 (A) Diagram of nanoplatform with two-photon imaging and ROS sensitivity. (B) Models for inflammation theranostics. (C) Synthesis route. (D) The fluorescence spectra. (E) Accumulative Pred release. The *ex vivo* fluorescent images (F) and quantitative result (G). (H) Single-photon and two-photon confocal images of joint tissue. (I) Photographs of the right hind limbs with different treatments. Adapted with permission from ref. 269. Copyright 2020 American Chemical Society.

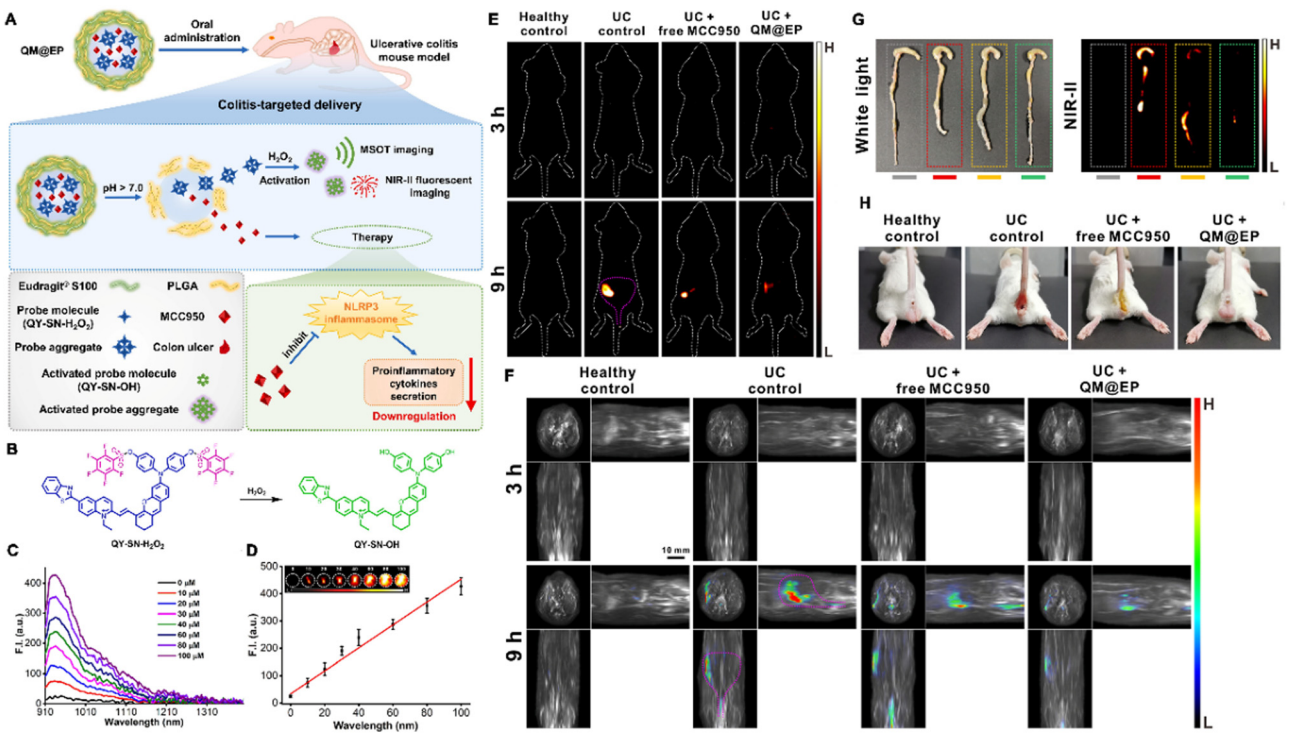

Fig. 28 Diagram of the nanosystem's action (A) and molecule transformation (B). (C) The NIR-II fluorescence spectra. (D) Fluorescence intensity. (E) NIR-II fluorescence imaging. (F) Orthogonal-view: 3D MSOT images. (G) Photographs under white light (left) and NIR-II fluorescence images (right) of the excised colons. (H) Photographs of the mice after different treatments. Adapted with permission from ref. 216. Copyright 2022 Elsevier Ltd.

H_2O_2 and act as a fluorescence quencher. Meanwhile, poly(lactic-*co*-glycolic acid) (PLGA) served as the sustained release excipient, whereas Eudragit® S100 was the excipient enabling the pH-controlled release of the drug formulation in the colon, while preventing premature release in the stomach (Fig. 28B). QM@EP emissions were ranged in 910–1200 nm (centered at 935 nm) (Fig. 28C) and showed ROS- and H_2O_2-responsive releases (Fig. 28D). Following oral administration in an animal model of ulcerative colitis, the pentafluorobenzenesulfonate moieties in QY–SN–H_2O_2 were cleaved and activated by the H_2O_2 and ROS present in the inflammatory environment, generating the AIE-active chromophore Q–SN–OH, as a result, strong fluorescence and PA signals were observed, enabling NIR-II fluorescence imaging (Fig. 28E) and MSOT imaging (Fig. 28F)-guided therapeutic efficacy against ulcerative colitis through inhibiting the information of NLRP3 inflammasome (Fig. 28G and H).[216] BPN-BBTD, another type of AIEgen, was found to be capable of imaging-guided surgery in the treatment of IBD.[136] Owing to their tunable emission wavelengths, AIEgens could contribute to the treatment of inflammatory diseases, even in deep tissues. However, reports on their applications in this area are limited, calling for new AIEgen-based strategies targeting improvements in therapeutic outcomes.

4.8 Senescence therapeutics

Senescence is an inevitable and natural process observed in all living systems. A senescence-associated secretory phenotype promotes the immune clearance of cells, driving chronic sterile inflammation and inducing a series of aging-related diseases. So far, some senolytic drugs, such as dasatinib, quercetin, and curcumin, have been developed for reducing the rate of aging.[270] Other strategies have also been adopted to reduce senescence, including heterochronic blood exchange.[271] These methods have shown positive effects in reducing senescence and its effects. However, senescent cells can promote senescence in normal cells. Thus, the timely elimination of senescent cells can also reduce the negative impact of senescence-related processes. Disappointingly, there is currently no effective tool for the guided and specific removal of senescent cells. By taking advantage of fluorescence imaging-guided therapy, Yang *et al.* designed a molecule called TPE-ETh-R-GFFY(gal)ERGD (Comp. 1) that can serve as a substrate for β-Gal and thereby generated TPE-ETh-R-GFFYERGD (Comp. 3). Subsequently, the supramolecular assembly of TPE-ETh-R was generated. This component showed fluorescence and an ROS-generating capacity, the TPE-ETh-R was found to exhibit fluorescence emission at 680 nm following aggregation. Meanwhile, Comp. 1 exhibited no fluorescence. Therefore, Comp. 1 could label and target senescent cells that overexpress β-Gal. Under white-light irradiation, higher levels of ROS could be detected, achieving PDT and completely killing senescent cells.[148] This first work inspired the further exploration of AIEgens in treating senescence. Owing to the excellent bioimaging capability of AIEgens and their therapeutic potentials in killing senescent cells, AIEgens could serve as excellent senolytic agents.

5. Perspectives and conclusions

Noncancerous diseases encompass a wide range of diseases that threaten public health and survival, beyond cancer and natural disasters. Due to a lack of unified criteria for disease classification, in the present review, we classified noncancerous diseases into the following categories: infectious diseases, wounds or injuries, metabolic diseases, CVDs, neurodegenerative diseases, orthopedic diseases, surface organ-associated diseases, inflammation, mental disorders, autoimmune diseases, and senescence. Each of these categories contains a group of specific diseases. Among these diseases, there is a close association and cascaded interaction between different diseases. Unfortunately, there is a lack of clear biomarkers for the detection and diagnosis of these diseases and specific targets for effective treatment are also lacking. Although innumerable efforts have been dedicated to strategize and develop solutions, the results remain far below expectations. Hence, advanced theranostic-based strategies are being pursued as part of both the fundamental and clinical research and will likely remain a hotspot of the research in the near future.

The past few decades have witnessed a dramatic development of nanomaterials for biomedical applications, especially the treatment of cancer.[272] Among all these nanomaterials, AIEgens are emerging as a group of luminescent nanomaterials that appear non-emissive when present as single molecules but show intense emission upon aggregate formation. They can thus help in overcoming the shortcoming caused by the notorious ACQ effects seen in traditional fluorescent molecules and generate new avenues of applications and the research across many fields.[273] Meanwhile, AIEgens have been proven to show multifunctional effects, which demonstrate their values in synergistic therapies. So far, AIEgens have helped in significantly promoting the development of bio-nanomedicines owing to their intrinsic properties, such as bright emission in the aggregate form, good biocompatibility, high photobleaching threshold, and high SNR, among others. Thus, AIEgens can be used to create effective tools for disease detection, bioimaging, and therapy in noncancerous diseases *via* rational design and fabrication and they have shown promising results in all aspects.[26,35,274–276] As detailed and discussed in the previous sections of this review, AIEgens exhibit a range of excellent properties, following rational design and incorporation into nanoplatforms, they can be applied further for efficacious and simplistic theranostics in patients with noncancerous diseases.

Despite the remarkable progresses in the application of AIEgens in the diagnosis, bioimaging, and treatment of noncancerous diseases, the research remains in its infancy and there has been limited scientific exploration. In some fields, inroads are yet to be made. From our perspective, there are several key challenges that need to be addressed before the further applications of AIEgen-based nanomaterials in the broader research and their clinical translation. The examples covered in this review demonstrate the following: first of all, the exploration and application of AIEgens to specific diseases, such as metabolic diseases, senescence, mental disorders, and

autoimmune diseases, can be expanded further, especially with respect to therapeutics. Second, although the AIEgens and related NPs show reasonable *in vitro* and *in vivo* biocompatibility and long-term stability,[277] there are few studies on their bio-interaction and their wide-ranging biological effects remain to be explored in detail.[278] Thus, the simplification of the design and the integration of nanoplatforms are required, along with a more comprehensive assessment of the alteration in biological systems. The biological degradation and metabolism of these compounds and the absence of obvious biological effects also need to be ensured. Third, inspired by the previous studies of other nanomaterials associated with negative roles of the nanomaterials-induced endothelial leakiness (NanoEL effect) in bio-nanomedicine,[279–282] one should be vigilant with the NanoEL effect in further applications and the utilization of the NanoEL effect combined with EPR effect and other targeting assistants could further enhance the targeting capability of AIEgen-based nanoplatforms.[283,284] Thus, the NanoEL effect is valuable to be explored for further and better applications in the field of AIEgens and non-cancer diseases. Fourth, more endeavors are necessary to elucidate the biological effects of AIEgens and their potentials for *in vivo* treatments in other non-tumor disease modelss beyond rodents. Tests must be conducted toward larger-size animals with more complicated tissues and organs in order to facilitate clinical translation in the future. Finally, as proposed by Prof. Liu, the short-wavelength absorption, broad emission, and aggregation-dependent brightness of AIEgens limit their practical performance in multiple areas of biomedicine.[285] Although various approaches have been developed to overcome these shortcomings, more convenient, easy, and effective strategies are still urgently needed. In other words, more novel AIEgens with longer wavelength absorption that can be extended to the NIR-IIb range, the narrow emission spectra, and aggregation-independent brightness will be the key to overcoming these aforementioned disadvantages.

In summary, this review summarizes the progresses in the development of smart AIEgen-based science for the detection, diagnosis, bioimaging, and bioimaging-guided treatments of noncancerous diseases. In addition, future and clinical perspectives of their applications have also been dissected in detail. Considering the short history and explosive development of AIEgens for biological applications, more viable solutions to their intrinsic shortcomings could be developed to enable their broader applications and ensure biosafety. This will allow AIEgens being ultimately useful for detection, diagnosis, bioimaging, and bioimaging-guided therapeutics in noncancerous diseases, promoting health outcomes. Collectively, this review seeks to motivate additional interest and novel ideas for the further exploration of a broad range of biomedical applications of AIEgens in noncancerous diseases *via* the development of more advanced AIEgens and improved clinical applications.

Conflicts of interest

There are no conflicts to declare.

Acknowledgements

This work was supported by grants from the National Natural Science Foundation of China (82102904) and the Science, Technology & Innovation Commission of Shenzhen Municipality (No. JCYJ20190807144605514, JCYJ20210324113405014, and JCYJ20190808154213097). And J. Yoon thanks the National Research Foundation of Korea for the grant funded by the Korean government (MSIT) (No. 2021R1A6A1A10039823).

References

1 M. Zhou, H. Wang, X. Zeng, P. Yin, J. Zhu, W. Chen, X. Li, L. Wang, L. Wang, Y. Liu, J. Liu, M. Zhang, J. Qi, S. Yu, A. Afshin, E. Gakidou, S. Glenn, V. S. Krish, M. K. Miller-Petrie, W. C. Mountjoy-Venning, E. C. Mullany, S. B. Redford, H. Liu, M. Naghavi, S. I. Hay, L. Wang, C. J. L. Murray and X. Liang, *Lancet*, 2019, **394**, 1145–1158.
2 D. F. Mackay, E. R. Russell, K. Stewart, J. A. MacLean, J. P. Pell and W. Stewart, *N. Engl. J. Med.*, 2019, **381**, 1801–1808.
3 P. Saeedi, I. Petersohn, P. Salpea, B. Malanda, S. Karuranga, N. Unwin, S. Colagiuri, L. Guariguata, A. A. Motala, K. Ogurtsova, J. E. Shaw, D. Bright, R. Williams, R. Almutairi, P. A. Montoya, A. Basit, S. Besanccon, C. Bommer, W. Borgnakke, E. Boyko, J. L. Chan, H. Divakar, A. Esteghamati, N. Forouhi, L. Franco, E. Gregg, M. Hassanein, C. Ke, D. Levitt, L. L. Lim, G. D. Ogle, D. Owens, M. Pavkov, J. Pearson-Stuttard, A. Ramachandran, W. Rathmann, M. Riaz, D. Simmons, A. Sinclair, E. Sobngwi, R. Thomas, H. Ward, S. Wild, X. L. Yang, L. L. Yuen, P. Zhang and I. D. A. Comm, *Diabetes Res. Clin. Pract.*, 2019, **157**, 107843.
4 L. F. Wang, F. S. Wang and M. E. Gershwin, *J. Intern. Med.*, 2015, **278**, 369–395.
5 S. S. Virani, A. Alonso, H. J. Aparicio, E. J. Benjamin, M. S. Bittencourt, C. W. Callaway, A. P. Carson, A. M. Chamberlain, S. Cheng, F. N. Delling, M. S. V. Elkind, K. R. Evenson, J. F. Ferguson, D. K. Gupta, S. S. Khan, B. M. Kissela, K. L. Knutson, C. D. Lee, T. T. Lewis, J. Liu, M. S. Loop, P. L. Lutsey, J. Ma, J. Mackey, S. S. Martin, D. B. Matchar, M. E. Mussolino, S. D. Navaneethan, A. M. Perak, G. A. Roth, Z. Samad, G. M. Satou, E. B. Schroeder, S. H. Shah, C. M. Shay, A. Stokes, L. B. VanWagner, N. Y. Wang, C. W. Tsao, E. American Heart Association Council on, C. Prevention Statistics and S. Stroke Statistics, *Circulation*, 2021, **143**, e254–e743.
6 D. W. Zhao, F. Zhang, B. J. Wang, B. Y. Liu, L. Li, S. Y. Kim, S. B. Goodman, P. Hernigou, Q. J. Cui, W. C. Lineaweaver, J. K. Xu, W. R. Drescher and L. Qin, *J. Orthop. Transl.*, 2020, **21**, 100–110.
7 B. Hu, H. Guo, P. Zhou and Z. L. Shi, *Nat. Rev. Microbiol.*, 2021, **19**, 141–154.
8 J. T. Chang, *N. Engl. J. Med.*, 2020, **383**, 2652–2664.
9 L. A. Clark, B. Cuthbert, R. Lewis-Fernandez, W. E. Narrow and G. M. Reed, *Psychol. Sci. Public Interest*, 2017, **18**, 72–145.
10 C. Abbafati, K. M. Abbas, M. Abbasi, M. Abbasifard, M. Abbasi-Kangevari, H. Abbastabar, F. Abd-Allah,

A. Abdelalim, M. Abdollahi, I. Abdollahpour, A. Abedi, P. Abedi, K. H. Abegaz, H. Abolhassani, A. E. Abosetugn, V. Aboyans, E. M. Abrams, L. G. Abreu, M. R. M. Abrigo and A. K. Abu Haimed, *et al.*, *Lancet*, 2020, **396**, 1204–1222.

11 M. Filippi, W. Bruck, D. Chard, F. Fazekas, J. J. G. Geurts, C. Enzinger, S. Hametner, T. Kuhlmann, P. Preziosa, A. Rovira, K. Schmierer, C. Stadelmann, M. A. Rocca and A. C. B. Path, *Lancet Neurol*, 2019, **18**, 198–210.

12 M. Pietzner, E. Wheeler, J. Carrasco-Zanini, A. Cortes, M. Koprulu, M. A. Worheide, E. Oerton, J. Cook, I. D. Stewart, N. D. Kerrison, J. A. Luan, J. Raffler, M. Arnold, W. Arlt, S. O'Rahilly, G. Kastenmuller, E. R. Gamazon, A. D. Hingorani, R. A. Scott, N. J. Wareham and C. Langenberg, *Science*, 2021, **374**, 839.

13 J. Luo, Z. Xie, J. W. Lam, L. Cheng, H. Chen, C. Qiu, H. S. Kwok, X. Zhan, Y. Liu, D. Zhu and B. Z. Tang, *Chem. Commun.*, 2001, 1740–1741, DOI: **10.1039/b105159h**.

14 Z. Zhao, H. K. Zhang, J. W. Y. Lam and B. Z. Tang, *Angew. Chem., Int. Ed.*, 2020, **59**, 9888–9907.

15 Y. Hong, J. W. Lam and B. Z. Tang, *Chem. Commun.*, 2009, 4332–4353.

16 Y. C. Chen, J. W. Y. Lam, R. T. K. Kwok, B. Liu and B. Z. Tang, *Mater. Horiz.*, 2019, **6**, 428–433.

17 M. M. Kang, Z. J. Zhang, N. Song, M. Li, P. P. Sun, X. H. Chen, D. Wang and B. Z. Tang, *Aggregate*, 2020, **1**, 80–106.

18 Y. Yu, H. Xing, D. Liu, M. Zhao, H. H. Sung, I. D. Williams, J. W. Y. Lam, G. Xie, Z. Zhao and B. Z. Tang, *Angew. Chem.*, 2022, **61**, e202204279.

19 Y. B. Yang, Q. Y. Li, H. W. Zhang, H. Liu, X. F. Ji and B. Z. Tang, *Adv. Mater.*, 2021, **33**, 2105418.

20 P. B. Han, A. J. Qin and B. Z. Tang, *Chem. Res. Chin. Univ.*, 2021, **37**, 16–24.

21 G. Feng and B. Liu, *Small*, 2016, **12**, 6528–6535.

22 Y. Gu, Z. Zhao, H. Su, P. Zhang, J. Liu, G. Niu, S. Li, Z. Wang, R. T. K. Kwok, X. L. Ni, J. Sun, A. Qin, J. W. Y. Lam and B. Z. Tang, *Chem. Sci.*, 2018, **9**, 6497–6502.

23 D. Liu, Z. Zhao and B. Z. Tang, *Sci. Sin.: Chim.*, 2022, **52**, 1524–1546.

24 J. Y. Gong, W. J. Gong, B. Wu, H. R. Wang, W. He, Z. Y. Dai, Y. Z. Li, Y. Liu, Z. M. Wang, X. J. Tuo, J. W. Y. Lam, Z. J. Qiu, Z. Zhao and B. Z. Tang, *Aggregate*, 2022, e263.

25 S. X. Lei, J. Tian, Y. T. Kang, Y. F. Zhang and I. Manners, *J. Am. Chem. Soc.*, 2022, **144**, 17630–17641.

26 G. R. Suman, M. Pandey and A. S. J. Chakravarthy, *Mater. Chem. Front.*, 2021, **5**, 1541–1584.

27 X. L. Cai and B. Liu, *Angew. Chem., Int. Ed.*, 2020, **59**, 9868–9886.

28 H. Q. Gao, X. Y. Zhang, C. Chen, K. Li and D. Ding, *Adv. Biosyst.*, 2018, **2**, 1800074.

29 G. H. Luo, T. Z. Xu, X. Li, W. Jiang, Y. H. Duo and B. Z. Tang, *Coord. Chem. Rev.*, 2022, **462**, 214508.

30 J. Zhang, B. Z. He, Y. B. Hu, P. Alam, H. K. Zhang, J. W. Y. Lam and B. Z. Tang, *Adv. Mater.*, 2021, **33**, 2008071.

31 S. D. Xu, Y. K. Duan and B. Liu, *Adv. Mater.*, 2020, **32**, 1903530.

32 J. Liang, B. Tang and B. Liu, *Chem. Soc. Rev.*, 2015, **44**, 2798–2811.

33 H. T. Bai, W. He, J. H. C. Chau, Z. Zheng, R. T. K. Kwok, J. W. Y. Lam and B. Z. Tang, *Biomaterials*, 2021, **268**, 120598.

34 T. Gao, Y. Wu, W. Y. Wang, C. Deng, Y. H. Chen, L. Y. Yi, Y. S. Song, W. Q. Li, L. L. Xu, Y. J. Xie, L. Y. Fang, Q. F. Jin, L. Zhang, B. Z. Tang and M. X. Xie, *ACS Nano*, 2021, **15**, 11908–11928.

35 R. T. K. Kwok, C. W. T. Leung, J. W. Y. Lam and B. Z. Tang, *Chem. Soc. Rev.*, 2015, **44**, 4228–4238.

36 Y. Z. Xu, R. H. Xu, Z. Wang, Y. Zhou, Q. F. Shen, W. C. Ji, D. F. Dang, L. J. Meng and B. Tang, *Chem. Soc. Rev.*, 2021, **50**, 667–690.

37 Q. Wu, Y. Li, L. Wang, D. Wang and B. Z. Tang, *Biomaterials*, 2022, **286**, 121581.

38 N. R. Barthelemy, Y. Li, N. Joseph-Mathurin, B. A. Gordon, J. Hassenstab, T. L. S. Benzinger, V. Buckles, A. M. Fagan, R. J. Perrin, A. M. Goate, J. C. Morris, C. M. Karch, C. J. Xiong, R. Allegri, P. C. Mendez, S. B. Berman, T. Ikeuchi, H. Mori, H. Shimada, M. Shoji, K. Suzuki, J. Noble, M. Farlow, J. Chhatwal, N. R. Graff-Radford, S. Salloway, P. R. Schofield, C. L. Masters, R. N. Martins, A. O'Connor, N. C. Fox, J. Levin, M. Jucker, A. Gabelle, S. Lehmann, C. Sato, R. J. Bateman, E. McDade, R. Allegri, R. Allegri, R. Bateman, J. Bechara, T. Benzinger, S. Berman, C. Bodge, S. Brandon, W. Brooks, J. Buck, V. Buckles, S. Chea, J. Chhatwal, P. C. Mendez, H. L. Chui, J. Cinco, J. Clifford, C. Cruchaga, T. Donahue, J. Douglas, N. Edigo, N. Erekin-Taner, A. Fagan, M. Farlow, C. Fitzpatrick, G. Flynn, N. Fox, E. Franklin, H. Fujii, C. Gant, S. Gardener, B. Ghetti, A. Goate, J. Goldman, B. Gordon, N. Graff-Radford, J. Gray, A. Groves, J. Hassenstab, L. Hoechst-Swisher, D. Holtzman, R. Hornbeck, S. H. DiBari, T. Ikeuchi, S. Ikonomovic, G. Jerome, M. Jucker, C. Karch, K. Kasuga, T. Kawarabayashi, W. Klunk, R. Koeppe, E. Kuder-Buletta, C. Laske, J. H. Lee, J. Levin, R. Martins, N. S. Mason, C. Masters, D. Maue-Dreyfus, E. McDade, H. Mori, J. Morris, A. Nagamatsu, K. Neimeyer, J. Noble, J. Norton, R. Perrin, M. Raichle, A. Renton, J. Ringman, J. H. Roh, S. Salloway, P. Schofield, H. Shimada, W. Sigurdson, H. Sohrabi, P. Sparks, K. Suzuki, K. Taddei, P. T. Wang, C. J. Xiong, X. Xu and D. I. A. Net, *Nat. Med.*, 2020, **26**, 398.

39 M. Gao and B. Z. Tang, *ACS Sens.*, 2017, **2**, 1382–1399.

40 C. C. Zhou, W. H. Xu, P. B. Zhang, M. J. Jiang, Y. C. Chen, R. T. K. Kwok, M. M. S. Lee, G. G. Shan, R. L. Qi, X. Zhou, J. W. Y. Lam, S. Wang and B. Z. Tang, *Adv. Funct. Mater.*, 2019, **29**, 1805986.

41 Y. T. Gao, Z. Y. He, X. W. He, H. K. Zhang, J. Weng, X. L. Yang, F. L. Meng, L. Luo and B. Z. Tang, *J. Am. Chem. Soc.*, 2019, **141**, 20097–20106.

42 D. Shen, W. H. Jin, Y. L. Bai, Y. N. Huang, H. C. Lyu, L. G. Zeng, M. D. Wang, Y. Q. Tang, W. Wan, X. P. Dong, Z. M. Gao, H. L. Piao, X. J. Liu and Y. Liu, *Angew. Chem., Int. Ed.*, 2021, **60**, 16067–16076.

43 H. Bai, Z. Y. Liu, T. F. Zhang, J. Du, C. C. Zhou, W. He, J. H. C. Chau, R. T. K. Kwok, J. W. Y. Lam and B. Tang, *ACS Nano*, 2020, **14**, 7552–7563.
44 J. Ouyang, L. H. Sun, F. Zeng and S. Z. Wu, *Coord. Chem. Rev.*, 2022, **458**, 214438.
45 H. Li, H. Kim, J. Han, V. Nguyen, X. J. Peng and J. Yoon, *Aggregate*, 2021, **2**, e51.
46 Y. Chen, W. Zhang, Z. Zhao, Y. Cai, J. Gong, R. T. K. Kwok, J. W. Y. Lam, H. H. Y. Sung, I. D. Williams and B. Z. Tang, *Angew. Chem.*, 2018, **57**, 5011–5015.
47 R. Zhang, G. Niu, Q. Lu, X. Huang, J. H. C. Chau, R. T. K. Kwok, X. Yu, M. H. Li, J. W. Y. Lam and B. Z. Tang, *Chem. Sci.*, 2020, **11**, 7676–7684.
48 G. B. D. A. R. Collaborators, *Lancet*, 2023, **400**(10369), 2221–2248.
49 K. F. Smith, M. Goldberg, S. Rosenthal, L. Carlson, J. Chen, C. C. Chen and S. Ramachandran, *J. R. Soc., Interface*, 2014, **11**, 20140950.
50 B. Stecher and W. D. Hardt, *Trends Microbiol.*, 2008, **16**, 107–114.
51 S. Akira, S. Uematsu and O. Takeuchi, *Cell*, 2006, **124**, 783–801.
52 T. C. Zortea, C. T. A. Brenna, M. Joyce, H. McClelland, M. Tippett, M. M. Tran, E. Arensman, P. Corcoran, S. Hatcher, M. J. Heise, P. Links, R. C. O'Connor, N. E. Edgar, Y. V. Cha, G. Guaiana, E. Williamson, M. Sinyor and S. Platt, *Crisis*, 2021, **42**, 474–487.
53 O. Lazcka, F. J. Del Campo and F. X. Munoz, *Biosens. Bioelectron.*, 2007, **22**, 1205–1217.
54 S. Unkel, C. P. Farrington, P. H. Garthwaite, C. Robertson and N. Andrews, *J. R. Stat. Soc., Ser. A*, 2012, **175**, 49–82.
55 W. Gu, S. Miller and C. Y. Chiu, *Annu. Rev. Pathol.: Mech. Dis.*, 2019, **14**, 319–338.
56 C. Wang, M. Liu, Z. F. Wang, S. Li, Y. Deng and N. Y. He, *Nano Today*, 2021, **37**, 101092.
57 P. Rajapaksha, A. Elbourne, S. Gangadoo, R. Brown, D. Cozzolino and J. Chapman, *Analyst*, 2019, **144**, 396–411.
58 C. Deusenbery, Y. Y. Wang and A. Shukla, *ACS Infect. Dis.*, 2021, **7**, 695–720.
59 V. N. Nguyen, Z. Zhao, B. Z. Tang and J. Yoon, *Chem. Soc. Rev.*, 2022, **51**, 3324–3340.
60 Z. Wang, T. D. Cong, W. Zhong, J. W. Lau, G. Kwek, M. B. Chan-Park and B. Xing, *Angew. Chem.*, 2021, **60**, 16900–16905.
61 X. H. Chen, H. J. Han, Z. Tang, Q. Jin and J. Ji, *Adv. Healthcare Mater.*, 2021, **10**, 2100736.
62 X. W. He, L. H. Xiong, Z. Zhao, Z. Y. Wang, L. Luo, J. W. Y. Lan, R. T. K. Kwok and B. Z. Tang, *Theranostics*, 2019, **9**, 3223–3248.
63 Y. M. Li, X. L. Hu, S. D. Tian, Y. Li, G. Q. Zhang, G. Y. Zhang and S. Y. Liu, *Biomaterials*, 2014, **35**, 1618–1626.
64 H. Chang, Y. Mei, Y. D. Li and L. Q. Shang, *Talanta*, 2022, **247**, 123583.
65 Q. Zhang, B. H. Yin, J. H. Hao, L. J. Ma, Y. Y. Huang, X. Y. Shao, C. Q. Li, Z. Q. Chu, C. Q. Yi, S. H. D. Wong and M. Yang, *Aggregate*, 2022, e195.
66 P. P. Bao, C. Li, H. L. Ou, S. L. Ji, Y. Chen, J. Gao, X. Yue, J. Shen and D. Ding, *Biomater. Sci.*, 2021, **9**, 437–442.
67 E. Zhao, Y. Hong, S. Chen, C. W. Leung, C. Y. Chan, R. T. Kwok, J. W. Lam and B. Z. Tang, *Adv. Healthcare Mater.*, 2014, **3**, 88–96.
68 T. T. Kong, Z. Zhao, Y. Li, F. Wu, T. Jin and B. Z. Tang, *J. Mater. Chem. B*, 2018, **6**, 5986–5991.
69 E. Kuru, S. Tekkam, E. Hall, Y. V. Brun and M. S. Van Nieuwenhze, *Nat. Protoc.*, 2015, **10**, 33–52.
70 D. Mao, F. Hu, Kenry, S. L. Ji, W. B. Wu, D. Ding, D. L. Kong and B. Liu, *Adv. Mater.*, 2018, **30**, 1706831.
71 M. C. Fisher, D. A. Henk, C. J. Briggs, J. S. Brownstein, L. C. Madoff, S. L. McCraw and S. J. Gurr, *Nature*, 2012, **484**, 186–194.
72 D. S. J. Ting, C. S. Ho, R. Deshmukh, D. G. Said and H. S. Dua, *Eye*, 2021, **35**, 1084–1101.
73 C. C. Zhou, M. J. Jiang, J. Du, H. T. Bai, G. G. Shan, R. T. K. Kwok, J. H. C. Chau, J. Zhang, J. W. Y. Lam, P. Huang and B. Tang, *Chem. Sci.*, 2020, **11**, 4730–4740.
74 A. Kathiravan, K. Sundaravel, M. Jaccob, G. Dhinagaran, A. Rameshkumar, D. Arul Ananth and T. Sivasudha, *J. Phys. Chem. B*, 2014, **118**, 13573–13581.
75 X. Hu, P. Zhang, D. Wang, J. Jiang, X. Chen, Y. Liu, Z. Zhang, B. Z. Tang and P. Li, *Biosens. Bioelectron.*, 2021, **182**, 113188.
76 X. X. Ge, M. Gao, B. R. He, N. N. Cao, K. R. Li, Y. Liu, S. M. Tang, K. Liu, J. Zhang, F. Hu, L. Zheng and B. Situ, *Biomaterials*, 2022, **287**, 121618.
77 C. Bambra, R. Riordan, J. Ford and F. Matthews, *J. Epidemiol. Commun. Health*, 2020, **74**, 964–968.
78 Z. Liu, T. Meng, X. Tang, R. Tian and W. Guan, *Front. Immunol.*, 2021, **12**, 635558.
79 K. Tanneeru, N. K. Bhatraju, R. S. Bhosale and S. K. Kalangi, *Front. Microbiol.*, 2021, **12**, 766351.
80 T. Kato, A. Kawaguchi, K. Nagata and K. Hatanaka, *Biochem. Biophys. Res. Commun.*, 2010, **394**, 200–204.
81 L. H. Xiong, X. He, Z. Zhao, R. T. K. Kwok, Y. Xiong, P. F. Gao, F. Yang, Y. Huang, H. H. Sung, I. D. Williams, J. W. Y. Lam, J. Cheng, R. Zhang and B. Z. Tang, *ACS Nano*, 2018, **12**, 9549–9557.
82 R. Chen, C. Ren, M. Liu, X. Ge, M. Qu, X. Zhou, M. Liang, Y. Liu and F. Li, *ACS Nano*, 2021, **15**, 8996–9004.
83 R. L. Smith, M. R. Soeters, R. C. I. Wust and R. H. Houtkooper, *Endocr. Rev.*, 2018, **39**, 489–517.
84 H. Yki-Jarvinen, *Lancet Diabetes Endocrinol.*, 2014, **2**, 901–910.
85 E. A. Day, R. J. Ford and G. R. Steinberg, *Trends Endocrinol. Metab.*, 2017, **28**, 545–560.
86 S. Chatterjee, K. Khunti and M. J. Davies, *Lancet*, 2017, **389**, 2239–2251.
87 H. Teymourian, A. Barfidokht and J. Wang, *Chem. Soc. Rev.*, 2020, **49**, 7671–7709.
88 C. C. Liu, Y. D. Hang, T. Jiang, J. Yang, X. Zhang and J. L. Hua, *Talanta*, 2018, **178**, 847–853.
89 Y. Jia, S. Guo, Q. Han, J. Zhu, X. Zhang, N. Na and J. Ouyang, *J. Mater. Chem. B*, 2021, **9**, 5128–5135.

90 A. C. Sedgwick, K. C. Yan, D. N. Mangel, Y. Shang, A. Steinbrueck, H. H. Han, J. T. Brewster, X. L. Hu, D. W. Snelson, V. M. Lynch, H. Tian, X. P. He and J. L. Sessler, *J. Am. Chem. Soc.*, 2021, **143**, 1278–1283.
91 Y. Zhou, J. Hua, G. Barritt, Y. Liu, B. Z. Tang and Y. Tang, *ChemBioChem*, 2019, **20**, 1256–1259.
92 H. N. Tan and Y. H. Li, *Microchim. Acta*, 2021, **188**, 254.
93 G. G. Yu, Z. Sun, Y. T. Wu and N. Sai, *Spectrochim. Acta, Part A*, 2022, **268**, 120641.
94 F. Sun, W. Zhao, H. Shen, N. Fan, J. Zhang, Q. Liu, C. Xu, J. Luo, M. Zhao, Y. Chen, K. W. K. Lam, X. Yang, R. T. K. Kwok, J. W. Y. Lam, J. Sun, H. Zhang and B. Z. Tang, *Adv. Mater.*, 2022, e2207671, DOI: **10.1002/adma.202207671**.
95 R. L. Sacco, G. A. Roth, K. S. Reddy, D. K. Arnett, R. Bonita, T. A. Gaziano, P. A. Heidenreich, M. D. Huffman, B. M. Mayosi, S. Mendis, C. J. Murray, P. Perel, D. J. Pineiro, S. C. Smith Jr., K. A. Taubert, D. A. Wood, D. Zhao and W. A. Zoghbi, *Circulation*, 2016, **133**, e674–690.
96 W. Wang, Y. Liu, J. Liu, P. Yin, L. Wang, J. Qi, J. You, L. Lin, S. Meng, F. Wang and M. Zhou, *Int. J. Cardiol.*, 2021, **340**, 105–112.
97 I. Csige, D. Ujvarosy, Z. Szabo, I. Lorincz, G. Paragh, M. Harangi and S. Somodi, *J. Diabetes Res.*, 2018, **2018**, 3407306.
98 D. H. Wilson, D. M. Rissin, C. W. Kan, D. R. Fournier, T. Piech, T. G. Campbell, R. E. Meyer, M. W. Fishburn, C. Cabrera, P. P. Patel, E. Frew, Y. Chen, L. Chang, E. P. Ferrell, V. von Einem, W. McGuigan, M. Reinhardt, H. Sayer, C. Vielsack and D. C. Duffy, *JALA*, 2016, **21**, 533–547.
99 A. Y. Hannun, P. Rajpurkar, M. Haghpanahi, G. H. Tison, C. Bourn, M. P. Turakhia and A. Y. Ng, *Nat. Med.*, 2019, **25**, 65.
100 N. Zhao, Q. Gong, R. X. Zhang, J. Yang, Z. Y. Huang, N. Li and B. Z. Tang, *J. Mater. Chem. C*, 2015, **3**, 8397–8402.
101 R. Y. Zhang, S. H. P. Sung, G. X. Feng, C. J. Zhang, Kenry, B. Tang and B. Liu, *Anal. Chem.*, 2018, **90**, 1154–1160.
102 Y. W. Zhang, S. H. Wang, X. D. Wang, Q. Zan, X. Yu, L. Fan and C. A. Dong, *Anal. Bioanal. Chem.*, 2021, **413**, 3823–3831.
103 K. Li, M. Yamamoto, S. J. Chan, M. Y. Chiam, W. Qin, P. T. H. Wong, E. K. F. Yim, B. Z. Tang and B. Liu, *Chem. Commun.*, 2014, **50**, 15136–15139.
104 S. Jebari-Benslaiman, U. Galicia-Garcia, A. Larrea-Sebal, J. R. Olaetxea, I. Alloza, K. Vandenbroeck, A. Benito-Vicente and C. Martin, *Int. J. Mol. Sci.*, 2022, **23**, 3346.
105 K. Wang, H. Q. Gao, Y. W. Zhang, H. Y. Yan, J. H. Si, X. Y. Mi, S. A. Xia, X. Q. Feng, D. B. Liu, D. L. Kong, T. Wang and D. Ding, *Adv. Mater.*, 2022, **34**, 2106994.
106 B. N. Dugger and D. W. Dickson, *Cold Spring Harbor Perspect. Biol.*, 2017, **9**, a028035.
107 Y. J. Hou, X. L. Dan, M. Babbar, Y. Wei, S. G. Hasselbalch, D. L. Croteau and V. A. Bohr, *Nat. Rev. Neurol.*, 2019, **15**, 565–581.
108 O. Hansson, *Nat. Med.*, 2021, **27**, 954–963.
109 G. Bivona, C. M. Gambino, B. Lo Sasso, C. Scazzone, R. V. Giglio, L. Agnello and M. Ciaccio, *Diagnostics*, 2022, **12**, 130.
110 A. Jeromin and R. Bowser, *Adv Neurobiol*, 2017, **15**, 491–528.
111 L. Parnetti, L. Gaetani, P. Eusebi, S. Paciotti, O. Hansson, O. El-Agnaf, B. Mollenhauer, K. Blennow and P. Calabresi, *Lancet Neurol.*, 2019, **18**, 573–586.
112 B. R. Groveman, C. D. Orru, A. G. Hughson, L. D. Raymond, G. Zanusso, B. Ghetti, K. J. Campbell, J. Safar, D. Galasko and B. Caughey, *Acta Neuropathol. Commun.*, 2018, **6**, 7.
113 J. Zhou, P. Jangili, S. Son, M. S. Ji, M. Won and J. S. Kim, *Adv. Mater.*, 2020, **32**, 2001945.
114 M. Wang, X. Gu, G. Zhang, D. Zhang and D. Zhu, *Anal. Chem.*, 2009, **81**, 4444–4449.
115 Y. J. Tang, D. Zhang, Y. X. Zhang, Y. L. Liu, L. R. Cai, E. Plaster and J. Zheng, *J. Mater. Chem. B*, 2022, **10**, 2280–2295.
116 Y. Yang, S. Li, Q. Zhang, Y. Kuang, A. Qin, M. Gao, F. Li and B. Z. Tang, *J. Mater. Chem. B*, 2019, **7**, 2434–2441.
117 F. Jia, F. Chibhabha, Y. Yang, Y. Kuang, Q. Zhang, S. Ullah, Z. Liang, M. Xie and F. Li, *J. Mater. Chem. B*, 2021, **9**, 731–745.
118 J. Shi, Q. Deng, Y. Li, M. Zheng, Z. Chai, C. Wan, Z. Zheng, L. Li, F. Huang and B. Tang, *Anal. Chem.*, 2018, **90**, 13775–13782.
119 N. R. Marzano, K. M. Wray, C. L. Johnston, B. P. Paudel, Y. Hong, A. van Oijen and H. Ecroyd, *ACS Chem. Neurosci.*, 2020, **11**, 4191–4202.
120 J. D. Zhang, J. Mei, X. L. Hu, X. P. He and H. Tian, *Small*, 2016, **12**, 6562–6567.
121 M. Kumar, Y. Hong, D. C. Thorn, H. Ecroyd and J. A. Carver, *Anal. Chem.*, 2017, **89**, 9322–9329.
122 R. Jakob-Roetne and H. Jacobsen, *Angew. Chem., Int. Ed.*, 2009, **48**, 3030–3059.
123 W. Fu, C. Yan, Z. Guo, J. Zhang, H. Zhang, H. Tian and W. H. Zhu, *J. Am. Chem. Soc.*, 2019, **141**, 3171–3177.
124 A. G. Robling and L. F. Bonewald, *Annu. Rev. Physiol.*, 2020, **82**, 485–506.
125 S. Safiri, A. A. Kolahi, D. Hoy, E. Smith, D. Bettampadi, M. A. Mansournia, A. Almasi-Hashiani, A. Ashrafi-Asgarabad, M. Moradi-Lakeh, M. Qorbani, G. Collins, A. D. Woolf, L. March and M. Cross, *Ann. Rheum. Dis.*, 2019, **78**, 1463–1471.
126 W. Z. Jiang, H. Liu, R. X. Wan, Y. J. Wu, Z. J. Shi and W. H. Huang, *Ageing Res. Rev.*, 2021, **67**, 101315.
127 W. H. Robinson, C. M. Lepus, Q. Wang, H. Raghu, R. Mao, T. M. Lindstrom and J. Sokolove, *Nat. Rev. Rheumatol.*, 2016, **12**, 580–592.
128 R. J. Wakefield, W. W. Gibbon, P. G. Conaghan, P. O'Connor, D. McGonagle, C. Pease, M. J. Green, D. J. Veale, J. D. Isaacs and P. Emery, *Arthritis Rheum.*, 2000, **43**, 2762–2770.
129 J. M. Li, W. Y. Lee, T. Y. Wu, C. W. Leung, J. B. Xu, D. S. Wong, R. Li, G. Li, B. Z. Tang and L. M. Bian, *Adv. Biosyst.*, 2018, **2**, 1800010.

130 P. C. Robinson, S. van der Linden, M. A. Khan and W. J. Taylor, *Nat. Rev. Rheumatol.*, 2021, **17**, 109–118.
131 D. J. Hunter and S. Bierma-Zeinstra, *Lancet*, 2019, **393**, 1745–1759.
132 J. S. Smolen, D. Aletaha and I. B. McInnes, *Lancet*, 2016, **388**, 2023–2038.
133 R. Medzhitov, *Science*, 2021, **374**, 1070–1075.
134 Y. X. Li, M. L. Zha, G. Yang, S. X. Wang, J. S. Ni and K. Li, *Chem. – Eur. J.*, 2021, **27**, 13085–13091.
135 W. F. Xu, L. Y. He, Q. Xia, C. H. Jia, L. L. Geng, M. Yang, Z. H. Xu, P. Y. Chen, Y. Cheng, J. H. Zhao, H. L. Wang, H. Chen, Y. H. Zhang, S. T. Gong and R. Y. Liu, *J. Mater. Chem. B*, 2018, **6**, 809–815.
136 X. X. Fan, Q. M. Xia, Y. Y. Zhang, Y. R. Li, Z. Feng, J. Zhou, J. Qi, B. Z. Tang, J. Qian and H. Lin, *Adv. Healthcare Mater.*, 2021, **10**, 2101043.
137 T. Kisseleva and D. Brenner, *Nat. Rev. Gastroenterol. Hepatol.*, 2021, **18**, 151–166.
138 D. Yan, T. Li, Y. Yang, N. Niu, D. Wang, J. Ge, L. Wang, R. Zhang, D. Wang and B. Z. Tang, *Adv. Mater.*, 2022, e2206643, DOI: **10.1002/adma.202206643**.
139 N. E. Sharpless and C. J. Sherr, *Nat. Rev. Cancer*, 2015, **15**, 397–408.
140 A. Hernandez-Segura, J. Nehme and M. Demaria, *Trends Cell Biol.*, 2018, **28**, 436–453.
141 M. J. Yousefzadeh, R. R. Flores, Y. Zhu, Z. C. Schmiechen, R. W. Brooks, C. E. Trussoni, Y. X. Cui, L. Angelini, K. A. Lee, S. J. McGowan, A. L. Burrack, D. Wang, Q. Dong, A. P. Lu, T. Sano, R. D. O'Kelly, C. A. McGuckian, J. I. Kato, M. P. Bank, E. A. Wade, S. P. S. Pillai, J. Klug, W. C. Ladiges, C. E. Burd, S. E. Lewis, N. F. LaRusso, N. V. Vo, Y. S. Wang, E. E. Kelley, J. Huard, I. M. Stromnes, P. D. Robbins and L. J. Niedernhofer, *Nature*, 2021, **594**, 100.
142 E. Sikora, T. Arendt, M. Bennett and M. Narita, *Ageing Res. Rev.*, 2011, **10**, 146–152.
143 V. Gorgoulis, P. D. Adams, A. Alimonti, D. C. Bennett, O. Bischof, C. Bishop, J. Campisi, M. Collado, K. Evangelou, G. Ferbeyre, J. Gil, E. Hara, V. Krizhanovsky, D. Jurk, A. B. Maier, M. Narita, L. Niedernhofer, J. F. Passos, P. D. Robbins, C. A. Schmitt, J. Sedivy, K. Vougas, T. von Zglinicki, D. H. Zhou, M. Serrano and M. Demaria, *Cell*, 2019, **179**, 813–827.
144 F. Debacq-Chainiaux, J. D. Erusalimsky, J. Campisi and O. Toussaint, *Nat. Protoc.*, 2009, **4**, 1798–1806.
145 L. Peng, M. Gao, X. Cai, R. Zhang, K. Li, G. Feng, A. Tong and B. Liu, *J. Mater. Chem. B*, 2015, **3**, 9168–9172.
146 M. Li, M. Yang and W.-H. Zhu, *Mater. Chem. Front.*, 2021, **5**, 763–774.
147 Y. Yao, Y. Zhang, C. Yan, W. H. Zhu and Z. Guo, *Chem. Sci.*, 2021, **12**, 9885–9894.
148 Z. Gao, H. Gao, D. Zheng, T. Xu, Y. Chen, C. Liang, L. Wang, D. Ding and Z. Yang, *Sci. China: Chem.*, 2020, **63**, 398–403.
149 L. Dong, M. Y. Zhang, H. H. Han, Y. Zang, G. R. Chen, J. Li, X. P. He and S. Vidal, *Chem. Sci.*, 2021, **13**, 247–256.
150 S. Zhang, X. Wang, X. Wang, T. Wang, W. Liao, Y. Yuan, G. Chen and X. Jia, *Anal. Chim. Acta*, 2022, **1198**, 339554.
151 R. Long, C. Tang, Z. Yang, Q. Fu, J. Xu, C. Tong, S. Shi, Y. Guo and D. Wang, *J. Mater. Chem. C*, 2020, **8**, 11860–11865.
152 G. Jiang, G. Zeng, W. Zhu, Y. Li, X. Dong, G. Zhang, X. Fan, J. Wang, Y. Wu and B. Z. Tang, *Chem. Commun.*, 2017, **53**, 4505–4508.
153 Z. Zeng, X. Ren, T. Yin, X. Gao, M. Tsai, Y. Zhang and M. Gu, *Am. J. Transl. Res.*, 2019, **11**, 6907–6923.
154 X. L. Cai, A. Bandla, D. Mao, G. X. Feng, W. Qin, L. D. Liao, N. Thakor, B. Z. Tang and B. Liu, *Adv. Mater.*, 2016, **28**, 8760–8765.
155 H. G. Lu, Y. D. Zheng, X. W. Zhao, L. J. Wang, S. Q. Ma, X. Q. Han, B. Xu, W. J. Tian and H. Gao, *Angew. Chem., Int. Ed.*, 2016, **55**, 155–159.
156 J. Qian and B. Z. Tang, *Chemistry*, 2017, **3**, 56–91.
157 J. Qi, C. W. Sun, A. Zebibula, H. Q. Zhang, R. T. K. Kwok, X. Y. Zhao, W. Xi, J. W. Y. Lam, J. Qian and B. Z. Tang, *Adv. Mater.*, 2018, **30**, 1706856.
158 Z. Feng, S. Y. Bai, J. Qi, C. W. Sun, Y. H. Zhang, X. M. Yu, H. W. Ni, D. Wu, X. X. Fan, D. W. Xue, S. J. Liu, M. Chen, J. Y. Gong, P. F. Wei, M. B. He, J. W. Y. Lam, X. J. Li, B. Tang, L. X. Gao and J. Qian, *Adv. Mater.*, 2021, **33**, 2008123.
159 R. Hu, F. Zhou, T. T. Zhou, J. L. Shen, Z. M. Wang, Z. J. Zhao, A. J. Qin and B. Z. Tang, *Biomaterials*, 2018, **187**, 47–54.
160 M. J. Gu, Z. X. Zeng, M. Y. Wu, J. K. Leung, E. G. Zhao, S. D. Wang and S. J. Chen, *Chem. – Asian J.*, 2019, **14**, 775–780.
161 I. Z. Mukadam, J. Machhi, J. Herskovitz, M. Hasan, M. D. Oleynikov, W. R. Blomberg, D. Svechkarev, A. M. Mohs, Y. Zhou, P. Dash, J. McMillan, S. Gorantla, J. Garrison, H. E. Gendelman and B. D. Kevadiya, *Biomaterials*, 2020, **231**, 119669.
162 Q. S. Zhang, P. Yu, Y. Fan, C. X. Sun, H. S. He, X. Liu, L. F. Lu, M. Y. Zhao, H. X. Zhang and F. Zhang, *Angew. Chem., Int. Ed.*, 2021, **60**, 3967–3973.
163 J. Du, S. Liu, P. F. Zhang, H. X. Liu, Y. Y. Li, W. He, C. B. Li, J. H. C. Chau, R. T. K. Kwok, J. W. Y. Lam, L. T. Cai, Y. H. Huang, W. J. Zhang, J. Q. Hou and B. Z. Tang, *ACS Appl. Mater. Interfaces*, 2020, **12**, 8040–8049.
164 C. Peng, X. Y. Ma, D. Lin, X. W. Feng, H. Yu and Y. H. Li, *Anal. Chim. Acta*, 2021, **1187**, 339146.
165 Y. X. Li, M. L. Zha, T. Y. Kang, C. Li, X. Wu, S. X. Wang, S. B. Lu, Y. S. Lee, Y. R. Wu, J. S. Ni and K. Li, *Small*, 2022, **18**, 2105362.
166 C. Yang, X. Ni, D. Mao, C. Ren, J. Liu, Y. Gao, D. Ding and J. Liu, *Biomaterials*, 2019, **188**, 107–117.
167 L. Sun, J. Ouyang, Y. Ma, Z. Zeng, C. Zeng, F. Zeng and S. Wu, *Adv. Healthcare Mater.*, 2021, **10**, e2100867.
168 M. L. Steinhauser, A. P. Bailey, S. E. Senyo, C. Guillermier, T. S. Perlstein, A. P. Gould, R. T. Lee and C. P. Lechene, *Nature*, 2012, **481**, 516–519.
169 L. X. Shi, X. W. Liu, L. Y. Shi, H. T. Stinson, J. Rowlette, L. J. Kahl, C. R. Evans, C. Zheng, L. E. P. Dietrich and W. Min, *Nat. Methods*, 2020, **17**, 844.

170 M. M. Kim, A. Parolia, M. P. Dunphy and S. Venneti, *Nat. Rev. Clin. Oncol.*, 2016, **13**, 725–739.
171 F. Zhang, Z. Li, Y. M. Liu, B. S. Yang, H. Qiao, J. Chai, G. M. Wen and B. Liu, *J. Mater. Chem. B*, 2020, **8**, 9533–9543.
172 C. B. Xiang, J. J. Xiang, X. Yang, C. B. Li, L. H. Zhou, D. Y. Jiang, Y. L. Peng, Z. Xu, G. J. Deng, B. D. Zhu, P. F. Zhang, L. T. Cai and P. Gong, *J. Mater. Chem. B*, 2022, **10**, 4254–4260.
173 S. Wang, X. Li, S. Y. Chong, X. Wang, H. Chen, C. Chen, L. G. Ng, J. W. Wang and B. Liu, *Adv. Mater.*, 2021, **33**, e2007490.
174 H. K. Seitz, R. Bataller, H. Cortez-Pinto, B. Gao, A. Gual, C. Lackner, P. Mathurin, S. Mueller, G. Szabo and H. Tsukamoto, *Nat. Rev. Dis. Primers*, 2018, **4**, 16.
175 K. Sugimoto and Y. Takei, *Hepatol. Res.*, 2017, **47**, 70–79.
176 Y. Z. Feng, G. Nie, W. J. Liang, W. Q. Li, Y. Zhang, K. P. Wang and D. G. Chen, *Sens. Actuators, B*, 2022, **355**, 131285.
177 J. Klohs, A. Wunder and K. Licha, *Basic Res. Cardiol.*, 2008, **103**, 144–151.
178 G. Feng, J. L. Y. Li, C. Claser, A. Balachander, Y. Tan, C. C. Goh, I. W. H. Kwok, L. Renia, B. Z. Tang, L. G. Ng and B. Liu, *Biomaterials*, 2018, **152**, 77–85.
179 Y. Li, D. Hu, Z. Sheng, T. Min, M. Zha, J. S. Ni, H. Zheng and K. Li, *Biomaterials*, 2021, **264**, 120365.
180 W. Qin, N. Alifu, J. W. Y. Lam, Y. Cui, H. Su, G. Liang, J. Qian and B. Z. Tang, *Adv. Mater.*, 2020, **32**, e2000364.
181 M. X. Liu, B. B. Gu, W. B. Wu, Y. K. Duan, H. J. Liu, X. Q. Deng, M. Z. Fan, X. M. Wang, X. B. Wei, K. T. Yong, K. Wang, G. X. Xu and B. Liu, *Chem. Mater.*, 2020, **32**, 6437–6443.
182 B. Situ, M. Gao, X. He, S. Li, B. He, F. Guo, C. Kang, S. Liu, L. Yang, M. Jiang, Y. Hu, B. Z. Tang and L. Zheng, *Mater. Horiz.*, 2019, **6**, 546–553.
183 X. D. Lou, Z. J. Zhao and B. Z. Tang, *Small*, 2016, **12**, 6430–6450.
184 B. Situ, M. Gao, X. J. He, S. W. Li, B. R. He, F. X. Guo, C. M. Kang, S. Liu, L. Yang, M. J. Jiang, Y. W. Hu, B. Z. Tang and L. Zheng, *Mater. Horiz.*, 2019, **6**, 546–553.
185 Z. Yang, X. Fan, X. Liu, Y. Chu, Z. Zhang, Y. Hu, H. Lin, J. Qian and J. Hua, *Chem. Commun.*, 2021, **57**, 3099–3102.
186 J. Y. Xiang, X. L. Cai, X. D. Lou, G. X. Feng, X. H. Min, W. W. Luo, B. R. He, C. C. Goh, L. G. Ng, J. Zhou, Z. J. Zhao, B. Liu and B. Z. Tang, *ACS Appl. Mater. Interfaces*, 2015, **7**, 14965–14974.
187 J. Qi, N. Alifu, A. Zebibula, P. F. Wei, J. W. Y. Lam, H. Q. Peng, R. T. K. Kwok, J. Qian and B. Z. Tang, *Nano Today*, 2020, **34**, 100893.
188 Y. Li, Z. Cai, S. Liu, H. Zhang, S. T. H. Wong, J. W. Y. Lam, R. T. K. Kwok, J. Qian and B. Z. Tang, *Nat. Commun.*, 2020, **11**, 1255.
189 H. Zhang, P. Fu, Y. Liu, Z. Zheng, L. Zhu, M. Wang, M. Abdellah, M. He, J. Qian, A. W. Roe and W. Xi, *Biomaterials*, 2022, **289**, 121809.
190 W. Wu, Y. Q. Yang, Y. Yang, Y. M. Yang, K. Y. Zhang, L. Guo, H. F. Ge, X. W. Chen, J. Liu and H. Feng, *Small*, 2019, **15**, 1805549.
191 L. Lin, Z. He, T. Zhang, Y. Zuo, X. Chen, Z. Abdelrahman, F. Chen, Z. Wei, K. Si, W. Gong, X. Wang, S. He and Z. Chen, *J. Mater. Chem. B*, 2022, **10**, 887–898.
192 J. A. Li, Z. J. Zhang, X. Q. Deng, Z. R. Xu, L. Wang, G. X. Xu, K. Wang, D. Wang and B. Z. Tang, *Biomaterials*, 2022, **287**, 121612.
193 M. B. He, D. Y. Li, Z. Zheng, H. Q. Zhang, T. X. Wu, W. H. Geng, Z. W. Hu, Z. Feng, S. Y. Peng, L. Zhu, W. Xi, D. Zhu, B. Z. Tang and J. Qian, *Nano Today*, 2022, **45**, 101536.
194 D. Li, H. Zhang, L. L. Streich, Y. Wang, P. Lu, L. Wang, R. Prevedel and J. Qian, *Mater. Chem. Front.*, 2021, **5**, 3201–3208.
195 Z. Zheng, D. Y. Li, Z. Y. Liu, H. Q. Peng, H. H. Y. Sung, R. T. K. Kwok, I. D. Williams, J. W. Y. Lam, J. Qian and B. Z. Tang, *Adv. Mater.*, 2019, **31**, 1904799.
196 V. L. Villemagne, V. Dore, S. C. Burnham, C. L. Masters and C. C. Rowe, *Nat. Rev. Neurol.*, 2018, **14**, 225–236.
197 M. J. Betts, E. Kirilina, M. C. G. Otaduy, D. Ivanov, J. Acosta-Cabronero, M. F. Callaghan, C. Lambert, A. Cardenas-Blanco, K. Pine, L. Passamonti, C. Loane, M. C. Keuken, P. Trujillo, F. Lusebrink, H. Mattern, K. Y. Liu, N. Priovoulos, K. Fliessbach, M. J. Dahl, A. Maass, C. F. Madelung, D. Meder, A. J. Ehrenberg, O. Speck, N. Weiskopf, R. Dolan, B. Inglis, D. Tosun, M. Morawski, F. A. Zucca, H. R. Siebner, M. Mather, K. Uludag, H. Heinsen, B. A. Poser, R. Howard, L. Zecca, J. B. Rowe, L. T. Grinberg, H. I. L. Jacobs, E. Duzel and D. Hammerer, *Brain*, 2019, **142**, 2558–2571.
198 L. Q. Gao, W. Wang, X. Wang, F. Yang, L. X. Xie, J. Shen, M. A. Brimble, Q. C. Xiao and S. Q. Yao, *Chem. Soc. Rev.*, 2021, **50**, 1219–1250.
199 Y. Wang, Y. Qiu, A. Sun, Y. Xiong and J. J. A. C. A. Yan, *Anal. Chim. Acta*, 2020, **1133**, 109–118.
200 Z. Xu, Z. Zhang, X. Deng, J. Li, Y. Jiang, W. C. Law, C. Yang, W. Zhang, X. Chen, K. Wang, D. Wang and G. Xu, *ACS Nano*, 2022, **16**, 6712–6724.
201 Z. Zheng, H. Zhang, H. Cao, J. Gong, M. He, X. Gou, T. Yang, P. Wei, J. Qian, W. Xi and B. Z. Tang, *ACS Nano*, 2022, **16**, 6444–6454.
202 B. R. Bloem, M. S. Okun and C. Klein, *Lancet*, 2021, **397**, 2284–2303.
203 L. Liu, K. Zhang, H. Sandoval, S. Yamamoto, M. Jaiswal, E. Sanz, Z. H. Li, J. Hui, B. H. Graham, A. Quintana and H. J. Bellen, *Cell*, 2015, **160**, 177–190.
204 L. H. Li, F. Zhou, Q. Gao, Y. Lu, X. Y. Xu, R. Hu, Z. M. Wang, M. Y. Peng, Z. M. Yang and B. Tang, *iScience*, 2019, **21**, 261.
205 J. R. Plemel, W. Q. Liu and V. W. Yong, *Nat. Rev. Drug Discovery*, 2017, **16**, 617–634.
206 S. E. Nasrabady, B. Rizvi, J. E. Goldman and A. M. Brickman, *Acta Neuropathol. Commun.*, 2018, **6**, 22.
207 M. Y. Wu, A. Y. H. Wong, J. K. Leung, C. Kam, K. L. K. Wu, Y. S. Chan, K. Liu, N. Y. Ip and S. J. Chen, *Proc. Natl. Acad. Sci. U. S. A.*, 2021, **118**, e2106143118.

208 W. F. T. Lai, C. H. Chang, Y. Tang, R. Bronson and C. H. Tung, *Osteoarthr. Cartil.*, 2004, **12**, 239–244.
209 Q. Luo, Z. Y. Luo, H. Zeng, Y. Xiao, Y. B. Peng and G. Liu, *Spectrochim. Acta, Part A*, 2022, **273**, 121017.
210 M. Gao, J. J. Chen, G. W. Lin, S. W. Li, L. Wang, A. J. Qin, Z. J. Zhao, L. Ren, Y. J. Wang and B. Z. Tang, *ACS Appl. Mater. Interfaces*, 2016, **8**, 17878–17884.
211 Z. Y. Zheng, T. T. Zhou, R. Hu, M. J. Huang, X. Ao, J. Chu, T. Jiang, A. J. Qin and Z. M. Zhang, *Bioact. Mater.*, 2020, **5**, 1018–1025.
212 Y. Cheng, J. Dai, C. L. Sun, R. Liu, T. Y. Zhai, X. D. Lou and F. Xia, *Angew. Chem., Int. Ed.*, 2018, **57**, 3123–3127.
213 X. G. Liu, M. Wu, M. Wang, Y. K. Duan, C. U. Phan, H. Chen, G. P. Tang and B. Liu, *Angew. Chem., Int. Ed.*, 2021, **60**, 3175–3181.
214 X. Y. Gao, G. X. Feng, P. N. Manghnani, F. Hu, N. Jiang, J. Z. Liu, B. Liu, J. Z. Sun and B. Z. Tang, *Chem. Commun.*, 2017, **53**, 1653–1656.
215 Y. X. Ye, X. Y. Chen, Y. W. Yu, Q. Zhang, X. W. Wei, Z. C. Wang, B. Z. Wang, Q. C. Jiao and H. L. Zhu, *Analyst*, 2021, **146**, 6556–6565.
216 L. H. Sun, J. Ouyang, F. Zeng and S. Z. Wu, *Biomaterials*, 2022, **283**, 121468.
217 C. Chen, H. Q. Gao, H. L. Ou, R. T. K. Kwok, Y. H. Tang, D. H. Zheng and D. Ding, *J. Am. Chem. Soc.*, 2022, **144**, 3429–3441.
218 J. Lugrin, N. Rosenblatt-Velin, R. Parapanov and L. Liaudet, *Biol. Chem.*, 2014, **395**, 203–230.
219 Z. G. Song, D. Mao, S. H. P. Sung, R. T. K. Kwok, J. W. Y. Lam, D. L. Kong, D. Ding and B. Z. Tang, *Adv. Mater.*, 2016, **28**, 7249–7256.
220 Y. Li, Z. Cai, S. Liu, H. Zhang, S. T. H. Wong, J. W. Y. Lam, R. T. K. Kwok, J. Qian and B. Z. Tang, *Nat. Commun.*, 2020, **11**, 1255.
221 K. Gu, Y. Xu, H. Li, Z. Guo, S. Zhu, S. Zhu, P. Shi, T. D. James, H. Tian and W. H. Zhu, *J. Am. Chem. Soc.*, 2016, **138**, 5334–5340.
222 S. Koo, M. Won, H. Li, W. Y. Kim, M. Li, C. Yan, A. Sharma, Z. Guo, W. H. Zhu, J. L. Sessler, J. Y. Lee and J. S. Kim, *Chem. Sci.*, 2021, **12**, 10054–10062.
223 X. Yu, Y. Ying, Z. Feng, J. Qi, J. Zheng, Y. Zhang, J. Liu, J. Qian, B. Z. Tang and D. Zhang, *Nano Today*, 2021, **39**, 101235.
224 X. Shi, N. Yan, G. Niu, S. H. P. Sung, Z. Liu, J. Liu, R. T. K. Kwok, J. W. Y. Lam, W. X. Wang, H. H. Sung, I. D. Williams and B. Z. Tang, *Chem. Sci.*, 2020, **11**, 3152–3163.
225 G. C. Ma, Z. K. Liu, C. G. Zhu, H. J. Chen, R. T. K. Kwok, P. F. Zhang, B. Z. Tang, L. T. Cai and P. Gong, *Angew. Chem., Int. Ed.*, 2022, **61**, 2207213.
226 D. Yan, M. Wang, Q. Wu, N. Niu, M. Li, R. Song, J. Rao, M. Kang, Z. Zhang, F. Zhou, D. Wang and B. Z. Tang, *Angew. Chem.*, 2022, **61**, e202202614.
227 H. Wang, Z. He, X.-A. Liu, Y. Huang, J. Hou, W. Zhang and D. Ding, *Small Struct.*, 2022, **3**, 2200036.
228 W. Xu, M. M. S. Lee, J. J. Nie, Z. Zhang, R. T. K. Kwok, J. W. Y. Lam, F. J. Xu, D. Wang and B. Z. Tang, *Angew. Chem.*, 2020, **59**, 9610–9616.
229 C. Y. Y. Yu, H. Xu, S. L. Ji, R. T. K. Kwok, J. W. Y. Lam, X. L. Li, S. Krishnan, D. Ding and B. Z. Tang, *Adv. Mater.*, 2017, **29**, 1606167.
230 S. R. Jia, *CCS Chem.*, 2022, **4**, 744.
231 M. Wang, D. Y. Yan, M. Wang, Q. Wu, R. X. Song, Y. M. Huang, J. Rao, D. Wang, F. F. Zhou and B. Z. Tang, *Adv. Funct. Mater.*, 2022, **32**, 2205371.
232 H. F. Wen, Z. J. Zhang, M. M. Kang, H. X. Li, W. H. Xu, H. Guo, Y. M. Li, Y. H. Tan, Z. Y. Wen, Q. Wu, J. C. Huang, L. Xi, K. Li, L. Wang, D. Wang and B. Z. Tang, *Biomaterials*, 2021, **274**, 120892.
233 J. Qi, H. L. Ou, Q. Liu and D. Ding, *Aggregate*, 2021, **2**, 95–113.
234 G. X. Feng, G. Q. Zhang and D. Ding, *Chem. Soc. Rev.*, 2020, **49**, 8179–8234.
235 M. Li, H. F. Wen, H. X. Li, Z. C. Yan, Y. Li, L. Wang, D. Wang and B. Z. Tang, *Biomaterials*, 2021, **276**, 121007.
236 Z. D. Qiu, X. X. Yu, J. Y. Zhang, C. J. Xu, M. Y. Gao, Y. H. Cheng and M. F. Zhu, *Biomaterials*, 2022, **287**, 121666.
237 T. Zhou, R. Hu, L. Wang, Y. Qiu, G. Zhang, Q. Deng, H. Zhang, P. Yin, B. Situ, C. Zhan, A. Qin and B. Z. Tang, *Angew. Chem.*, 2020, **59**, 9952–9956.
238 M. Kang, C. Zhou, S. Wu, B. Yu, Z. Zhang, N. Song, M. M. S. Lee, W. Xu, F. J. Xu, D. Wang, L. Wang and B. Z. Tang, *J. Am. Chem. Soc.*, 2019, **141**, 16781–16789.
239 A. Wiehe, J. M. O'Brien and M. O. Senge, *Photochem. Photobiol. Sci.*, 2019, **18**, 2565–2612.
240 N. Kipshidze, N. I. Yeo and N. Kipshidze, *Nat. Photonics*, 2020, **14**, 651–652.
241 X. J. Shi, S. H. P. Sung, J. H. C. Chau, Y. Li, Z. Y. Liu, R. T. K. Kwok, J. K. Liu, P. H. Xiao, J. J. Zhang, B. Liu, J. W. Y. Lam and B. Z. Tang, *Small Methods*, 2020, **4**, 2000046.
242 M. Y. Wu, M. J. Gu, O. K. Leung, X. M. Li, Y. C. Yuan, C. Shen, L. R. Wang, E. G. Zhao and S. J. Chen, *Small*, 2021, **17**, 2101770.
243 Y. Cheng, A. E. Clark, J. J. Zhou, T. Y. He, Y. Li, R. M. Borum, M. N. Creyer, M. Xu, Z. C. Jin, J. C. Zhou, W. Yim, Z. H. Wu, P. Fajtova, A. J. O'Donoghue, A. F. Carlin and J. V. Jokerst, *ACS Nano*, 2022, **16**, 12305–12317.
244 B. Li, W. Wang, W. F. Song, Z. Zhao, Q. Q. Tan, Z. Y. Zhao, L. T. Tang, T. C. Zhu, J. L. Yin, J. Bai, X. Dong, S. Y. Tan, Q. Y. Hu, B. Z. Tang and X. Huang, *Adv. Sci.*, 2021, **8**, 2003556.
245 R. Hu, Q. Y. Deng, Q. Y. Tang, R. Y. Zhang, L. R. Wang, B. Situ, C. Gui, Z. M. Wang and B. Z. Tang, *Biomaterials*, 2021, **271**, 120725.
246 Y. H. Liao, B. Li, Z. Zhao, Y. Fu, Q. Q. Tan, X. Y. Li, W. Wang, J. L. Yin, H. Shan, B. Z. Tang and X. Huang, *ACS Nano*, 2020, **14**, 8046–8058.
247 B. Li, Q. Q. Tan, Z. J. Fan, K. Xiao and Y. H. Liao, *Adv. Ther.*, 2020, **3**, 1900189.
248 M. Wu, W. B. Wu, Y. K. Duan, X. G. Liu, M. Wang, C. U. Phan, G. B. Qi, G. P. Tang and B. Liu, *Adv. Mater.*, 2020, **32**, 2005222.

249 M. M. S. Lee, W. H. Xu, L. Zheng, B. R. Yu, A. C. S. Leung, R. T. K. Kwok, J. W. Y. Lam, F. J. Xu, D. Wang and B. Tang, *Biomaterials*, 2020, **230**, 119582.
250 J. S. Ni, T. L. Min, Y. X. Li, M. L. Zha, P. F. Zhang, C. L. Ho and K. Li, *Angew. Chem., Int. Ed.*, 2020, **59**, 10179–10185.
251 D. Mao, F. Hu, Kenry, G. B. Qi, S. L. Ji, W. B. Wu, D. L. Kong and B. Liu, *Mater. Horiz.*, 2020, **7**, 1138–1143.
252 Y. Y. Xie, Y. W. Zhang, X. Z. Liu, X. F. Ma, X. T. Qin, S. R. Jia and C. Zhong, *Chem. Eng. J.*, 2021, **413**, 127542.
253 Y. L. Xu, W. Tuo, L. Yang, Y. Sun, C. L. Li, X. Q. Chen, W. C. Yang, G. F. Yang, P. J. Stang and Y. Sun, *Angew. Chem., Int. Ed.*, 2022, **61**, e202110048.
254 Y. Li, F. Liu, J. J. Zhang, X. Y. Liu, P. H. Xiao, H. T. Bai, S. Chen, D. Wang, S. H. P. Sung, R. T. K. Kwok, J. Z. Shen, K. Zhu and B. Z. Tang, *Adv. Sci.*, 2021, **8**, 2001750.
255 G. X. Feng, Y. Y. Yuan, H. Fang, R. Y. Zhang, B. G. Xing, G. X. Zhang, D. Q. Zhang and B. Liu, *Chem. Commun.*, 2015, **51**, 12490–12493.
256 M. Y. Wu, L. Chen, Q. Chen, R. Hu, X. Xu, Y. Wang, J. Li, S. Feng, C. Dong, X. L. Zhang, Z. Li, L. Wang, S. Chen and M. Gu, *Adv. Mater.*, 2022, e2208578, DOI: **10.1002/adma.202208578**.
257 X. L. Liu, M. G. Li, T. Han, B. Cao, Z. J. Qiu, Y. Y. Li, Q. Y. Li, Y. B. Hu, Z. Y. Liu, J. W. Y. Lam, X. L. Hu and B. Z. Tang, *J. Am. Chem. Soc.*, 2019, **141**, 11259–11268.
258 R. H. Dong, Y. Li, M. A. Chen, P. H. Xiao, Y. F. Wu, K. Zhou, Z. Zhao and B. Z. Tang, *Small Methods*, 2022, **6**, 2101247.
259 Y. Li, Z. Zhao, J. J. Zhang, R. T. K. Kwok, S. Xie, R. B. Tang, Y. X. Jia, J. C. Yang, L. Wang, J. W. Y. Lam, W. F. Zheng, X. Y. Jiang and B. Z. Tang, *Adv. Funct. Mater.*, 2018, **28**, 1804632.
260 B. X. Ma, H. Xu, W. H. Zhuang, Y. N. Wang, G. C. Li and Y. B. Wang, *Small*, 2020, **16**, 2003253.
261 H. Cao, Y. Cheng, H. Gao, J. Zhuang, W. Zhang, Q. Bian, F. Wang, Y. Du, Z. Li, D. Kong, D. Ding and Y. Wang, *ACS Nano*, 2020, **14**, 4014–4026.
262 T. Zhang, X. Chen, C. Yuan, X. Pang, S. Ping, Y. Liu, L. Han, J. Sun, J. W. Y. Lam, Y. Liu, J. Wang, B. Shi and B. Z. Tang, *Angew. Chem.*, 2022, e202211550, DOI: **10.1002/anie.202211550**.
263 R. Li, Y. Li, M. Mu, B. Yang, X. Chen, W. Y. W. Lee, Y. Ke, W. H. Yung, B. Z. Tang and L. Bian, *ACS Appl. Mater. Interfaces*, 2021, **13**, 11609–11620.
264 L. G. Jia, W. J. Wang, Y. S. Yan, R. Hu, J. C. Sang, W. P. Zhao, Y. Wang, W. Wei, W. Cui, G. Q. Yang, F. P. Lu, J. Zheng and F. F. Liu, *ACS Appl. Mater. Interfaces*, 2020, **12**, 31182–31194.
265 T. T. Li, Y. Wu, W. T. Cai, D. Wang, C. D. Ren, T. Y. Shen, D. H. Yu, S. J. Qiang, C. Y. Hu, Z. Zhao, J. Yu, C. Peng and B. Z. Tang, *Adv. Sci.*, 2022, **9**, e2202485.
266 C. Peng, W. J. Sun, C. C. Zhou, S. J. Qiang, M. J. Jiang, J. W. Y. Lam, Z. Zhao, R. T. K. Kwok, W. T. Cai and B. Z. Tang, *Biomaterials*, 2021, **279**, 121227.
267 S. Mahmoudi, A. Masoomi, K. Ahmadikia, S. A. Tabatabaei, M. Soleimani, S. Rezaie, H. Ghahvechian and A. Banafsheafshan, *Mycoses*, 2018, **61**, 916–930.
268 C. C. Zhou, C. Peng, C. Z. Shi, M. J. Jiang, J. H. C. Chau, Z. Y. Liu, H. T. Bai, R. T. K. Kwok, J. W. Y. Lam, Y. X. Shi and B. Z. Tang, *ACS Nano*, 2021, **15**, 12129–12139.
269 B. X. Ma, H. Xu, W. H. Zhuang, Y. N. Wang, G. C. Li and Y. B. Wang, *ACS Nano*, 2020, **14**, 5862–5873.
270 P. D. Robbins, D. Jurk, S. Khosla, J. L. Kirkland, N. K. LeBrasseur, J. D. Miller, J. F. Passos, R. J. Pignolo, T. Tchkonia and L. J. Niedernhofer, *Annu. Rev. Pharmacol. Toxicol.*, 2021, **61**, 779–803.
271 I. M. Conboy, M. J. Conboy, A. J. Wagers, E. R. Girma, I. L. Weissman and T. A. Rando, *Nature*, 2005, **433**, 760–764.
272 J. J. Chen, Y. F. Zhu, C. T. Wu and J. L. Shi, *Chem. Soc. Rev.*, 2020, **49**, 9057–9094.
273 J. Mei, N. L. C. Leung, R. T. K. Kwok, J. W. Y. Lam and B. Z. Tang, *Chem. Rev.*, 2015, **115**, 11718–11940.
274 J. Li, J. X. Wang, H. X. Li, N. Song, D. Wang and B. Z. Tang, *Chem. Soc. Rev.*, 2020, **49**, 1144–1172.
275 P. Alam, N. L. C. Leung, J. Zhang, R. T. K. Kwok, J. W. Y. Lam and B. Z. Tang, *Coord. Chem. Rev.*, 2021, **429**, 213693.
276 Z. J. Zhang, M. M. Kang, H. Tan, N. Song, M. Li, P. H. Xiao, D. Y. Yan, L. P. Zhang, D. Wang and B. Z. Tang, *Chem. Soc. Rev.*, 2022, **51**, 1983–2030.
277 Y. Cheng, C. L. Sun, X. W. Ou, B. F. Liu, X. D. Lou and F. Xia, *Chem. Sci.*, 2017, **8**, 4571–4578.
278 H. B. Wu, W. Huang, X. Y. Zhou and Y. Z. Min, *Front. Immunol.*, 2020, **11**, 575816.
279 M. I. Setyawati, C. Y. Tay, S. L. Chia, S. L. Goh, W. Fang, M. J. Neo, H. C. Chong, S. M. Tan, S. C. J. Loo, K. W. Ng, J. P. Xie, C. N. Ong, N. S. Tan and D. T. Leong, *Nat. Commun.*, 2013, **4**, 1673.
280 F. Peng, M. I. Setyawati, J. K. Tee, X. G. Ding, J. P. Wang, M. E. Nga, H. K. Ho and D. T. Leong, *Nat. Nanotechnol.*, 2019, **14**, 279.
281 M. I. Setyawati, C. Y. Tay, D. Docter, R. H. Stauber and D. T. Leong, *Chem. Soc. Rev.*, 2015, **44**, 8174–8199.
282 J. K. Tee, L. X. Yip, E. S. Tan, S. Santitewagun, A. Prasath, P. C. Ke, H. K. Ho and D. T. Leong, *Chem. Soc. Rev.*, 2019, **48**, 5381–5407.
283 J. P. Wang, L. Y. Zhang, F. Peng, X. H. Shi and D. T. Leong, *Chem. Mater.*, 2018, **30**, 3759–3767.
284 N. Y. Ni, W. Y. Wang, Y. Sun, X. Sun and D. T. Leong, *Biomaterials*, 2022, **287**, 121640.
285 B. B. Gu, K. T. Yong and B. Liu, *Small Methods*, 2018, **2**, 1700392.